POLITECNICO DI TORINO

MASTER'S DEGREE IN MECHATRONIC ENGINEERING

MODELLING AND CONTROL OF SEMI-ACTIVE FLUID VISCOUS DAMPERS IN STRUCTURAL VIBRATION OPTIMIZATION

SUPERVISORS:

PROF. G. C. MARANO

PROF. A. RIZZO

PROF. N. D. LAGAROS

CANDIDATE:

ANDREA TROISE

OCTOBER 2022

A.Y. 2021/2022

Abstract

In this original final project, called “Modelling and control of semi-active fluid viscous dampers in structural vibration optimization” the behaviour and usefulness of a device referred to as “variable orifice fluid viscous damper” is analysed in the context of improving the dynamic response of structures. Nowadays, in the civil engineering field, the presence of strategies to act on the behaviour of structures subjected to external inputs such as earthquakes or wind gusts is more and more often present. These strategies in literature are divided into three main approaches: passive control, semi-active control, and active control. Passive control of structures consists in exploiting devices that are fixated on a certain behaviour that cannot be modified in real-time it can be also considered a redesign of the structure parameters. Active control of structures, instead, exploits solutions that are capable of dynamically modifying the characteristics of the structure, requiring a relevant amount of energy to the actuators (which is particularly critical during an exceptional event such as an earthquake) that must be perfectly controlled to avoid the destabilization of the structure. Semi-active control of structures represents the compromise between the two previous approaches, it exploits devices that are capable of modifying their mechanical parameters in real-time, that do not need a relevant amount of power to work, and also are not capable of destabilizing a structure because they do not possess actuators. In this context, the specific “variable orifice fluid viscous damper” device was considered and studied starting from a literature survey that was fundamental to obtaining the necessary information for building a model that could integrate the device to analyse its effect. In the MATLAB/Simulink environment, the equation of motion of the systems was linearized and put into state-space form to create an LTI system for the simulations. After this step two main control algorithms were considered, the PID and the MPC controller. Many simulations were carried out considering various tuning of the controllers, different levels of approximation of the model, and also different sampling times, which is a fundamental parameter for the computational weight of the controller. After this step, the sensors, filters, and delay of the real components were added to the model to decrease even the approximation and move closer to a hypothetical real application of the device in a specific structure.

Acknowledgements

I would like to express my most sincere gratitude towards Professor G. C. Marano and Professor A. Rizzo for the opportunity to work with them during these months and for being always present to guide me and entrusting my proposals for the direction of this work. I deeply thank Ph.D. candidates M. M. Rosso and E. Bruschi for all the time that they dedicated to me and all the precious advice that resulted in a fundamental part of this project. My sincere gratitude goes also towards Eng. R. Cucuzza and Ph.D. candidate J. Melchiorre, with whom I had the chance to work during my experience in Athens. I would also like to thank Professor N. D. Lagaros for guiding me, especially in the first steps of this dissertation.

Dedico questo lavoro di tesi alla mia famiglia ed ai miei amici, senza il loro affetto ed il loro tempo non sarei nulla.

Vi voglio bene.

"Dai un cuore al cervello e un cervello al cuore"

Table of contents

List of figures

List of tables

Introduction

Engineering is defined as the activity of applying scientific knowledge to the design, building and control of systems and devices. It branches into many subjects that developed each other at times independently from the others. This thesis work, developed in collaboration with the National Technical University of Athens, focuses on the combination of two different branches: control theory and structural engineering.

A civil engineering structure represents a system that is often subject to dynamic loadings, such as natural events, for which the energy input must be dissipated guaranteeing that the integrity of the construction is not compromised. The strategies to improve the dynamic response of a structure are three: active control, passive control, and semi-active control. Passive control of structures exploits the implementation of devices that are capable of dissipating the energy input to the system without any real-time modification, which is substantially a redesign of the characteristic parameters of the structure; active control relies on actuators capable of modifying the behaviour of the structure through an input force, it requires a vast amount of energy and a careful design to avoid the destabilization of the system itself; semi-active control represents a trade-off between the two previous approaches, in this method the devices require a small amount of energy, they are capable of varying their behaviour in real-time, and intrinsically guarantee the stability of the structure thanks to their working principle that does not input energy to the construction but only dissipates it. In this context, control theory represents a fundamental building block for the optimization of the structure, since the thorough research on the topic of the last decades created a wide range of algorithms that can be applied to the specific case under study, also with algorithms based on artificial intelligence that are constantly being researched and developed in the field.

In chapter one of the present document, a state-of-art review is argued, presenting the various devices used in the context of vibration control optimization, categorized into active, passive, and semi-active approaches. Chapter two focuses on the specific device chosen for the application, i.e., a semi-active fluid viscous damper capable of varying its damping coefficient in a certain range and analyses it thoroughly from a technical and an analytical point of view. Chapter three focuses on the control algorithms chosen for the specific application of the thesis, which are Proportional Derivative Integrative and Model Predictive Control algorithms, introducing the mathematical theory behind them and allowing to grasp the differences

between the two. Chapter four explores how the model was built highlighting the most important aspects and illustrates the various simulations evaluating the results through the comparison of two performance indexes.

Chapter 1

State of the art in vibration control

1.1 Introduction to vibration control

Structural control devices have been the subject of research in the field of engineering for many decades. The objective of these devices is the alleviation of the response in buildings and bridges to a dynamic loading given typically by a seismic event or strong gusts of wind. The task of structural control is to determine a technique that, after measuring a response of the system, determines the action to enhance its safety and dynamic behaviour. There are various approaches to the problem given by natural hazards, such as active, passive, hybrid, and semi-active damping strategies.

An active structural control system consists of sensors located about the structure to measure either external excitations or structural response variables, or both, devices to process the measured information and compute the necessary control force needed based on a given control algorithm, and actuators powered by external sources to produce the required forces [83], these forces can be both used to add and dissipate energy in the structure [37]. The control strategy is called feedback control when only the structural response is measured, instead, it is referred to as feedforward control when only the excitation to the building is measured. A third scenario is called feedback-feedforward control, and it exploits the measurements of both the response and the excitation quantities [83].

The advantages of an active control system with respect to a passive one are the following: (a) improved response control of the structure; (b) lower sensitivity to ground behaviour; (c) mitigation of many kinds of input to the structure; (d) selectivity of the control strategy; for example, it could be chosen to improve human comfort over structural behaviour under some peculiar circumstances and so on [83]. Active damping strategies of structures rely on the input forces given by electrohydraulic or electromechanical actuators, these actuators are designed to influence several vibration modes of the system; hence this technique is most suited for structures with many degrees of freedom. The actuators used for an active control strategy of the system require an external power source of considerable energy. Active control systems can adapt to a wide range of operating conditions and structures.

The main drawbacks of active control systems are:

- The implementation costs
- The need for a high energy source during a natural event such as an earthquake
- The possibility of destabilizing the structure if the control system is not well designed, or has a malfunction

Passive damping strategies do not rely on actuators of any sort, they do not require an external power source for operation and they utilize the motion of the structure to develop the control forces; they are used to increase the energy dissipation capacity of a structure through localized, discrete devices, and may increase the stiffness and strength of the structure to which they are attached; the forces imparted by passive devices are developed in response to the motion of the structure. The dissipated energy in a passively controlled structural system cannot be increased in any way by passive control devices [37]. The passive technique for protecting structures is based on the principle that the input energy to the system is transformed into both kinetic and potential (strain) energy which must be either absorbed or dissipated through heat. The performance of the structure can be improved if a part of this input energy is absorbed by the passive devices instead of the structure itself. Passive systems are unable to adapt to changes in the structural properties and the stochastic nature of external excitations due to their fixed behaviour.

Hybrid vibration control refers to a combined application of active and passive control systems. A hybrid system incorporates both typologies of devices, this allows the structure to reach the highest levels of performance exploiting the best features of both strategies, also, the presence of passive elements allows for a smaller effort of active components. Hybrid techniques are utilized typically in very high-end applications, such as skyscrapers or viaducts, and they incorporate both actuators connected to a high-power source of energy and devices such as isolators. Notably, also hybrid systems are not free of the necessity for a reliable and high-power source of energy in critical conditions.

Control strategies based on semi-active devices appear to combine the best features of both passive and active control systems [83]. Typically, semiactive control devices do not add mechanical energy to the structural system, therefore bounded-input bounded-output stability is always guaranteed; semiactive control devices, moreover, are often viewed as controllable passive devices [37]. A semi-active system exploits passive devices capable of varying their characteristic parameters such as damping coefficient and/or stiffness in real time. It does so by modifying its mechanical properties or some other specific feature. The approach is possible thanks to the measurement of the structural response and/or the excitation given by the input

and a control loop that computes the necessary action of the device. Since there are no actuators in this strategy, also in this case as in the passive approach the motion of the structure is used to develop the control forces. The variation of the properties of the device is possible thanks to a small source of energy such as a battery pack, this allows to solve the energy issue typically related to active control systems.

Control strategies, also in this kind of application, are referred to as: feedback, feedforward, or feedback-feedforward depending on if the sensors compute the control action measuring respectively: the response of the system, the excitation of the input, or both. Preliminary results have shown that "*well-designed semiactive systems perform significantly better than passive ones and that they also have the potential to achieve, or even surpass, the performance of active systems"* [37].

Semi-active, hybrid and active control of structures are considered the natural evolution of passive control techniques. They rely on devices capable of processing the data in real time, to develop control actions with the smallest time lag possible. This allows an improved structural behaviour and enhanced safety of the structure.

1.2 Typical devices employed in the passive control strategy

Vibrating structures dissipate energy due to internal stressing, rubbing, cracking, and plastic deformation. A large energy dissipation capacity implies also smaller amplitudes of vibration; some structures have a very low damping coefficient, which implies very large amplitudes of oscillation even for moderate inputs. Many different methods for increasing the damping are utilized in real-world applications, and they mainly focus on converting kinetic energy to heat or transferring energy among vibrating modes. These methods exploit a various range of materials and devices for enhancing damping, stiffness, and strength of the system and can be used also for the rehabilitation of ageing structures [37].

- Base isolation devices

The base isolation approach has the objective to decouple a superstructure from its substructure, therefore limiting the influence of the seismic input on the building. The devices aim to reduce the fundamental frequency of structural vibration to a value lower than the main frequency of the earthquake input, which is equivalent to increasing the natural period of the structure and dissipating a part of the energy to reduce the acceleration transmitted to the

superstructure. The energy given by the ground motion at higher frequencies is deflected, and this makes the solution very attractive for a building containing expensive equipment.

Natural rubber bearings (NRB) are a very common type of base isolation device built of alternating steel with a thickness between 2.5 to 4.5 mm and rubber layers with thickness from 3 to 9 mm, showing high damping, horizontal flexibility, and high vertical stiffness. High damping rubber bearings (HDRB) are similar to this design, using a special synthetic rubber that can dissipate energy through loop cycles. Notably, the size, height, and fundamental natural period of base-isolated buildings increase steadily with time, indicating that base-isolation is reaching maturity [64].

Pure friction base isolators base their working principle on sliding friction, they are effective for a wide range of input frequencies. The frictional force is proportional to the mass of the structure, and they have the capability of reducing torsional effects given by asymmetric buildings [43].

Lead rubber bearing systems are laminated elastomeric bearings with a lead plug down their centre used to increase the hysteretic energy dissipation capabilities of the device. An issue with the device is the impossibility to check the conditions of the core from outside after a seismic event. The behaviour can be modelled with a set of nonlinear equations. In [70] the author describes the tests on the devices, the results, and a design procedure for selecting the size of the lead plug.

Resilient friction base isolation systems (R-FBI) are made of concentric layers of polytetrafluoroethylene plates containing a central core of rubber. The system can mix the best features of friction damping with the resistance of rubber, which allows spreading the displacement and the velocity throughout the height of the device [59].

Electric de France (EDF) systems represent an accustomed device for nuclear power plants in high seismicity regions, this kind of isolator is made by a double raft interposed with reinforced neoprene pads and friction plates, therefore typically overlapping various layers of laminated neoprene with lead-bronze plate on top. The plate exploits friction with a steel plate on the base of the structure to decouple the structure from the ground. The neoprene pads behave as a filter between the primary structures and the ground, limiting the horizontal earthquake forces and accelerations experienced by the structures, while the low natural frequency of the predominant horizontal mode minimizes participation of higher structural modes [35].

Sliding bearings combine the best characteristics of EDF and R-FBI base isolation devices, it is therefore made by alternating layers of polytetrafluoroethylene with a central core of rubber with a frictional plate on top. The resulting behaviour is the one of an R-FBI system for low

seismic excitation, and a frictional behaviour (EDF) for high seismic inputs, which improves the safety of the system [85].

- Metallic yield dampers

Inelastic deformation of metals is exploited in metallic yield dampers as a technique to dissipate the energy input to a structure. These devices, often referred to as "ADAS" (added damping and stiffness), are built using mild steel plates shaped in various ways, such as triangular, x-shaped, honeycomb, and others, also exploiting materials such as shape-memory alloys, they include torsional beams, flexural beams, and U-strip energy dissipators [19,87,92].

Metallic yield dampers possess many desirable characteristics such as stable hysteretic behaviour, low-cycle fatigue property, high reliability, and low sensitivity to temperature variations [37]. The amount of energy dissipated by the device can be measured by evaluating the area within a hysteresis loop of displacement vs shear force, nevertheless, it is not easy to characterize the hysteretic behaviour of the component under arbitrary cyclic loading given that inelastic behaviour follows non-linear relations and depends on microscopic mechanics factors.

To utilize metallic dampers within a structural system, design guidelines and theoretical plus experimental studies are necessary, moreover, the devices transform a linear system into a non-linear one due to their behaviour [37].

- Friction dampers

The friction that develops between two solid bodies sliding on each other is utilized as an energy-dissipation technique in the friction dampers.

The stick-slip phenomenon consists of the abrupt variation of the friction coefficient between the two bodies within its static and dynamic value, and this effect must be minimized during the design of the friction damper device because it introduces a high-frequency excitation that is counterproductive to the energy dissipation objective.

During the load, the friction damper imposes slippage in both compression and tension, dissipating the energy input and avoiding its damaging effect on the structure, furthermore it is important to choose compatible materials for the device to maintain a constant behaviour during the period of use. The sliding interfaces are made of steel on steel, brass on steel, or graphite impregnated bronze on stainless steel; the choice of the interface composition is very relevant in terms of the time resistance features of the device [37].

A very common device is called the "Pall device", and it has been extensively studied in the field; it is installed in an X-braced frame, and it is designed not to slip during windstorms or moderate earthquakes; under the severe working condition the devices slip at a predetermined optimum load before yielding occurs in primary structural members; the devices often require a nonlinear analysis to explore the behaviour under stress conditions. Experimental and analytical results show that the devices can reduce inelastic deformation demands, and reduce damage quantified by monitoring permanent deformations [63].
For its characteristics and ease of installation, the device is well fit in the context of retrofitting old structures to improve their seismic behaviour and therefore enhance their protection. Some specific devices incorporate a mixture of a friction damping and viscoelastic damping mechanism in series, in such a way it is possible to manage the inputs by entrusting the most severe inputs to the friction damper and the milder ones to the viscoelastic damper [67,68,89]. This kind of device generates a hysteretic loop that has the same features of Coulomb's model of friction hysteresis, it provides a good performance that is not significantly affected by the number of loading cycles.

- Viscoelastic dampers

For seismic applications, only a certain class of viscoelastic dampers is exploited, which can dissipate energy at all deformation levels, but these devices are primarily intended for alleviating wind inputs. The dissipation of energy inside the device starts when the vibration of the structure causes relative motion between the outer and the inner layer of the device.
To dissipate energy by exploiting the shear deformation of the viscoelastic layers, the dampers employ materials such as copolymers or glass-like matter. They are built by bonding steel plates with viscoelastic material layers. The behaviour of the device under dynamic loadings depends on vibrational frequency, strain, and ambient temperature. The device is effective in reducing the inelastic ductility demand of the test structure under severe seismic phenomena; the design damping ratio added by the dampers should be higher than the one of the structures itself to reduce the inelastic response, because the equivalent damping ratio of the structure after yielding would be much higher than the inherent damping ratio of the linear structure [37]. A linear structural system stays linear even after the insertion of viscoelastic dampers because the devices increase damping and stiffness properties without exploiting nonlinear effects, differently from what happens with metallic or frictional dampers [98,99].

The natural period of a visco-elastically damped system varies slightly with the temperature, but if the design is developed as a stiff device, then the damping ratio shows to be much less sensitive to the temperature variation [45].
The effectiveness of viscoelastic dampers applied to reinforced concrete structures or steel structures under a various range of seismic inputs was demonstrated in [22,23,32,52,81], in which the in-depth analysis showed that the addition of viscous fluid dampers can reduce the damage to the structure by limiting inelastic deformations.
The material of the damper shows linearity over a broad range of strains with constant temperature, but with large strains, the self-heating effect is evident because the dissipated energy is converted into heat. This results in a nonlinear behaviour of the component, which is present also if the stress-strain response of the material is linear because in general, it represents only an approximation of the behaviour [37].

- Fluid viscous damper

Viscous fluid dampers over the years have been widely used in the military, aerospace, and automotive industry. This kind of damper exploits the technique of fluid orificing in order to dissipate the energy input to the structure. The device consists of a housing filled with highly viscous fluid and a piston that has a certain number of orifices that allow the fluid to pass from one side to the other of the chamber. The dissipation of the energy takes place due to the movement of the piston in the fluid. Considering a Newtonian fluid inside the chamber, the force produced by the device is directly proportional to the velocity of the piston [37].
The devices have some features that make them very appealing in the structural engineering context, in particular the linear behaviour over a very broad range of frequencies of the inputs, the very low sensitivity to temperature variations, and the reduced dimensions.
In [25,55], the study of the device is modelled in the following way:

$$F + \lambda^r D^r[F] = C_0 D^q[X] \tag{1.2.1}$$

In which F = output force, λ, C_0, r and q are constants that depend on the material, $D^r[F]$ and $D^q[X]$ are fractional derivatives. Choosing r and q equal to 1 yields the Maxwell model, in which λ is the relaxation time and C_0 the constant damping coefficient. The second term in the equation disappears for a low damping force rate, which translates to input frequencies lower than a value close to 4 Hz. The model in that case becomes:

$$F = C_0 \dot{X} \tag{1.2.2}$$

The device is often described through another relationship:

$$F = C_0 V^{\sigma} \tag{1.2.3}$$

In which n is an exponent in the range $\sigma \in [0.1; 2]$ and V is the velocity of the piston head inside the damper. For the special design of the orifices, it is possible to obtain lower values of σ, which causes the force to flatten at high velocities.

- Tuned mass dampers

Passive tuned mass dampers are devices consisting of a mass mounted on one or more damped springs, which are tuned to have an oscillation frequency as close as possible to the resonant frequency of the building, in order to reduce the amplitude of the oscillations.
TMDs are used mostly to alleviate wind excitations in high-rise structures such as skyscrapers, they can be tuned to a single structural frequency, therefore, more than one device may be necessary to reach the desired level of safety in the building.
Both analytical and numerical results demonstrate that the capability of TMDs of improving the dynamic behaviour of the same structure during different earthquakes or of different structures during the same earthquake is dramatically different, varying from good performance to no effect. This behaviour highlights a certain dependency of the attained reduction in response to the characteristics of the ground motion that stimulates the structure. The reduction is large for resonant inputs and becomes less evident as the main frequency of the input gets further away from the natural frequency of the structure to which the device is tuned [37].
[48,57] Highlight how the optimal configuration of a TMD system can be very different depending on the individual features of a structure, from the spring-mass type to the circular track type and the pendulum type.
Some design features must be carefully controlled in a TMD system: for sliding masses, a surface with low-friction bearings is necessary for a response at any level of excitation. The travel of the TMD with respect to the building is a key factor as well, as the amount of mass that can be positioned on the top of the structure [37].
In [62] analytical results highlight how applying TMDs to base-isolated systems allows for the absorption of the seismic input without degradation of the isolating effect given by base isolation devices.

- Tuned liquid dampers

The tuned liquid dampers principle for dissipating energy and reducing the dynamic response of structures is like the one of tuned mass dampers, with the difference that the mass is in a liquid state and is generally placed on the highest floor of the building. The dissipative effect takes place by means of wave breaking and viscous action. A variant of the device consists in tuned liquid column dampers (TLCD), which dissipate energy by the motion of the liquid through an orifice with some specific design characteristics. The devices are cheaper than TMD and are easier to tune to the desired frequency.

The improvement in structural performance given by the device has been proved in [44], pointing out that it is able to add indirect damping to the system. The performance was analysed also in [86,90], with reference to the wind inputs and the analysis of a single degree of freedom structure, with positive results that led to many practical applications, in particular for wind response alleviation. In [91] the analysis of the device focuses on the shape of the container, which is geometrically the same as a nutation damper, in [15] a rectangular container filled with two immiscible fluids is used for adding damping to the response of the structure; [33] studies containers with rectangular shape partially filled with water.

TLD must be tuned to the desired frequency, they provide a highly non-linear response due to the liquid sloshing and going through orifices. In TLCDs the fundamental frequency of the device depends on the length of the column of fluid. A good fit between the real behaviour and the hypothetic one was found in the small oscillations case. It is also possible to tune the TLD to two different frequencies in two orthogonal directions of motion, by adjusting tank length in those directions. With respect to TMDs, the maintenance costs are much smaller and the excitation threshold for the response of the device is also lower. The tank is typically made of polypropylene, which makes the installation of the device sufficiently easy, also for existing buildings. For large oscillation inputs, the system is not very sensitive to tuning, which happens instead for small oscillations [37].

1.3 Typical devices employed in the semiactive control strategy

- Variable orifice dampers

Variable orifice dampers are devices that can be controlled by varying the aperture of the orifices present on the piston, therefore varying the resistance to the flow of the viscous fluid present in the chamber; this allows the modification of the force/velocity characteristics of the device. The typical time required to vary from a fully open valve configuration to a fully closed

one is in the order of milliseconds. They typically operate with a low energy requirement (50W).

In [66] the device is characterized in-depth and a flow model is built for it; the dissipator is referred to as the "Semiactive Vibration Absorber" (SAVA). The procedures to identify model parameters in the laboratory are described as the device results able both to store and dissipate energy. The results show that the variable orifice dampers are a robust, reliable, and inexpensive mean of improving the dynamic behaviour of a structure.

In [60] a semiactive control strategy based on variable slip-force level dampers is presented, it exhibits bilinear hysteresis with a ductility factor equal to two. The device behaves linearly regardless of the seismic input and a decentralized control algorithm is employed which utilizes local response information. The system is applied initially to a single degree of freedom structure and then in a 20 DOF multi-story structure. The results show how the device allowed to maintain the structure in linear behaviour.

A fuzzy control methodology is used in [20] to control semi active hydraulic dampers (SHD) installed in combination with steel bracings and placed at different floor levels on a five-story steel building. The FLC is used for the bottom device and other controllers are assumed to provide control commands for the variable damping coefficient of the device in a certain proportion to that obtained for the bottom-most controller. The simulation is developed in MATLAB Simulink environment using the 1940 El Centro earthquake signal as input. The results highlight how the SHD are able to provide an efficient semi active control strategy and that the maximum damping coefficient and damper capacity are the most important factors in the response of the structure.

Pneumatic and hydraulic versions of the device with resettable characteristics are used in [42] to control a three-story scaled frame subject to random inputs. The device under study is modelled like a linear spring that is occasionally reset to extract energy from the vibrating structure. The results highlight that the device employed can provide good structural control.

An on/off oil damper with a built-in controller is presented in [47], using a decentralized algorithm for control that gives independence to each device and allows a simple implementation. A two-dimensional 20-story frame is controlled with the device which results able to dissipate twice as much energy as an ordinary passive damper.

- Smart tuned mass dampers

Smart TMDs are an improvement of standard TMD since their varying stiffness allows the device to alleviate more than one resonant frequency thanks to real-time control of the device. The variation of stiffness of the device is strongly dependent on the instantaneous estimation of frequency and period by a controller. This sort of improvement to the passive version of the device can also be applied to TLDs.

In [50] a semiactive TMD with MR implementation is used for a 2-dimensional model of a 12-story frame subject to seismic inputs. The performance of the system is evaluated by comparison with an active TMD, and the system is controlled online with a saturated optimal control strategy. The results show that the STMD is not as effective as the active version, but it is cheaper and has lower power requirements. In [80] the device referred to as a "ground hook tuned mass damper" (GHTMD) is used for the reduction of floor vibrations due to human movements. The structure tested is a metal deck on a shaker table. The results are compared with the behaviour of a passive TMD, and they show that the STMD is better at reducing uneven weight distribution caused by equipment or other loads.

- Electro and magnetorheological dampers

Electro and magnetorheological dampers rely on controllable fluids, which are able to reversibly change from a free-flowing, linear viscous fluid to a semi-solid when exposed to an electric (for electrorheological fluids) or magnetic (for magnetorheological fluids) field [83].

In presence of a strong field, the particles of the liquid polarize and align, thus increasing exponentially the resistance to the flow. The presence of the field can modify the behaviour from a viscous fluid to a yielding solid within milliseconds.

Magnetorheological fluids typically consist of micron-sized magnetically polarizable particles dispersed in a medium such as mineral or silicone oil. The sudden transition allows the construction of large bandwidth devices. The fluids can operate from -40°C to 150°C with slight variations in the yield stress. They show a certain sensitivity to impurities and many additives can be used to enhance properties such as stability, seal life, bearing life, and so on.

The behaviour of the device can be modulated by varying the field and therefore obtaining different kinds of responses depending on the need and the control strategy utilized.

In [36] magnetorheological dampers in active bracings are used in a scaled model subject to earthquake loadings, and the results highlight how Sliding Mode Control (SMC) performs better than both Linear Quadratic Regulator (LQR) and skyhook controllers.

The use of the MR dampers for bridge control is analysed in [51] on a 1:12 scaled model with two dampers. The damping force is controlled aiming at minimizing the rate of change of energy in the system with Fuzzy Logic (FLC), fuzzy logic plus sliding mode, and Lyapunov-based control strategies. The results show how in general the use of dampers improves the behaviour and, more specifically, how FLC has the best performance out of the three methods.
A wireless control system for a half-scaled three-story steel structure is employed in [54] and it is subjected to the El Centro earthquake signal on a shaking table. Linear Quadratic Gaussian (LQG) control was used in a centralized and decentralized fashion. The results suggest that the performance of the decentralized strategy is better due to robustness and performance factors.
In [53] centralized and decentralized LQG control of a 20-story frame with MR dampers were analysed with four different scenarios ranging from fully centralized to fully decentralized control. The study concluded stating that the performance difference between the strategies is almost neglectable, but the decentralized control is more robust.
Podium structure buildings behaviour was analysed in [95] using scaled models, testing 4 different scenarios, ranging from no control to multilevel logic control algorithm of MR dampers. The tests highlighted how the values of displacements and acceleration decreased up to 70% with respect to the uncontrolled system and about 35% for the passive version of the system.
In [29] the Cape Girardeau Bridge is used as a benchmark problem with 24 magnetorheological fluid dampers with 1000 kN capacity each. The system is controlled with H_2 and LQG control strategies and subjected to the 1985 Mexico City, 1999 Gebze and 1940 El Centro earthquakes. The conclusion highlights an improvement in all responses. In [58] the same bridge was controlled with Sliding Mode Control (SMC) and Linear Quadratic Gaussian (LQG) methods, and the SMC resulted being the more effective.
In [69] shake table tests were performed on a steel frame model with MR dampers in active bracing using the signals from the 1976 Friuli, and the 1994 Northridge earthquakes. The study exploited an instantaneous optimal control algorithm and the presence of MR dampers allowed a reduction in displacements of about 35% with respect to the passive device condition.

- Variable friction dampers

This improvement of passive friction damper, typically made by a structural bracing connected to a friction shaft, allows the control of the device by adjusting the presence of slippage to the

desired amount, this can be achieved by varying the normal component of the force to the surfaces by hydraulic, electromagnetic, and piezoelectric actuators.
In [96] the authors tested the device proving that it can reduce displacement, as well as velocity and acceleration of a high-rise building. In [28] a smart piezoelectric friction damper is used for a tall building to improve the dynamic behaviour under wind loadings, the results show how the device results efficient also with different control strategies.

1.4 Typical devices employed in the active control strategy

- Active tuned mass damper

ATMDs, also known as "active mass drivers", exploit actuators connected to a TMD to control the vibration of a structure. The forces from the actuator can be employed to increase the efficiency of the device and its robustness to changes in the dynamic behaviour [83]. The device can overcome the main issue of passive TMDs by being able to counteract more than one resonant frequency of the structure with a single device. It works well for wind gusts and earthquakes, but it is difficult to accurately compute the fundamental frequency of a structure. The device also, is not as effective for irregular structures under strong ground motion, because the presence of many different modes of vibration may significantly increase the dynamic response [31].
It is possible to distinguish between two alternative versions of this device, one is also called a "hybrid mass damper"; it needs more space for the installation and is able to act on both longitudinal and torsional motion, while the other is referred to as "active mass damper" and can act only on one specimen of motion, either torsional or longitudinal, which is the reason why more than one of these devices is usually installed in active control applications.
Li et al. in [49] exploit the H_2 control strategy to analyze the response of a big offshore platform, and the results highlight how the ATMD strategy performs better than the TMD one.
In [93] an ATMD is analysed on a possible installation to counteract wind gusts with different control algorithms: Linear Quadratic Gaussian (LQG), H∞ and Sliding Mode Control (SMC), all three strategies performed well in improving the dynamic response of the structure.
Most of the research in the field is focused on implementing a single ATMD on structures, but there are some exceptions, in [41] Ikeda et al. discuss the use of two ATMD to counteract both lateral and torsional dynamic effects on a ten-story building with steel frame. The discussion highlights how the reduction in lateral and torsional vibration is respectively at 26% and 11% for earthquake inputs.

In [34] Guclu and Yazici analyse the behaviour of a two-dimensional 15-story structure with 15 degrees of freedom controlled with a Proportional Derivative (PD) and a Fuzzy Logic controller to control ATMDs placed on the first and on the 15th floor. The results of the analysis show that the Fuzzy Logic controller is more effective than the PD in improving the behaviour of the system.

- Distributed actuators

Active strategies often exploit inputs from several actuators spread across the structure. The control strategy used, and the placement of actuators are strongly dependent on the individual properties of a structure, and its simulated uncontrolled response. In this kind of solution, the control strategy used is typically a robust one since increasing the number of devices necessary for the control means increasing the failure or destabilisation probability. In fact, a supercomputer may be necessary to compute the necessary actions in real time, which increases the implementation costs and the algorithm complexity [31].

In [12] a computational model for control with thousands of distributed actuators for large structures is presented, focusing on different kinds of inputs such as wind, earthquake, and impact loadings.

In [1-11] Saleh and Adeli discuss parallel algorithms to simultaneously optimize and control structural systems with distributed actuators. In the study, they analyse micro and macro tasking on high-performance processors that share memory.

In [74,75] Saleh and Adeli focus on the solution of the Riccati equation, needed for the application of the LQR algorithm, using parallel vector algorithms optimized for shared-memory supercomputers.

The saturation working condition in which the force input by the actuators is not enough to stabilize the structure is analysed in [14], the results of the study show that the saturation is not detrimental for the 2D six-story frame analysed.

Saleh and Adeli in [78] analyse a 3D multi-storey building structure controlled with distributed actuators, subject to earthquake motions and wind gusts from both directions. Different options for the placement of the actuators are studied. The results highlight how the most effective placement depends on the specific characteristics of the structure and that the unbraced moment-resisting frames are the most effective.

Optimal control of multi-storey building structures subject to blast-type loadings is presented in [73], analysing both internal and external blasts on different floors. The results show how a careful placement of the controllers can improve considerably the behaviour of the structure.

Chase et al. in [24] analyse a 2D five-story frame with distributed actuators controlled by the H∞ control algorithm, which guarantees stability also in saturation and fault conditions.

- Active tendon systems

Active tendons are prestressed tendons placed between various stories of a structure, used to adjust the level of tension in the cables, thus controlling the magnitude of the controlled force to the construction. They exploit hydraulic or piezoelectric actuators and are utilized for active control. Active tendon systems act by modulating the level of tension of the tendons, hence controlling the amplitude of the force to the structure, they are typically used in cable suspended bridges.

In [71] an active tendon system is presented for a 142.5m cable-stayed pedestrian bridge subject to the 1952 Taft earthquake and controlled with a Lyapunov-based controller. The results show that the response of the bridge is significantly improved thanks to the system.

In [29] an active tendon system with either hydraulic or piezoelectric actuators is used to control two scaled models of cable-stayed bridges. The study focuses mainly on wind loadings.

Chapter 2

Variable aperture fluid viscous dampers

2.1 Sources and fundamentals of fluid viscous dampers

This chapter explores the fundamental characteristics of the dampers under study, it is mainly based on the very detailed technical report NCEER-95-0011 by M.D. Symans and M.C. Constantinou, which was the result of research conducted at the University of Buffalo, State University of New York. The results presented in the report represented a basis for all the studies of the device in the following years, this included. Moreover, the insights taken by other research papers are cited in the text itself with the classic square bracket format.

Fluid viscous dampers were first used in the French military field at the end of the nineteenth century. They were considered a national secret until the first world war when they were shared with French allies, the United Kingdom, and the United States of America. Since then, the application of the device has spread from the automotive field to the aerospace one, being used for suspensions and payload dampers, and has nowadays become ubiquitous in many fields of engineering. The extensive applications of fluid viscous dampers to vibration control of structures were proven in military applications during the decades of the cold war, but the devices were made commercially available only during the last decades of the twentieth century.

In physical systems, damping is produced by processes that dissipate the energy stored in the oscillation. The typical level of damping of a building is very low, and so is the amount of energy dissipated during an external disturbance such as a seismic input, bringing the structure beyond its elastic limit, and causing permanent deformations, therefore risking the collapse. The idea of additive damping elements is to make sure that the energy is dissipated by them, rather than by the structure itself, hence acting as a protective device. A fluid viscous damper generally consists of a piston in the damper housing typically filled with a compound of silicone oil with kinematic viscosity equal to $100\ \frac{mm^2}{s}$ and specific weight equal to $9.78\ \frac{kN}{m^3}$. The fluid is non-toxic, inert, non-flammable, modellable as an uncompressible fluid and stable for very long periods. A pressure differential across the piston head is responsible for the force generated by the fluid damper, which converts seismic energy into heat.

The presence of an accumulator and a control valve prevents the generation of a restoring force in the device, given by its compressibility. Typically, piston motions with a frequency lower than 4 Hz display no stiffness properties; this cut-off frequency may be desired, it is a function of the design of the device, and it depends on the dimension of the accumulator.

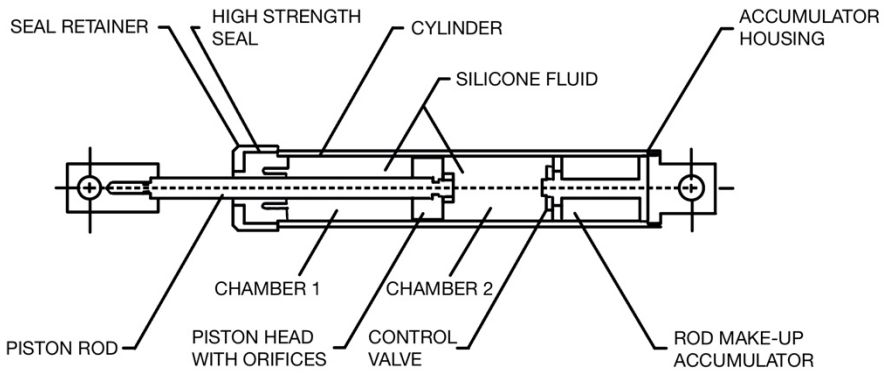

Figure 2.1: Passive fluid viscous damper, image inspired from technical report NCEER-95-0011

Viscous fluid dampers display a linear viscous response for a broadband range of frequencies and a compact design, they can reduce contemporarily both stress and deflection within a structure subjected to a transient. This happens because the device modulates the output force as a function of the velocity only, which inherently provides a behaviour that is out-of-phase with stresses due to the flexing of the structure.

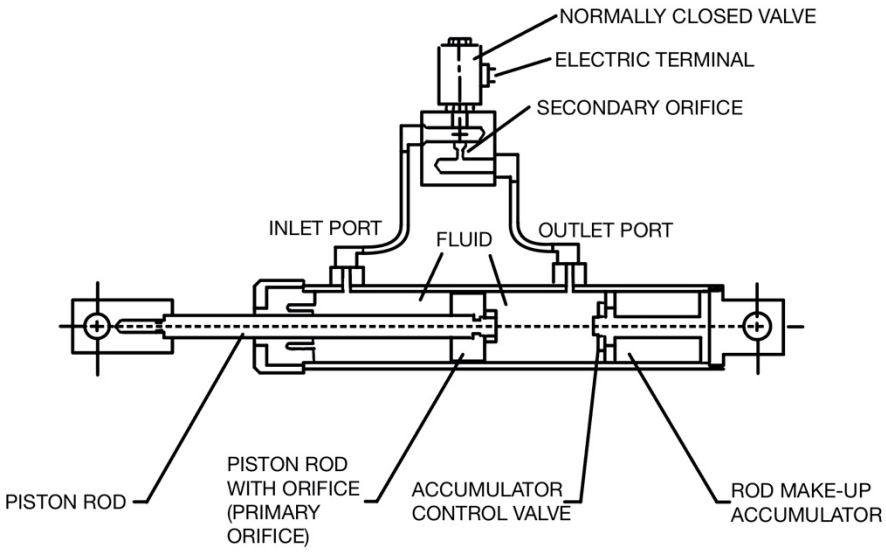

Figure 2.2: Semi-active fluid viscous damper, image inspired from technical report NCEER-95-0011

The dampers are often referred to as "inertial dampers" because of the dependence of the force output of the device on the speed of the fluid through the orifices. In figure 2.2 the modifications needed to create a semi-active device are visible, in particular the addition of an external bypass loop with a control valve. In this form, the device is referred to as a "two-stage damper", because typically the control valve can only be in the "fully open" or in the "fully closed" position. The control valve is a D.C. solenoid valve in which the solenoid coil can either be fully energized or de-energized.

2.2 Integrated electronics and solenoid valve

As shown in figure 2.3, the external valve possesses a whole apparatus that must receive a certain number of signals, both to supply power to the valve and to monitor its proper behaviour. The voltage supply required is typically $24\ V_{DC}$ which is very low. The complete list of signals is presented in the following table

Table 2.1: List of electric signals necessary for the functioning of the solenoid valve

Signal	Technical Specifications	Notes
V_+	Power supply at $24\ V_{DC}$ for solenoid power stage and driver logic	Input – power supply
V_0	Power supply at $0\ V_{DC}$ for solenoid power stage and driver logic	Gnd – power supply
AGND	Ground signal	Gnd – analog signal
ENABLE	Enable or disable the driver ($4 \div 20\ mA$ for current-input version)	Input – on/off signal
INPUT+	Reference analog differential input of $\pm 10\ V_{DC}$ maximum range ($4 \div 20\ mA$ for current-input version)	Input – analog signal
INPUT-		
MONITOR	Monitor analog input $\pm 10\ V_{DC}$ maximum range	Output – analog signal
FAULT	Fault $(0V)$ or normal working $(24V)$	Output – on/off signal

As reported in the table, the inputs to the integrated electronics of the valve can either be voltages or currents, this clearly implies that the command signal for the algorithm will be in the respective form. The datasheet of this specific valve reports a maximum power supply needed equal to $35W$, this allows battery operation during blackouts, which is a critical advantage in the context of control during extreme events.

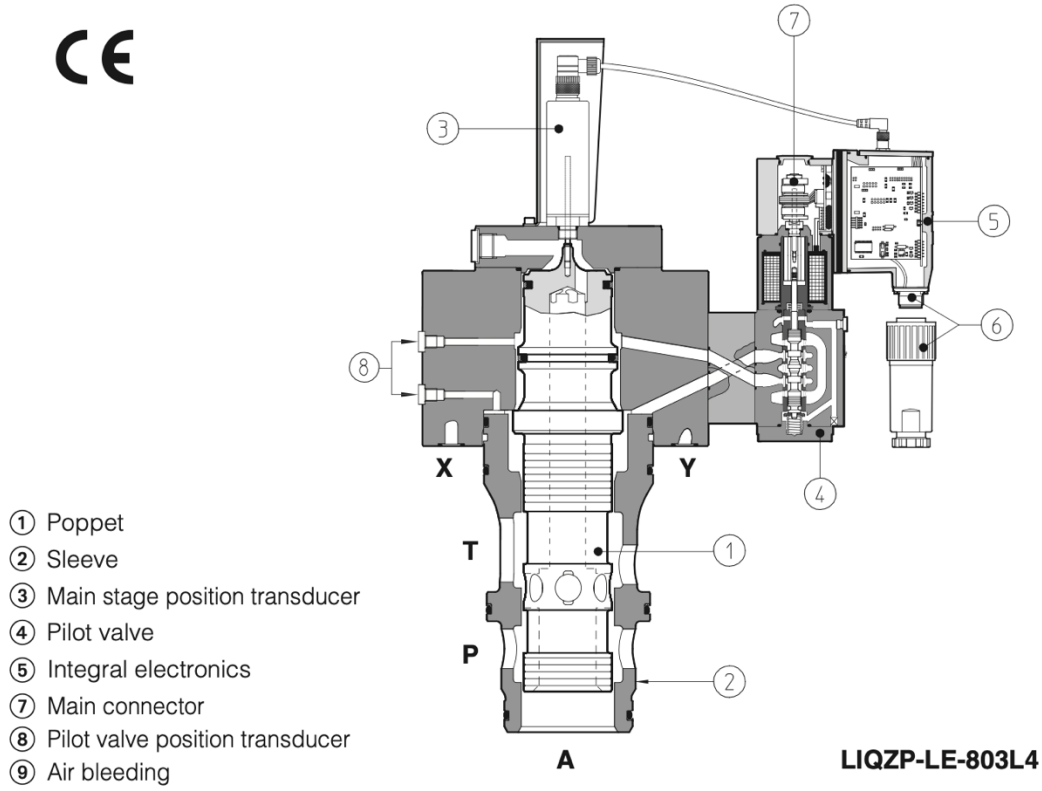

Figure 2.3: Functioning scheme of the solenoid valve from ATOS® datasheet of LIQZP-LE-803L4

The valve present in the external bypass loop can be described as a two-stage normally closed valve. When no input signal is applied the valve stays closed, and the resulting behaviour is the one of a standard passive fluid viscous damper. Conversely, when the electric signal is active the solenoid creates an electromagnetic force that opens the spool. The force that the solenoid exerts must overcome a certain threshold, which is the force of the reset spring placed inside the valve. When the spool is in an open position the damping level is much lower than the passive value. Another very important feature of this kind of valve is its "failsafe" characteristic, which automatically closes the spool in case of a power loss, allowing maximum damping in an emergency situation.

The solenoid valve actually allows also partial openings of the spool, which create a broader range of possible damping coefficients, nevertheless the control of the two-stage damper is easier and often more convenient than the other variants.

Figure 2.4 from the datasheet results particularly useful in terms of understanding the behaviour of the valve with respect to the control signal given. The control signal can be in two different ranges: $-10 \div +10V$, $4 \div 20\,mA$. These ranges allow the movement of the spool in two opposite directions as indicated by the $A \rightarrow T$ and the $P \rightarrow A$ notation, which are highlighted

in figure 2.3. The curve that describes the flow variance with the control signal is bilinear, it has a slope of 5 $\frac{\%\ of\ max\ flow}{Voltage}$ in the central zone and a slope of 11,25 $\frac{\%\ of\ max\ flow}{Voltage}$ for the remaining portion of the graph. The variation is slower for voltages up to an absolute value of $2V$, from that point on the increase of the flow is quicker. Depending on the dimension of the valve, the maximum flow rate can vary from 500 $^{lt}/_{min}$ to 5000 $^{lt}/_{min}$ and the maximum pressure from 350 bar to 420 bar. From the diagram, it can be noticed that one side only of the whole graph can be considered since a change in the sign of the reference signal does not change the percentage of the regulated flow with respect to the maximum value.
Typically, current control has some advantages compared to voltage control, it allows a more precise behaviour due to the fact that the current build-up effect is neglectable.

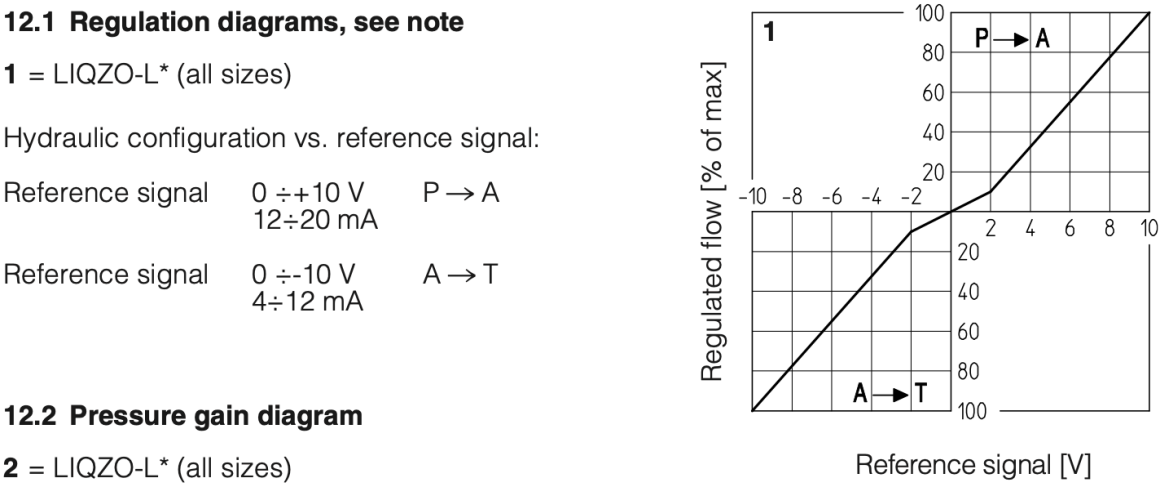

Figure 2.4: Regulation diagram of the solenoid valve from ATOS® datasheet of LIQZP-LE-803L4

Following the arrival of the control signal (either in voltage or current) an oscillator excites the position transducer present inside the valve, which produces an electric signal proportional to the position of the spool, the signal of the desired spool position gets compared with the one of the instantaneous position and the error is reduced to zero. This feedback loop allows precise positioning of the spool at every time instant.

2.3 Dissipation of energy and theoretical considerations

The output force of the damper can be written as:

$$F = C(t)|\dot{u}|^{\alpha} sgn(\dot{u}) \tag{2.3.1}$$

Where $\dot{u}$ is the velocity of the piston head, C is expressed as a function of time because in variable devices the damping coefficient changes depending on the aperture of the orifices. α is a coefficient that is a function of the design of the orifice on the piston head, typical values range from 0.1 to 2. The orifice design is typically referred to as "fluidic control orifice", a low value of α is desired in presence of high-velocity shocks, very common in military applications. It is not rare to find devices with a unitary value of α.

Supposing a sinusoidal cycle of the fluid damper described by equation 1, the trajectory of the piston head can be expressed as:

$$u = u_o \sin(\omega_o t) \tag{2.3.2}$$

The energy dissipated in the previously defined cycle is:

$$W = \int_0^T P\dot{u}dt = \oint Pdu = \pi P_o u_o \sin(\delta) \tag{2.3.3}$$

T is the period $T = \frac{2\pi}{\omega_0}$, ω_0 the frequency and u_0 the amplitude of the sinusoidal cycle. P is the force needed to keep the device in motion.

Integrating equation (2.3.1) and equation (2.3.3) yields the expression of the dissipated work:

$$W_{diss} = \frac{\Gamma^2\left(1+\frac{\alpha}{2}\right)}{\Gamma(2+\alpha)} \cdot 4 \cdot 2^{\alpha} \cdot C \cdot u_o^{1+\alpha} \cdot \omega_o^{\alpha} \tag{2.3.4}$$

With Γ equal to the gamma function $\Gamma(z) = (z-1)!$

It may be useful to express the dissipated energy as a function of the maximum value of the dissipator response $P_{max} = Cu_0^{\alpha}\omega_0^{\alpha}$, this brings to:

$$W_{diss} = \frac{\Gamma^2\left(1+\frac{\alpha}{2}\right)}{\Gamma(2+\alpha)} \cdot 4 \cdot 2^{\alpha} \cdot P_{max} \cdot u_o \tag{2.3.5}$$

This equation is very interesting in terms of understanding the effect of the coefficient α on the behaviour of the damper.

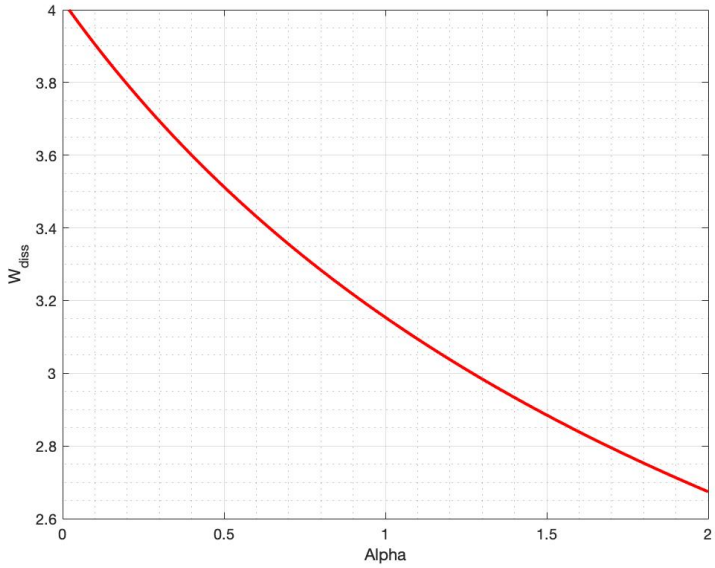

Figure 2.5: Plot of the energy dissipated by the device as a function of the coefficient Alpha

Parametrizing the value of $P_{max}u_0$ and plotting the expression it is possible to notice how, for low values of alfa, the energy dissipated by the damper is higher.

In detail, the case of $\alpha = 0.1$ yields dissipated energy equal to $W_{diss} = 3.88245 \cdot P_{max}u_0$, while for $\alpha = 2$, the value is $W_{diss} = 2.667 \cdot P_{max}u_0$.

A choice of a damper with $\alpha = 0.1$ ensures therefore that the device dissipates 45.57% more energy compared to a device with $\alpha = 2$.

Values of $\alpha = 2$ are very common for dampers with common cylindrical orifices, instead, devices with low values of α require a more complex and technologically advanced design of orifices.

Considering equation (2.3.2), the force needed to maintain the sinusoidal motion can be expressed in the following way:

$$P = P_O \sin(\omega t + \delta) \tag{2.3.6}$$

In which P_O is the amplitude of the force exerted, and δ is the phase angle between the force and the imposed displacement. This relation can be expanded in this form:

$$P = P_O \sin(\omega t)\cos(\delta) + P_O \cos(\omega t)\sin(\delta) \tag{2.3.7}$$

Using the following quantities:

$$K_1 = \frac{P_0}{u_0}\cos(\delta)\,;\; K_2 = \frac{P_0}{u_0}\sin(\delta) \tag{2.3.8}$$

Which represent two different typologies of stiffness, K_1 is called "storage stiffness" which is recoverable energy, instead K_2 is called "loss stiffness", associated with energy that is not stored anywhere, that has just been lost during the motion.

Equation (2.3.7) can be rewritten in the following form:

$$P = K_1 u + \frac{K_2}{\omega}\dot{u} \tag{2.3.9}$$

The force represented in this form has two contributions, the first is in phase with the motion and is due to the stiffness of the damper, the second term is 90° out of phase with the motion and is given by the viscosity of the damper.

From (9) the damping coefficient of the device can be obtained, and it has the following form:

$$C = \frac{K_2}{\omega} \tag{2.3.10}$$

Combining equation (2.3.8) and (2.3.3) the following expression is obtained:

$$K_2 = \frac{W_d}{\pi u_O^2} \tag{2.3.11}$$

The expression just shown becomes very useful because it allows to obtain the specific parameters of the device from the values measured during a test. Therefore, knowing the dissipated energy W_d, the amplitude of both the velocity and the force, u_O and P_O all the other relevant parameters are easily found.

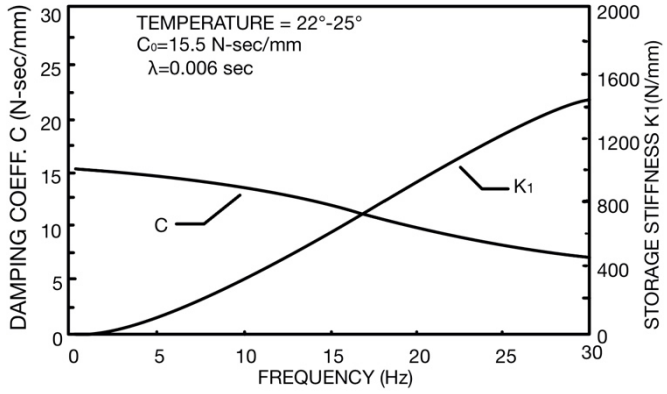

Figure 2.6: Bode plot of the coefficients C and K_1 with frequency, from [87]

Figure 2.6, from [56], shows how the values of the damping coefficient C and the storage stiffness K_1 have an almost constant behaviour below a certain frequency of motion of the device, which can be considered equal to $4 \div 5Hz$. The damping coefficient tends to get smaller for higher frequency inputs, while the storage stiffness quickly increases moving towards the right of the bode diagram.

The graph below shows a typical displacement-force plot of the device under a complete sinusoidal motion with the damping switching from low to high values. These graphs consider motion below the cut-off frequency pointed out before because at higher frequencies the behaviour does not result linear anymore.

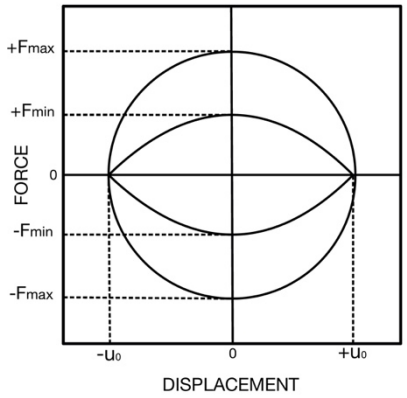

Figure 2.7: Theoretical plot of displacement of the device as a function of the force

Often the tests on the device are multi-stage, which means that the damping coefficient gradually increases during the sinusoidal motion, giving rise to a more cyclical behaviour as shown below.

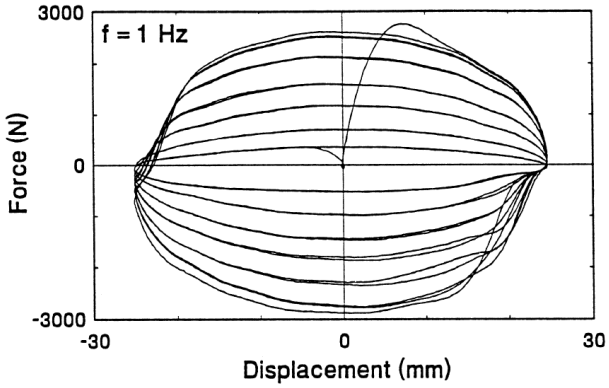

Figure 2.8: Experimental plot of displacement of the device versus the force, with a variation of the damping coefficient, from technical report NCEER-95-0011

2.4 System response time

A fundamental parameter of the semi-active fluid damper is the response time, which is the time needed for a complete variation of the damping coefficient, from minimum to maximum or vice versa. This parameter is clearly important because it causes a certain delay from the ideal behaviour of the device in which the variation happens instantly.

The response time is evaluated during the saturation condition of the command signal, and it can be separated into two different contributions, the first is a static response time, t_1 and is relative to the delay given by the electronic response of the integrated ECU together with the presence of static friction, the second one, t_2 counts the time needed from the initial motion of the spool to the final position of the control valve, so the actual time in which the damping coefficient varies.

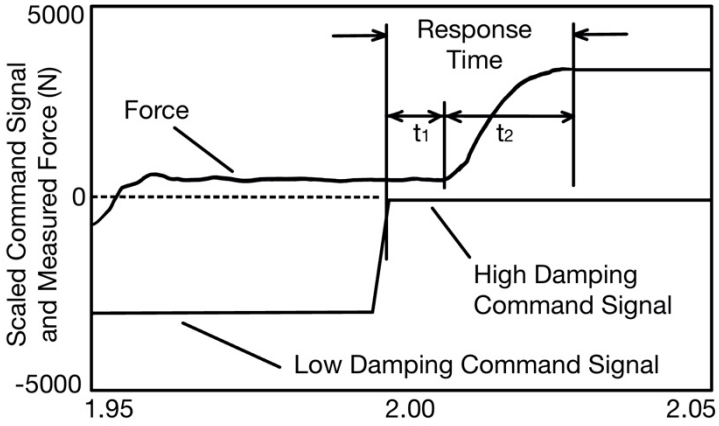

Figure 2.9: Variation of the command signal in saturation conditions, from technical report NCEER-95-0011

Depending on the structure of the valve in the application, the response time may or may not be identical for the opening procedure and the closing one, both for reasons related to the flow of oil inside the cylinder and for the presence of the reset spring.

In general, this kind of delay is quite reduced and allows proper control of the device during the whole period. The specific value depends on the particular dimension of the valve and the damper used in the application, but in general the sum of t_1 and t_2 is safely in the range $20 \div 35\ ms$.

2.5 Analytical models

The fundamental equation of the device, representative of the force being exerted is (1):

$$F = C(t)|\dot{u}|^{\alpha} sgn(\dot{u}) \tag{2.5.1}$$

In which $C(t)$, which is the damping coefficient of the device, can vary inside a certain range:

$$C_{min} \leq C(t) \leq C_{max} \tag{2.5.2}$$

Where C_{min} is the damping coefficient corresponding to the valve fully open, while C_{max} is the damping coefficient related to a passive behaviour with the control valve completely closed. This model, which is called the "Viscous Dashpot Model" represents very well the behaviour of the device for inputs with frequencies lower than the cut-off frequency, so around 4 Hz, nevertheless it is representative of a broader range of frequencies when the damper is built with a balanced piston rod structure instead of a rod make-up accumulator.

An alternative model to evaluate the viscoelastic effects inside the device is referred to as the "Viscoelastic Maxwell model", and it is dependent on the force as well as its derivative and the velocity of the piston rod:

$$F(t) + \lambda \dot{F}(t) = C(t)\dot{u}(t) \tag{2.5.3}$$

In which the constant λ represents the "relaxation time" and $C(t)$ is the damping coefficient value at a generic instant of time. The model has to be calibrated with the values of the damping coefficient with respect to the frequency of the input.

A different kind of approach that can be exploited to build an analytical model of the device is the fluid dynamics one. The mass flow rate equilibrium is equal to:

$$\frac{d}{dt}(m) = \frac{d}{dt}(\rho V) = \rho_i Q_i - \rho_o Q_o \tag{2.5.4}$$

In which t is time, m is the mass of fluid inside the volume V, ρ is the fluid mass density and Q is the flow rate, and in the equilibrium equation, the subscript i and o refer to input and output respectively. The previous equation can be expanded as:

$$\frac{d}{dt}(\rho V) = \rho \frac{dV}{dt} + \frac{d\rho}{dt} V = \rho \frac{dV}{dt} + V \frac{d\rho}{dP} \frac{dP}{dt} \tag{2.5.5}$$

In which P represents the pressure within the fluid volume. It is now useful to analyse the definition of the bulk modulus of a fluid β:

$$dP = -\beta \frac{dV}{V} \tag{2.5.6}$$

β is a function of the pressure and the temperature of the fluid under study. Now considering an infinitesimal amount of mass:

$$dm = d(\rho V) = \rho dV + V d\rho \tag{2.5.7}$$

The following is obtained:

$$\frac{dV}{V} = -\frac{d\rho}{\rho} \tag{2.5.8}$$

And putting together equations (2.5.5), (2.5.6) and (2.5.8) the following relation is obtained:

$$\frac{d}{dt}(\rho V) = \rho\left(\frac{dV}{dt} + \frac{V}{\beta}\frac{dP}{dt}\right) \tag{2.5.9}$$

And in this relation $\rho\frac{dV}{dt}$ is related to the boundary deformations and $\rho\frac{V}{\beta}\frac{dP}{dt}$ describes instead the compressibility of the fluid. Combining (2.5.9) with (2.5.4) and assuming a constant fluid density yields the following:

$$\frac{dV}{dt} + \frac{V}{\beta}\frac{dP}{dt} = Q_i - Q_o \tag{2.5.10}$$

In a closed chamber condition Q_i is equal to zero and Q_o is equal to:

$$Q_o = k_{pr}A_{pr}v_{pr} + k_{au}A_{au}v_{au} \tag{2.5.11}$$

In which A is the orifice area, v is the velocity of the fluid through the orifice, the subscript pr refers to the primary orifice, while the subscript au refers to the auxiliary orifice present on the outside loop and regulated by the control valve.
Using the conservation of energy is possible to relate the velocity of the fluid through the orifice with the pressure drop ΔP across the orifice:

$$v = \left(\frac{2\Delta P}{\rho}\right)^{\frac{1}{2}} \tag{2.5.12}$$

This representation works well for the orifice present in the external loop, containing the control valve, but not for the one present in the piston head of the damper, due to the peculiar shape of the orifices in the piston head which guarantee a linear relationship between the output force and the relative velocity of the piston within the fluid, which is the following:

$$v_p = \delta\left(\frac{2\Delta P}{\rho}\right)^{1} \tag{2.5.13}$$

Where the exponent of unity is present to emphasize the linearity of the relation, and δ is necessary to maintain dimensional equivalence.

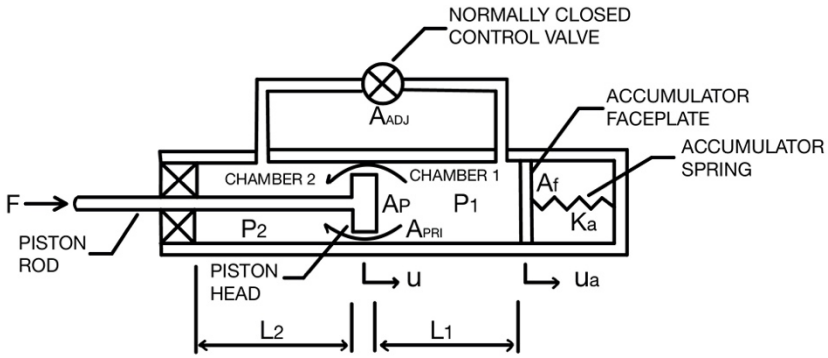

Figure 2.10: Functioning scheme of the semi-active fluid viscous damper, inspired by technical report NCEER-95-0011

Referring to the scheme in figure 2.9, it is possible to write the mass conservation equations for chamber 1 and chamber 2, which are respectively:

$$\frac{dV_1}{dt} + \frac{V_1}{\beta_1}\frac{dP_1}{dt} = -k_{pr}A_{pr}\delta\left[\frac{2(P_1 - P_2)}{\rho}\right]^1 + -k_{au}A_{au}\left[\frac{2|P_1 - P_2|}{\rho}\right]^{\frac{1}{2}}\text{sgn}(P_1 - P_2) \tag{2.5.14}$$

$$\frac{dV_2}{dt} + \frac{V_2}{\beta_2}\frac{dP_2}{dt} = k_{pr}A_{pr}\delta\left[\frac{2(P_1 - P_2)}{\rho}\right]^1 + +k_{au}A_{au}\left[\frac{2|P_1 - P_2|}{\rho}\right]^{\frac{1}{2}}\text{sgn}(P_1 - P_2) \tag{2.5.15}$$

In these equations, it has been assumed that the fluid cannot enter the accumulator chamber when in the actual dynamics of the damper it does through a small orifice. To account for the accumulator effect the spring stiffness and face plate area of the scheme can be adjusted properly. Equating the fluid pressure force to the spring stiffness force it is obtained the following:

$$K_a u_a = P_1 A_f \tag{2.5.16}$$

In which K_a is the accumulator spring stiffness, u_a is the accumulator faceplate relative displacement, and A_f the faceplate area. The total volume of the first chamber can be found as:

$$V_1 = (L_1 - u + u_a)A_p \tag{2.5.17}$$

Where L_1 is the length of the chamber, u is the relative displacement of the piston head and A_p is the piston head area. The volume of chamber two instead can be written as:

$$V_2 = (L_2 + u)\big(A_p - A_r\big) \tag{2.5.18}$$

Where L_2 is the length of the chamber, and A_r is the piston rod area. The values of L_1 and L_2 are changed to account for the quantity of fluid present in the bypass loop. The last four equations are put together to obtain the following two first-order nonlinear differential equations:

$$\frac{dP_1}{dt} = \frac{\left\{A_{pr}\dot{u} - k_{pr}A_{pr}\delta\left[\frac{2(P_1 - P_2)}{\rho}\right]^1 - k_{au}A_{au}\left[\frac{2|P_1 - P_2|}{\rho}\right]^{\frac{1}{2}}\operatorname{sgn}(P_1 - P_2)\right\}}{\left[\left(L_1 - u + \frac{P_1A_f}{K_a}\right)\frac{A_p}{\beta_1} + \frac{A_fA_p}{K_a}\right]} \tag{2.5.19}$$

$$\begin{aligned}\frac{dP_1}{dt} = &\left\{\big(A_r - A_p\big)\dot{u} + k_{pr}A_{pr}\delta\left[\frac{2(P_1 - P_2)}{\rho}\right]^1 + \right.\\ &\left. + k_{au}A_{au}\left[\frac{2|P_1 - P_2|}{\rho}\right]^{\frac{1}{2}}\operatorname{sgn}(P_1 - P_2)\right\}\left\{\frac{\beta_2}{\big(A_p - A_r\big)(L_2 + u)}\right\}\end{aligned} \tag{2.5.20}$$

There exist a relation useful to compute the bulk modulus of the silicone fluid:

$$\beta_i = 864 + 4.166P_i \tag{2.5.21}$$

Where P_i represents the pressure in chamber i. The equation relating the force output with the pressure differential across the chambers is the following:

$$F = P_1A_p - P_2\big(A_p - A_r\big) + F_f\operatorname{sgn}(\dot{u}) \tag{2.5.22}$$

In which F_f represents the force threshold to overcome the friction between the piston rod and the oil seals. The force can be computed after solving the differential equations that require the knowledge of displacement u, the velocity $\dot{u}$, and the adjustable area of the orifice A_{adj}. This fluid mechanics model does not account for the dynamics of the control valve in the external bypass loop. The fluid mechanics model can be used to make predictions on force-displacement

loops with some small approximations, in fact, it results possible to relate the aforementioned area with the displacement of the spool:

$$A_{adj}(t) = \pi d s(t) \tag{2.5.23}$$

Where d is the diameter of the spool and $s(t)$ is the spool displacement.
The relation between the damping coefficient and the control voltage is given by the following equation:

$$C = C_{min} + (C_{max} - C_{min}) \exp -\mu V^{\varphi} \tag{2.5.24}$$

In which C_{max} is the damping coefficient with a fully closed valve, C_{min} is the damping coefficient with a fully open valve and the parameters μ and φ are evaluated through curve fitting. The adjustable area as a function of the command voltage ε can be expressed in the following way:

$$A_{adj}(\varepsilon) = A_{max}\left[1 - \exp -\gamma \varepsilon^{\zeta}\right] \tag{2.5.25}$$

Again, γ and ζ must be determined empirically.

Chapter 3

Control theory and algorithms

3.1 General notions of Control theory

This chapter contains many mathematical results which are pertinent for the application, it presents the fundamentals of Proportional Integrative Derivative and Model Predictive Control algorithms. The detailed source of the results is present in the bibliography, but it is important to highlight that for the PID results the book "PID Control" by Michael A. Johnson and Mohammad H. Moradi has been an essential source, and for what concerns the MPC part the book "Predictive Control" by F. Borrelli, A. Bemporad and M. Morari and the many research papers by A. Bemporad on the topic have been fundamental to synthesize the theory behind the algorithms. In the appendix A, some basic results of control theory are presented, therefore it can be considered as an introductive part to chapter 3.

Structural vibration control nowadays is a field of interdisciplinary research. Structures must be designed to withstand a specific range of disturbances, which depend mainly on geographical factors, for which the design objective concerning the physical system focuses on keeping all the stresses and strain below a certain bound. This can be obtained using different techniques, very commonly with energy considerations, the bounds imposed on the system itself represent a trade-off between human comfort and safety, where the first one concerns accelerations, while the second one typically covers displacements and velocities.

The Physical Design Problem can be tackled either with or without a mathematical modelling phase. The modelling phase starts by noting that any model of the system, depending on the complexity, always represents an idealization of the actual physical dynamics. This simplification of the system, in order to be well-posed, relies on the guarantee that all the defined parameters remain within a specified bound in presence of disturbances. It is then necessary to select the design parameters (sensor type and location, actuator specifications, various transfer functions) to choose the type of bound on the output responses.

The simplification of the system dynamics aims for a set of equations that can easily be solved and also grasp the highlights of the overall behaviour, which is clearly not always possible.

The model of the system can be built from two starting points: input-output data or first principles, both yielding a set of partial or ordinary differential equations.

Modelling the system allows to make predictions on the behaviour, that would otherwise be obtained only after an infinite number of numerical computer simulations.
In control design theory, there is not a "best choice" for the controller, in fact, typically different alternatives are evaluated based on the specific application and computation requirements.
The second alternative consists instead directly in selecting some control parameters, which can be variables of the system on which some requirement is present or, alternatively, factors that can be modified directly in the loop. A strategy to control the parameters is then chosen (such as PID, CNN, FL) and through a trial-and-error procedure, a solution to the problem is then found. This approach does not give an exhaustive answer to the initial problem because in general it lacks a mathematical certainty and does not give any insurance on the effects of all the infinite untested inputs and disturbances.
An active or semiactive control system, in the civil engineering field, is composed of:

1. Sensors to measure the external inputs and the structural parameters required for the control
2. Processing devices, improving the quality of the signal coming from the sensors and performing the computation as instructed by the control algorithm
3. A certain number of actuators provide the necessary inputs, which are powered by an energy source having an entity that depends on the mechanical characteristics of the devices

In control system theory, when only the external excitation is measured, the strategy is referred to as open-loop control (or feedforward control). A closed-loop control (also referred to as feedback control) strategy requires instead the continuous measurement of the structural parameters to make real-time adjustments to the system through the actuators. The configuration which utilizes both the measurement of structural parameters and the external excitation is called feedback-feedforward control (or less often closed-open-loop control).

3.2 PID controllers

Proportional-Integrative-Derivative controllers are very common in many fields, because of their simplicity and low cost. The basic idea of a PID controller is to have a standard architecture for a system and to modify it simply by regulating the gain parameters of the proportional, derivative, and integrative blocks.

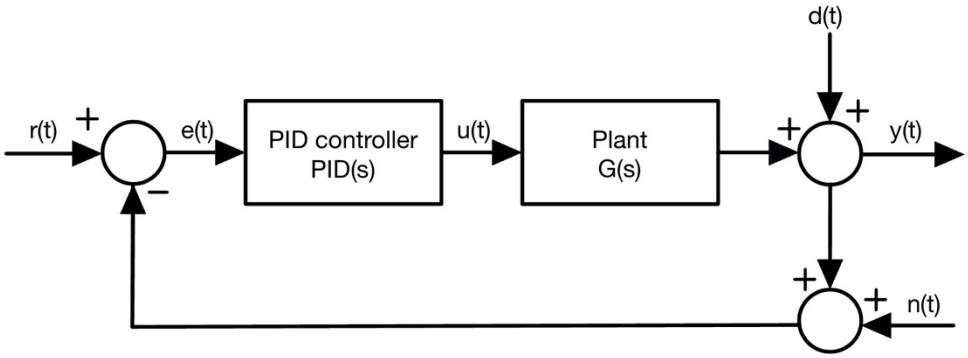

Figure 3.1: Architecture of a feedback system with PID controller

Three different representations of the PID controller can be given, the symbolic representation, the time domain representation, and the Laplace domain representation.

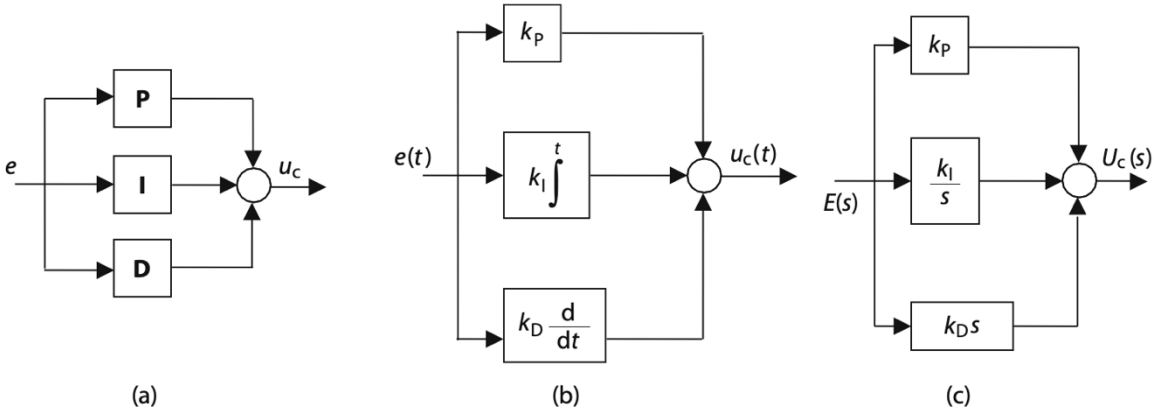

Figure 3.2: PID controller represented in three different domains (a) symbolic representation, (b) time domain representation, (c) Laplace domain representation. From [26].

In a PID controller, the output is computed as the sum of three contributions. The first contribution is proportional to the error signal between the reference and the actual value of the variable to be controlled. The second contribution is proportional to the integral of the error, so it is a function of the average value of the error itself. The third and final contribution is proportional to the derivative of the error, therefore it is a function of the variation velocity of the error value.

The control law of the PID controller can be written as

$$u(t) = K_P e(t) + K_I \int_0^t e(\tau)d\tau + K_D \frac{de(t)}{dt} \tag{3.2.1}$$

Where K_P is called *proportional gain*, K_I is called *integral gain*, and K_D is called *derivative gain*. There is, however, another way to write the control law, which is more common

$$u(t) = K_P \left(e(t) + \frac{1}{T_I} \int_0^t e(\tau)d\tau + T_D \frac{de(t)}{dt} \right) \tag{3.2.2}$$

With $T_I = K_P/K_I$, and $T_D = K_D/K_P$. In literature, it is also very common to use a quantity called *proportional bandwidth* B_P instead of the proportional gain K_P, where B_P represents the amount of error comparing it with the maximum value in percentage. $K_P = 100/B_P$.
Considering the Laplace transform of (3.6.2) the following relation is obtained

$$U(s) = K_P \left(1 + \frac{1}{T_I s} + T_D s\right) E(s) = K_P \left(\frac{T_D T_I s^2 + T_I s + 1}{T_I s} \right) E(s) \tag{3.2.3}$$

Which represents a dynamic LTI improper system, not physically realizable. Therefore, to solve the problem it is necessary to filter the derivative action, obtaining the real control law

$$U(s) = K_P \left(1 + \frac{1}{T_I s} + \frac{T_D s}{1 + s\frac{T_D s}{N}} \right) E(s) \tag{3.2.4}$$

The transfer function of the controller can now be written as:

$$\frac{U(s)}{E(s)} = K_P + \frac{K_P}{T_I s} + \frac{K_P T_D s}{1 + s\frac{T_D s}{N}} = P(s) + I(s) + D(s) \tag{3.2.5}$$

Which can be represented schematically as the sum of three contributions

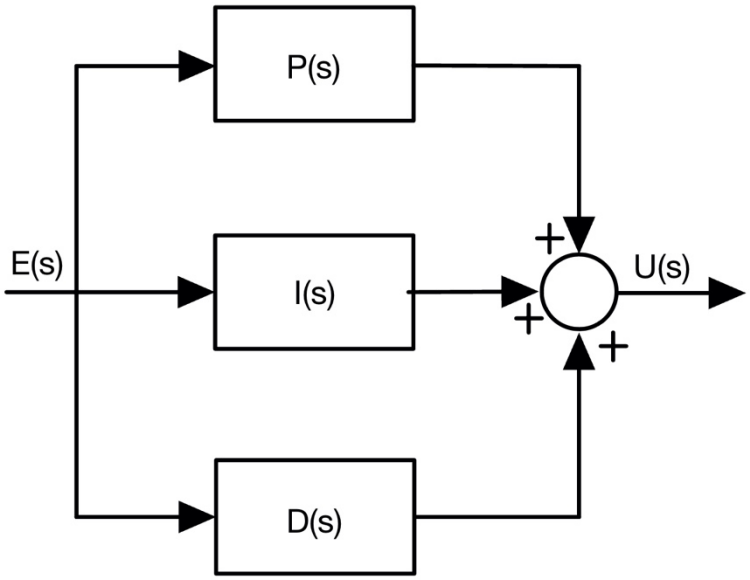

Figure 3.3: PID controller structure as a sum of Proportional, Integral and Derivative contributions

To have better insight into the effect of each component it is necessary to analyze them separately.

Proportional action can be expressed with the following relation

$$U_P(s) = K_P E(s) \tag{3.2.6}$$

Using only the proportional action, a difference between the requested value and the obtained value is produced. The difference can be reduced by increasing the gain K_P, but this can cause a highly rippled behaviour following transients. A purely proportional control is typically used only in asymptotically stable processes.

The integral action has the objective of bringing the controlled variable to the set-point value

$$U_I(s) = \frac{K_P}{T_I(s)} E(s) \tag{3.2.7}$$

It can be seen as a mechanism to put to zero the error caused by the proportional action. PI controllers (Proportional-Integrative) allow better precision without compromising the stability of the system, they also guarantee a shorter response time for the system.

The objective of the derivative action is to improve the stability of the control loop.

$$U_D(s) = \frac{K_P T_D}{1 + \frac{T_D}{N} s} E(s) \tag{3.2.8}$$

The derivative action outputs the derivative over time of the error, that is the reason why these kinds of controllers are called velocity controllers. Often this kind of action is not necessary for a controller, also because it has the drawback of amplifying the noise at high frequencies, which can destabilize the system compromising the quality of the control.
The instability can be explained considering that the dynamicity of the system causes a certain delay between the time in which the input changes to the time in which this change actually causes a sensible variation of the controlled variable. Nevertheless, from the knowledge of the rate of change is possible to predict the time course of the controlled variable through the derivative of the error curve.

3.3 Bandwidth-Limited derivative control

Real-world processes contain noise, which is typically represented by a high-frequency signal. In the bode plot of the PID controller, the behaviour of each of the three components is highlighted and allows to make some design considerations.
The control signal in the Laplace domain can be written in the following form:

$$U_c(s) = U_c^{nf}(s) - U_{noise}(s) \tag{3.3.1}$$

Where $U_c^{nf}(s)$ stands for the noise-free control signal and $U_{noise}(s) = [G_c(s)]N(s)$, with $N(s)$ equal to the Laplace transform of the noise signal.
Since the controller transfer function can be expressed as the sum of three terms (Proportional, Integrative and Derivative), then also the control signal given by the noise can be split into three contributions:

$$U_{noise}(s) = U_{noise}^P(s) + U_{noise}^I(s) + U_{noise}^D(s) \tag{3.3.2}$$

With

$$U_{noise}^P(s) = [G_P(s)]N(s),\ U_{noise}^I(s) = [G_I(s)]N(s),\ U_{noise}^D(s) = [G_D(s)]N(s) \tag{3.3.3}$$

And also

$$G_P(s) = k_P, \qquad G_I(s) = \frac{k_P}{\tau_i s}, \qquad G_D(s) = k_P \tau_D s \tag{3.3.4}$$

In figure 3.4, $k_P = 5$, $\tau_i = 5$ and $\tau_d = 5$

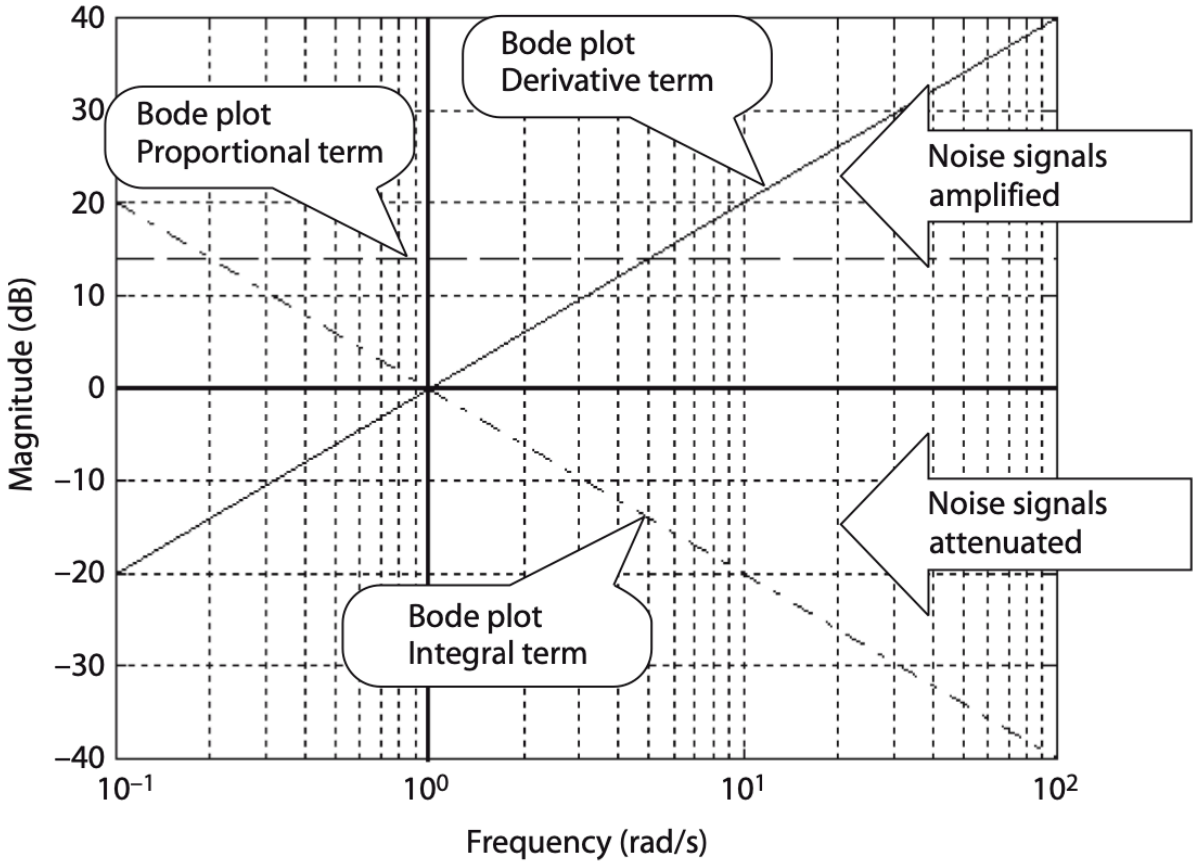

Figure 3.4: Bode plot of Proportional, Derivative, and Integral terms of the PID controller. From [26].

This plot shows that the Proportional term has a constant magnitude equal to 13.98 dB for the whole frequency range, the Integral term possesses a 20 dB/dec attenuation of the noise signals, while the Derivative term has the opposite behaviour with a 20 dB/dec amplification of the noise signals.

The solution for this phenomenon is given by a filtering action on the Derivative term, the filtering transfer function has the following form

$$G_f(s) = \left[\frac{1}{\tau_f s + 1}\right] \tag{3.3.5}$$

This yields a derivative term shown below

$$U^D_{noise}(s) = \left[k_P\left(\frac{\tau_d s}{\tau_f s + 1}\right)\right] N(s) \tag{3.3.6}$$

In which the modified derivative transfer function is expressed as:

$$G_{mD}(s) = \left[k_P\left(\frac{\tau_d s}{\tau_f s + 1}\right)\right] \tag{3.3.7}$$

And this modification in the transfer function of the Derivative term changes the high-frequency gain and its frequency response:

$$k_D^{\infty} = \lim_{\omega\to\infty} |G_{mD}(j\omega)| = k_P \frac{\tau_d}{\tau_f} \tag{3.3.8}$$

By setting $\tau_f = \frac{\tau_d}{n}$ the modified derivative term takes the following form:

$$G_{mD}(s) = \left[k_P\left(\frac{\tau_d s}{(\tau_d/n)s + 1}\right)\right] \tag{3.3.9}$$

Yielding the high-frequency gain:

$$k_D^{\infty} = k_P n \tag{3.3.10}$$

Typically, n is chosen to be inside the range $5 \leq n \leq 20$. Choosing $k_P = 5$, $\tau_d = 0.2$ and $n = 5$, k_D^{∞} results to be 27.95 dB, and this is shown in the bode plot below:

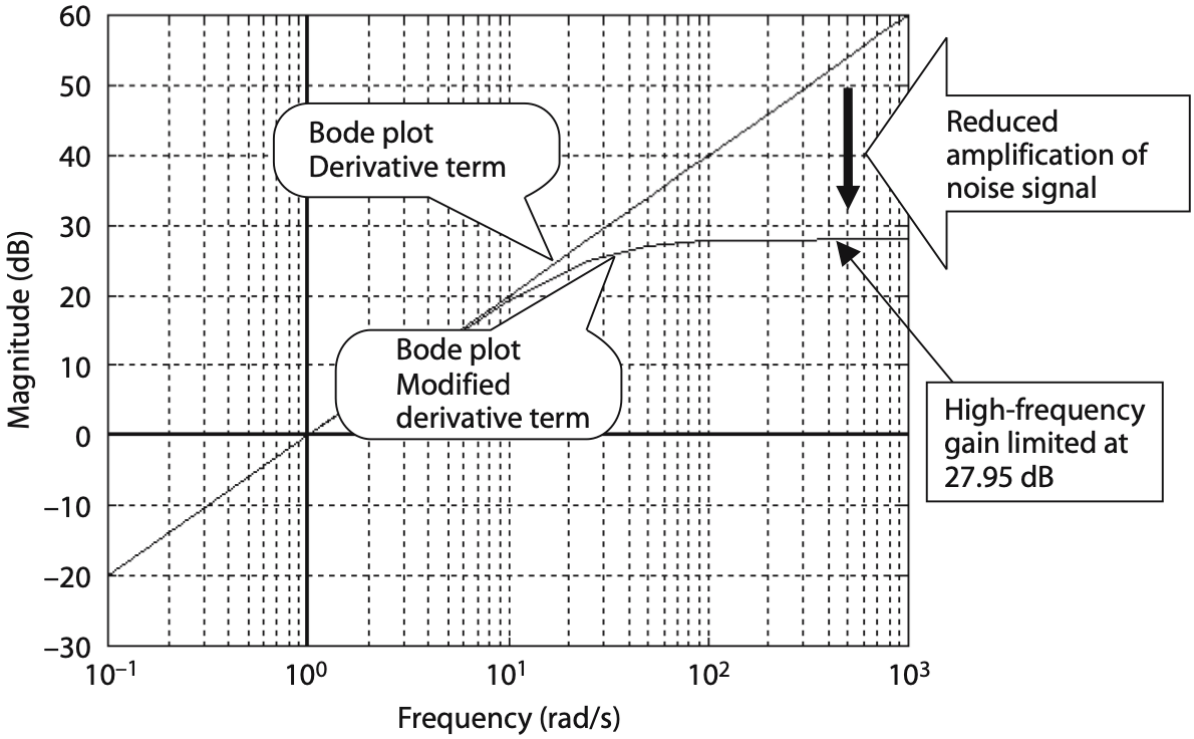

Figure 3.5: Modified Bode plot with limitation of the derivative term. From [26].

3.4 Tuning of a PID controller

The main advantage of the Proportional-Integrative-Derivative controller structure is that they do not need a detailed model of the system. This phenomenon is evident in the tuning process, which can be carried out through a series of experimental tests on the system, or in the simulation environment. The direct results of these tests are the gains of the controller to be implemented.

$$PID(s) = \frac{U(s)}{E(s)} = K_P + \frac{K_P}{T_I s} + \frac{K_P T_D s}{1 + s\frac{T_D s}{N}} = P(s) + I(s) + D(s) \tag{3.4.1}$$

3.5 Open loop tuning of PID controllers

In this method the controller is not connected to the system, the plant of the system is excited through a step function, and the response amplitude and time are measured. The static gain of the process is computed from the obtained data.

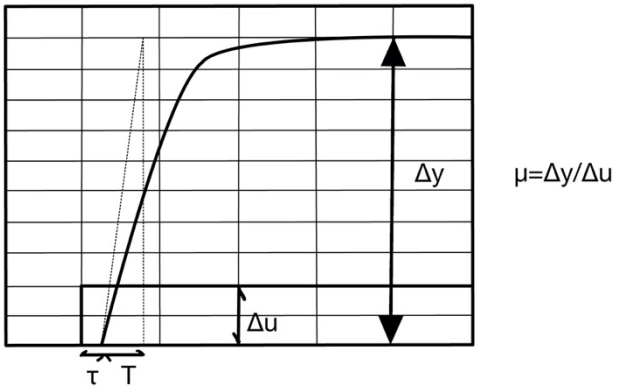

Figure 3.6: Time domain plot showing the variation of output consequently to a ramp input

Table 3.1: Values for open loop tuning of PID controllers

	K_I	T_I	T_D
P	$\frac{T}{\mu\tau}$		
PI	$\frac{0.9T}{\mu\tau}$	3τ	
PID	$\frac{1.2T}{\mu\tau}$	2τ	5τ

3.6 Cohen-Coon tuning of PID controllers

This kind of tuning of the Proportional-Integrative-Derivative controller exploits the same data extrapolated from the step-function stimulus to the plant of the system but with different relations.

Table 3.2: Values for Cohen-Coon tuning of PID controllers

	K_I	T_I	T_D
P	$\frac{3T+\tau}{3\mu\tau}$		
PI	$\frac{10{,}8T+\tau}{12\mu\tau}$	$\tau\frac{30T+30\tau}{9T+20\tau}$	
PID	$\frac{16T+3\tau}{12\mu\tau}$	$\tau\frac{32T+6\tau}{13T+8\tau}$	$\frac{4T\tau}{11T+2\tau}$

3.7 Closed loop tuning of PID controllers (Zieger-Nichols method)

The Zieger-Nichols method starts the tuning process by inserting a purely proportional controller with a low K_P coefficient. The gain is progressively increased to the point in which a regular oscillation is present in the behaviour. K_U is defined as the value of the gain K_P for which the response of the system is represented by a sinusoidal behaviour with constant amplitude, and at that point the period of the oscillation T_U is measured.
The table below shows the formulas for each gain.

Table 3.3: Values for closed loop tuning of PID controllers

	K_I	T_I	T_D
P	$0{,}5Ku$		
PI	$0{,}45Ku$	$\frac{Tu}{1{,}2}$	
PID	$0{,}6Ku$	$\frac{Tu}{2}$	$\frac{Tu}{8}$

3.8 Limitation of the derivative action

Considering once again the derivative action:

$$U_D(s) = \frac{K_P T_D}{1 + \frac{T_D}{N} s} E(s) \tag{3.2.8}$$

It may occur that in presence of a step input, the output takes an impulsive form. This effect is clearly undesired, and it may cause a saturation of the actuator, as well as damages to it. To avoid this problem the derivative action is present only on the controlled variable, and not on the error:

$$U_D(s) = \frac{K_P T_D}{1 + \frac{T_D}{N} s} Y(s) \tag{3.8.1}$$

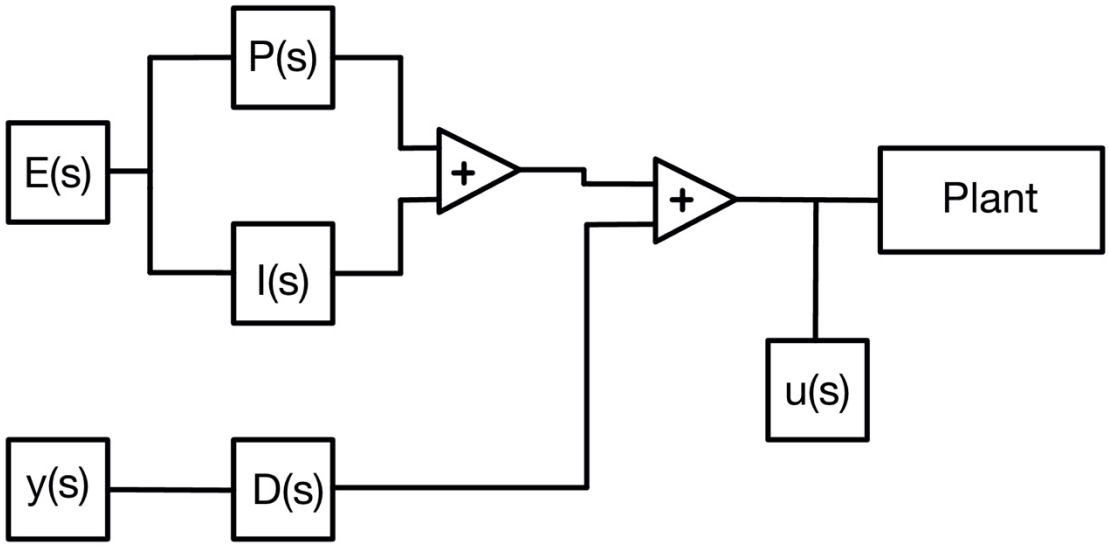

Figure 3.7: Structure of the PID controller and connection of the error and output signals

3.9 Desaturation of the integrative action (anti-wind-up)

At a steady state, the control variable $u(t)$ should be far from the saturation value, during the transient nevertheless it may happen that $u(t)$ overcomes the saturation levels. When $u(t)$ is saturated, the integral action keeps on integrating the error, causing a phenomenon known as "wind-up".

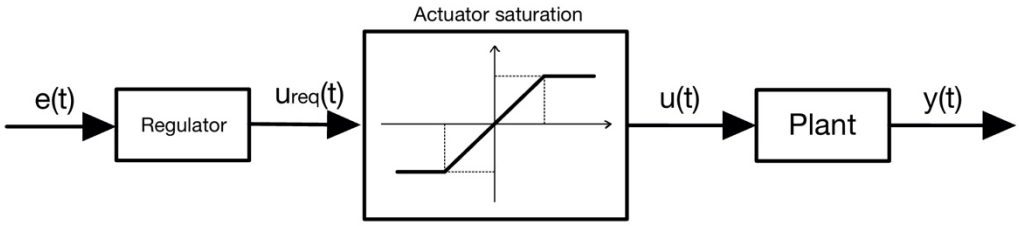

Figure 3.8: Saturation constraints on the actuator

To avoid this problem a desaturation system is introduced in the integrator: if the requested value overcomes the saturation value of the actuator, the value of the integral action is put to zero.

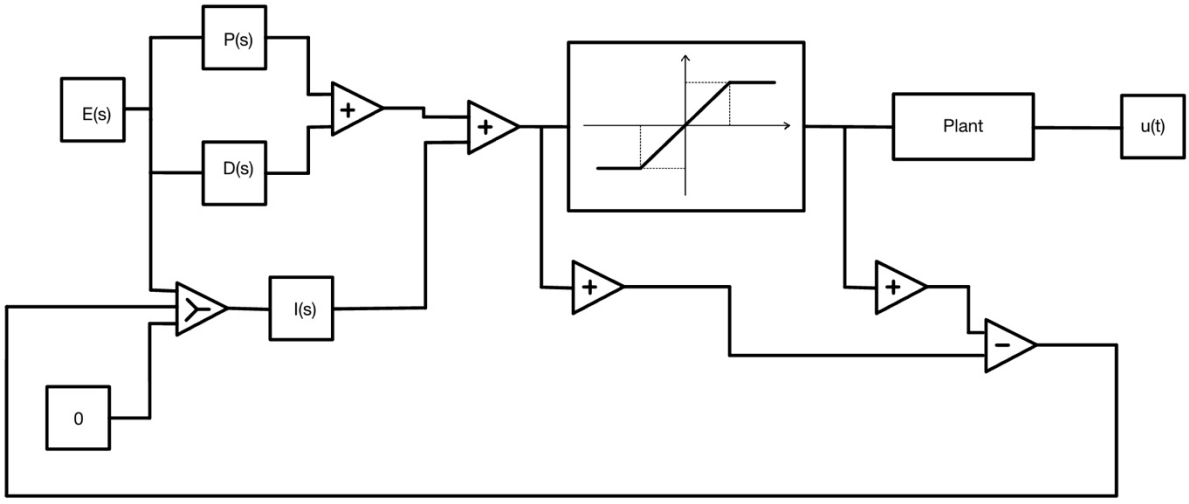

Figure 3.9: Saturation constraints on the actuator implemented inside the system

3.10 Model Predictive Control (MPC)

Model Predictive Control is a type of control algorithm that exploits a dynamic model to anticipate the system behaviour and compute the best control input for the successive time instant. Modelling is a fundamental phase of the MPC algorithm, together with the record of measurement, which is needed to determine the initial state of the system. The two previous steps are complementary, and their overall quality is an index of good state estimation. State estimation, therefore, consists in putting together past measurements with the system model to predict the most likely value of the state at the current time instant. This dissertation will limit

itself to the linear Model Predictive Control algorithm, which is by far the most common in both industrial and scientific contexts.

To properly discuss the MPC control algorithm it is necessary to introduce some basic constrained optimization results.

A set $S \subseteq \mathbb{R}^n$ is convex if, for all $x_1, x_2 \in S$

$$\lambda x_1 + (1-\lambda)x_2 \in S, \qquad \forall \lambda \in [0,1] \tag{3.10.1}$$

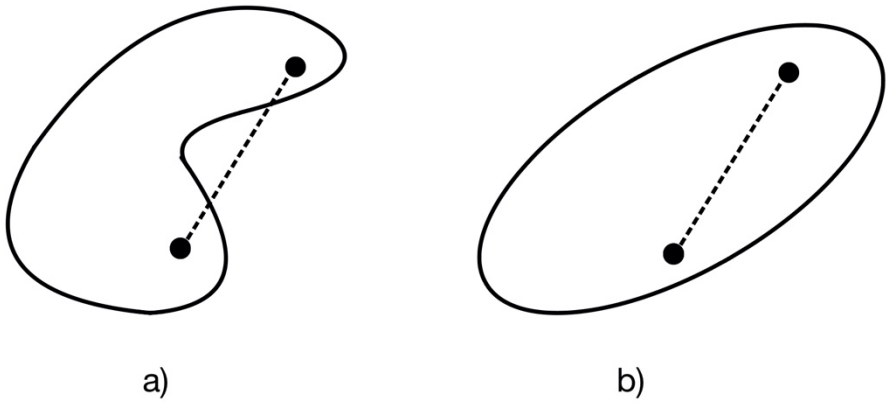

Figure 3.10: (a) 2D representation of a non-convex set, (b) 2D representation of a convex set

A function $f: S \to \mathbb{R}$ is a convex function if S is convex and

$$\begin{gathered} f(\lambda x_1 + (1-\lambda)x_2) \leq \lambda f(x_1) + (1-\lambda) f(x_2) \\ \forall\, x_1, x_2 \in S, \qquad \lambda \in [0,1] \end{gathered} \tag{3.10.2}$$

An optimization problem

$$\begin{gathered} \min f(x) \\ s.t.\ x \in S \end{gathered} \tag{3.10.3}$$

is called a convex optimization problem if S is a convex set and $f(x)$ is a convex function.

S is typically defined by linear equality constraints $Ax = b$ and convex inequality constraints $g(x) \leq 0,\ g: \mathbb{R}^n \to \mathbb{R}^m$.

A convex polyhedron is an intersection of a finite set of half-spaces of $\mathbb{R}^n$.

A convex polytope is a bounded convex polyhedron.

These objects can be represented in Hyperplane representation

$$P = \{x \in \mathbb{R}^n : Ax \leq b\} \tag{3.10.4}$$

Or in Vertex representation

$$\begin{gathered} P = \left\{ x \in \mathbb{R}^n : x = \sum_{i=1}^{q} \alpha_i v_i + \sum_{j=1}^{p} \beta_j r_j \right\} \\ \alpha_i, \beta_j \geq 0; \sum_{i=1}^{q} \alpha_i = 1; \;\; v_i, r_j \in \mathbb{R}^n \end{gathered} \tag{3.10.5}$$

Linear programming (LP) problems are defined as

$$\begin{gathered} \min c'x \\ s.t. \;\; Ax \leq b, x \in \mathbb{R}^n \\ Ex = f \end{gathered} \tag{3.10.6}$$

The LP problem in standard form is posed in this form

$$\begin{gathered} \min c'x \\ s.t. \;\; Ax \leq b, x \in \mathbb{R}^n \\ x \geq 0, x \in \mathbb{R}^n \end{gathered} \tag{3.10.7}$$

The conversion from the initial form to the standard form exploits slack variables and splits the positive values of x from the negative ones.

A trick often used to convert a maximization problem into a minimization one is the following

$$\max_x f(x) = -\min_x \{-f(x)\} \tag{3.10.8}$$

A Quadratic Programming (QP) optimization problem has the form:

$$\begin{gathered} \min \frac{1}{2} x'Qx + c'x \\ s.t. Ax \leq b, x \in \mathbb{R}^n \\ Ex = f \end{gathered} \tag{3.10.9}$$

A QP is convex if the Q matrix is positive semidefinite $Q \succcurlyeq 0$. Assuming that $Q = Q'$ does not cause a loss of generality.

$$\frac{1}{2} x'Qx = \frac{1}{2} x' \left(\frac{Q + Q'}{2} + \frac{Q - Q'}{2} \right) x = \frac{1}{2} x' \left(\frac{Q + Q'}{2} \right) x \tag{3.10.10}$$

Mixed-integer programming (MIP) can be split in the mixed-integer linear program (MILP)

$$\begin{gathered} \min c'x \\ Ax \leq b, x = \begin{bmatrix} x_c \\ x_b \end{bmatrix} \\ x_c \in \mathbb{R}^{n_c}, x_b \in \{0,1\}^{n_b} \end{gathered} \tag{3.10.11}$$

And mixed integer quadratic program (MIQP)

$$\begin{gathered} \min \frac{1}{2} x'Qx + c'x \\ s.t.\ Ax \leq b, x = \begin{bmatrix} x_c \\ x_b \end{bmatrix} \\ x_c \in \mathbb{R}^{n_c}, x_b \in \{0,1\}^{n_b} \end{gathered} \tag{3.10.12}$$

3.11 Linear unconstrained MPC

Given the state space model

$$\begin{cases} x_{k+1} = Ax_k + Bu_k \\ y_k = Cx_k \end{cases} \tag{3.11.1}$$

With

$$\begin{gathered} x \in \mathbb{R}^n, \quad u \in \mathbb{R}^m, \quad y \in \mathbb{R}^p \\ x_0 = x(t), \quad x_k = x(t+k|t), \quad u_k = u(t+k|t) \end{gathered} \tag{3.11.2}$$

The following equation relates the input and states of the model

$$x_k = A^k x_0 + \sum_{j=0}^{k-1} A^j B u_{k-1-j} \tag{3.11.3}$$

The performance index (also referred to as cost function) has this form

$$\begin{gathered} J(z, x_0) = x'_N P x_N + \sum_{k=0}^{N-1} x'_k Q x_k + u'_k R u_k \\ with\ R = R' \succ 0, P = P' \succcurlyeq 0\ and\ Q = Q' \succcurlyeq 0 \end{gathered} \tag{3.11.4}$$

The objective is to determine the sequence of inputs that optimally solves the optimization problem. Rewriting the cost function in an alternate form

$$J(z, x_0) = z'Hz + x_0'F'z + \frac{1}{2}x_0'Yx_0 \tag{3.11.5}$$

The solution is obtained by putting to zero the gradient

$$\nabla_z J(z, x_0) = Hz + Fx_0 = 0 \tag{3.11.6}$$

Which gives as an optimal sequence

$$z^* = -H^{-1}Fx_0 \tag{3.11.7}$$

Therefore, the algorithm to solve the unconstrained quadratic function finds the optimal sequence of inputs z^* by minimizing at each sampling step t the quadratic function below:

$$\min_z f(z) = \frac{1}{2}z'Hz + x'(t)F'z \tag{3.11.8}$$

With z being equal to:

$$z = \begin{bmatrix} u_0 \\ \vdots \\ u_{N-1} \end{bmatrix} \tag{3.11.9}$$

The solution is once again obtained putting to zero the gradient of the function $f(z)$

$$\begin{gathered} \nabla f(z) = Hz + Fx(t) = 0 \Rightarrow z^* = -H^{-1}Fx(t) \Rightarrow \\ \Rightarrow u(t) = -[I \quad 0 \quad \cdots \quad 0]H^{-1}Fx(t) = Kx(t) \end{gathered} \tag{3.11.10}$$

This is particularly interesting because it shows that an unconstrained linear Model Predictive Control algorithm equals a linear state feedback. It is important to highlight that for $J(z, x_0) = x_N'Px_N + \sum_{k=0}^{N-1} x_k'Qx_k + u_k'Ru_k, N_u = N$, with the matrix P being the solution of the algebraic Riccati equation. The MPC is equal to the Linear Quadratic Regulator control for any choice of the prediction horizon N.

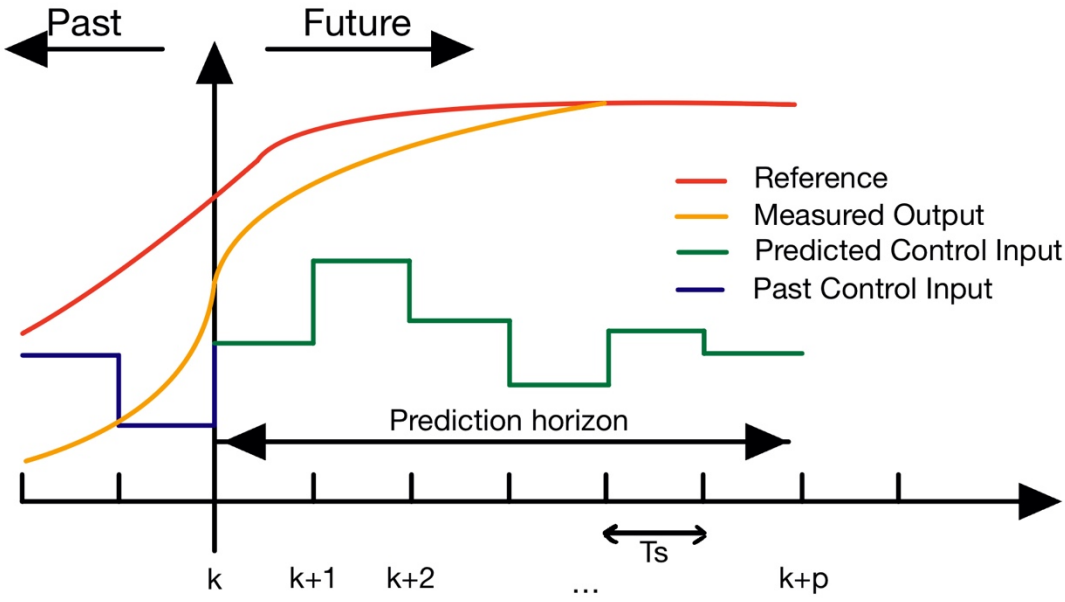

Figure 3.11: Various signals in the Model Predictive Controller

3.12 Constrained linear MPC

The constrained case results more interesting because it shows how MPC is a high-level control algorithm. The constraints are considered both on the input and output values.

$$\begin{cases} x_{k+1} = Ax_k + Bu_k \\ y_k = Cx_k \end{cases} \tag{3.12.1}$$

With the same dimension of the matrices as before, plus the enforced constraints

$$\begin{gathered} x \in \mathbb{R}^n, \quad u \in \mathbb{R}^m, \quad y \in \mathbb{R}^p \\ \begin{cases} u_{min} \leq u(t) \leq u_{max} \\ y_{min} \leq y(t) \leq y_{max} \end{cases} \\ u_{min}, u_{max} \in \mathbb{R}^m \\ y_{min}, y_{max} \in \mathbb{R}^p \end{gathered} \tag{3.12.2}$$

Therefore, this optimization problem is a constrained quadratic programming problem

$$\begin{gathered} \min_z x_N' P x_N + \sum_{k=0}^{N-1} x_k' Q x_k + u_k' R u_k \\ s.t.\ u_{min} \leq u(t) \leq u_{max}, k = 0, \cdots, N-1 \\ y_{min} \leq y(t) \leq y_{max}, k = 1, \cdots, N \\ with\ R = R' \succ 0, P = P' \succcurlyeq 0\ and\ Q = Q' \succcurlyeq 0 \end{gathered} \tag{3.12.3}$$

The optimization problem can be also expressed in the alternate form

$$\begin{gathered} V(x_0) = \frac{1}{2} x_0' Y x_0 + \min_z \frac{1}{2} z' H z + x_0' F' z \ \text{(Quadratic objective)} \\ s.t.\ Gz \leq W + S x_0 \ \ (Linear\ constraints) \\ with\ H = H' \succ 0 \end{gathered} \tag{3.12.4}$$

Which is a Convex Quadratic Program (CVX QP) in which z is the optimization vector containing the sequence of inputs from 0 to $N-1$. The H, F, Y, G, W, S matrices depend on Q, R, P, which are the weight matrices, the bounds on input variable u, the bounds on output variable y and the matrices of the model A, B, C.

The constrained linear MPC algorithm solves at each sampling step the constrained convex QP computing the solution z^*, which is the vector containing all the inputs from u_0^* to u_{N-1}^*, and applies only the first term of the vector discarding the others.

3.13 Tracking of a reference signal

To obtain an MPC control algorithm capable of tracking a certain given signal $r(t)$, it results necessary to extend the state space model with an adding state and to use an incremental increase of the input as follows

$$\begin{gathered} \Delta u(t) = u(t) - u(t-1) \\ x_u(t) = u(t-1) \end{gathered} \tag{3.13.1}$$

The new state space model assumes the following form:

$$\begin{cases} x(t+1) = Ax(t) + Bu(t-1) + B\Delta u(t) \\ x_u(t+1) = x_u(t) + \Delta u(t) \end{cases} \tag{3.13.2}$$

$$\begin{cases} \begin{bmatrix} x(t+1) \\ x_u(t+1) \end{bmatrix} = \begin{bmatrix} A & B \\ 0 & I \end{bmatrix} \begin{bmatrix} x(t) \\ x_u(t) \end{bmatrix} + \begin{bmatrix} B \\ I \end{bmatrix} \Delta u(t) \\ y(t) = \begin{bmatrix} C & 0 \end{bmatrix} \begin{bmatrix} x(t) \\ x_u(t) \end{bmatrix} \end{cases} \tag{3.13.3}$$

Which is still linear with states $x(t)$, $x_u(t)$ and has an input equal to $\Delta u(t)$.

The optimization problem takes the following form:

$$\begin{aligned} &\min_{z} \sum_{k=0}^{N-1} \left\| W^{y}\left(y_{k+1} - r(t)\right) \right\|_2^2 + \left\| W^{\Delta u} \Delta u_k \right\|_2^2 \\ &s.t.\ u_{min} \le u_k \le u_{max}, k = 0, \dots, N-1 \\ &y_{min} \le y_k \le y_{max}, k = 1, \dots, N \\ &\Delta u_{min} \le \Delta u_k \le \Delta u_{max}, k = 0, \dots, N-1 \\ &with\ [\Delta u_k \triangleq u_k - u_{k-1}], u_{-1} = u(t-1) \end{aligned} \tag{3.13.4}$$

In this context z keeps the same form of a row vector containing all the inputs value from the first time instant to the time instant $N-1$. The weight matrix W is the Cholesky factor of $Q^{(\cdot)} = \left(W^{(\cdot)}\right)' W^{(\cdot)}$, which is a diagonal matrix.

The optimization problem can be reformulated in the following structure:

$$\begin{aligned} &\min_{z} J\left(z, x(t)\right) = \frac{1}{2} z' H z + [x'(t)\ r'(t)\ u'(t-1)] F' z \\ &s.t.\ Gz \le W + S \begin{bmatrix} x(t) \\ r(t) \\ u(t-1) \end{bmatrix} \end{aligned} \tag{3.13.5}$$

It is possible to track the $r(t)$ by considering an additive penalty $\left\| W^{u}(u_k - u_{ref}(t)) \right\|_2^2$, plus, it is interesting to highlight that the constraints may also depend on the reference input.

3.18 Disturbance measurement

The measurement of disturbances is considered in the model as an unmeasured input $d(t)$ to the system, then the optimization problem is once again mathematically formulated, resulting very similar to the undisturbed process:

$$\begin{cases} x_{k+1} = Ax_k + Bu_k + B_d d(t) \\ y_k = Cx_k + D_d d(t) \end{cases} \tag{3.14.1}$$

$$x_k = A^k x_0 + \sum_{j=0}^{k-1} A^j B u_{k-1-j} + A^j B_d d(t) \tag{3.14.2}$$

The optimization problem is still a QP, and it is posed in the following:

$$\min_z \frac{1}{2} z'Hz + \left[x'(t)\, r'(t)\, u'(t-1)\, d'(t)\right] F'z$$
$$s.t.\ Gz \leq W + S \begin{bmatrix} x(t) \\ r(t) \\ u(t-1) \\ d(t) \end{bmatrix} \tag{3.14.3}$$

The Model Predictive Control intrinsically provides a feedforward action on the reference input and the measured disturbance.

3.15 Constraints softening

In an optimization problem, it often results useful to "soften" the constraints imposed on the various variables, in particular to prevent the unfeasibility of the solution. The optimization problem assumes the following structure:

$$\begin{gathered} \min_z \sum_{k=0}^{N-1} \left\| W^y \left(y_{k+1} - r(t)\right) \right\|_2^2 + \left\| W^{\Delta u} \Delta u_k \right\|_2^2 + \rho_\epsilon \epsilon^2 \\ \text{s.t. } u_{min} \leq u_k \leq u_{max}, k = 0, \dots, N-1 \\ y_{min} - \epsilon V_{min} \leq y_k \leq y_{max} + \epsilon V_{max}, k = 1, \dots, N \\ \Delta u_{min} \leq \Delta u_k \leq \Delta u_{max}, k = 0, \dots, N-1 \\ x_{k+1} = Ax_k + Bu_k, k = 0, \dots, N-1 \end{gathered} \tag{3.15.1}$$

And also, the vector z changes structure:

$$z = \begin{bmatrix} \Delta u(0) \\ \vdots \\ \Delta u(N-1) \\ \epsilon \end{bmatrix} \tag{3.15.2}$$

In this formulation $\epsilon_i \geq 0$ represents the amount of violation (misclassification) of the *i-th* point, having weight $\rho_\epsilon \gg W^y, W^{\Delta u}$. V_{min} and V_{max} are column vectors with all entries positive or null, which correspond to the amount of softening of the *i-th* constraint.

The infeasibility of an optimization problem can be related to design errors of the controller, modelling errors of the system and also the presence of disturbances during the working phase.

3.16 Feasibility of an optimization problem

Considering the QP optimization problem

$$\begin{gathered}\min_{z} \sum_{k=0}^{N-1} \left\| W^{y}\left(y_{k+1} - r(t)\right)\right\|_2^2 + \left\| W^{\Delta u}\Delta u_k \right\|_2^2 \\ s.t.\ u_{min} \le u_k \le u_{max}, k = 0, \dots, N-1 \\ y_{min} \le y_k \le y_{max}, k = 1, \dots, N \\ \Delta u_{min} \le \Delta u_k \le \Delta u_{max}, k = 0, \dots, N-1\end{gathered} \tag{3.16.1}$$

Concerning the input constraints, the feasibility is guaranteed if the equations of u and Δu are consistent, instead, the constraints on the output variable are more sensitive, having that for $N < \infty$ there is no guarantee that the optimization problem will be feasible at all times. Clearly, it results impossible to have $N = \infty$ because it would result in an infinite number of constraints.

3.17 Stability and convergence of an optimization problem

Considering the QP optimization problem in the following formulation

$$\begin{gathered}\min_{z} x_N' P x_N + \sum_{k=0}^{N-1} x_k' Q x_k + u_k' R u_k \\ s.t.\ u_{min} \le u(t) \le u_{max}, k = 0, \cdots, N-1 \\ y_{min} \le y(t) \le y_{max}, k = 1, \cdots, N \\ with\ R = R^{'} \succ 0, P = P^{'} \succcurlyeq 0\ and\ Q = Q' \succcurlyeq 0\end{gathered} \tag{3.17.1}$$

Stability depends on the model matrices A, B, C, also on matrices N, Q, R, P, and also on the saturation constraints on the control input and output variables $u_{min}, u_{max}, y_{min}, y_{max}$.
An important result in the context of MPC stability states that, considering the Model Predictive Control law stated in the following:

$$\begin{gathered}\min \sum_{k=0}^{N-1} x_k' Q x_k + u_k' R u_k \\ s.t. x_{k+1} = A x_k + B u_k \\ u_{min} \leq u_k \leq u_{max} \\ y_{min} \leq C x_k \leq y_{max} \\ x_N = 0 \leftarrow "terminal\ constraint" \\ R, Q \succ 0 \\ u_{min} < 0 < u_{max} \\ y_{min} < 0 < y_{max}\end{gathered} \tag{3.17.2}$$

The feasibility of the optimization problem at time $t = 0$ implies that

$$\begin{gathered}\lim_{t \to \infty} x(t) = 0 \\ \lim_{t \to \infty} u(t) = 0\end{gathered} \tag{3.17.3}$$

Moreover, it implies that the constraint are satisfied for $t \geq 0$ for all $R, Q \succ 0$.

An alternative result in the same context considers another formulation of the optimization problem:

$$\begin{gathered}\min \sum_{k=0}^{N-1} y_k' Q_y y_k + u_k' R u_k \\ s.t. x_{k+1} = A x_k + B u_k \\ u_{min} \leq u_k \leq u_{max} \\ y_{min} \leq C x_k \leq y_{max} \\ x_N = 0 \ or \ N = \infty\end{gathered} \tag{3.17.4}$$

The feasibility of the optimization problem at the initial time instant $t = 0$ implies that for all $R = R' \succ 0, Q_y = Q_y' \succ 0$:

$$\begin{gathered}\lim_{t \to \infty} y(t) = 0 \\ \lim_{t \to \infty} u(t) = 0\end{gathered} \tag{3.17.5}$$

For all $t \geq 0$ the constraints are satisfied. In the following some stability constraints are listed:

$$\begin{gathered} Infinite\ prediction\ horizon \quad N \to \infty \\ End - point\ constraint \quad x_N = 0 \\ Relaxed\ terminal\ constraint \quad x_n \in \Omega \\ Contraction\ constraint \quad \|x_{k+1}\| \leq \alpha \|x(t)\|, \alpha < 1 \end{gathered} \tag{3.17.6}$$

The proof of all the results stated before can be found in the bibliography.

3.18 Constraint horizon and control horizon

Considering the optimization problem with relaxed constraints in a slightly different version than the one stated before:

$$\begin{gathered} \min_z \sum_{k=0}^{N-1} \left\| W^y \left(y_k - r(t) \right) \right\|_2^2 + \left\| W^{\Delta u} \Delta u_k \right\|_2^2 + \rho_\epsilon \epsilon^2 \\ s.t.\ u_{min} \leq u_k \leq u_{max}, k = 0, \dots, N-1 \\ y_{min} - \epsilon V_{min} \leq y_k \leq y_{max} + \epsilon V_{max}, k = 1, \dots, N_c \\ \Delta u_{min} \leq \Delta u_k \leq \Delta u_{max}, k = 0, \dots, N-1 \\ \Delta u_k = 0, k = N_u, \dots, N-1 \end{gathered} \tag{3.18.1}$$

The constraint horizon N_c limits the number of constraints. Reducing the input horizon N_u lowers the performance of the controller but also reduces the computation time.

3.19 Kalman filter for MPC control

Kalman filter is a commonly used algorithm to filter the signals in a control loop, keeping count of the noise and estimating a joint probability distribution over the variables for each timeframe. The algorithm estimates the state variables together with their uncertainty range and updates these values through a weighted average once the next measurement is available. In the following, some important mathematical results are reported for completeness.
The plant model can be formulated as:

$$\begin{cases} x(t+1) = Ax(t) + B_u u(t) + B_v d_m(t) + B_d d_u(t) \\ y(t) = Cx(t) + D_v d_m(t) + D_d d_u(t) \end{cases} \tag{3.19.1}$$

$$with\ d_m(t) = measured\ disturbance\ and\ d_u(t) = unmeasured\ disturbance$$

The full mathematical model for the filter can be expressed as:

$$\begin{bmatrix} x(t+1) \\ x_d(t+1) \\ x_m(t+1) \end{bmatrix} = \begin{bmatrix} AB_d\bar{C} & 0 & 0 \\ 0 & \bar{A} & 0 \\ 0 & 0 & \tilde{A} \end{bmatrix} \begin{bmatrix} x(t) \\ x_d(t) \\ x_m(t) \end{bmatrix} + \begin{bmatrix} B_u \\ 0 \\ 0 \end{bmatrix} u(t) + \begin{bmatrix} B_v \\ 0 \\ 0 \end{bmatrix} d_m(t) + \\ + \begin{bmatrix} B_d \\ \bar{B} \\ 0 \end{bmatrix} n_d(t) + \begin{bmatrix} 0 \\ 0 \\ \tilde{B} \end{bmatrix} n_m(t) + \begin{bmatrix} B_u \\ 0 \\ 0 \end{bmatrix} n_u(t) \qquad (3.19.2)$$

$$y_m(t) = \begin{bmatrix} C_m & D_{dm}\bar{C} & \tilde{C} \end{bmatrix} \begin{bmatrix} x(t) \\ x_d(t) \\ x_m(t) \end{bmatrix} + D_{vm}v(t) + \bar{D}_m n_d(t) + \tilde{D}_m n_m(t)$$

In which, the various matrices are responsible for managing the inputs of the various signals, and then $n_d(t)$, $n_m(t)$ and $n_u(t)$ are, respectively, the modelling errors, the measurement noise, and the Gaussian noise on the input of the process.

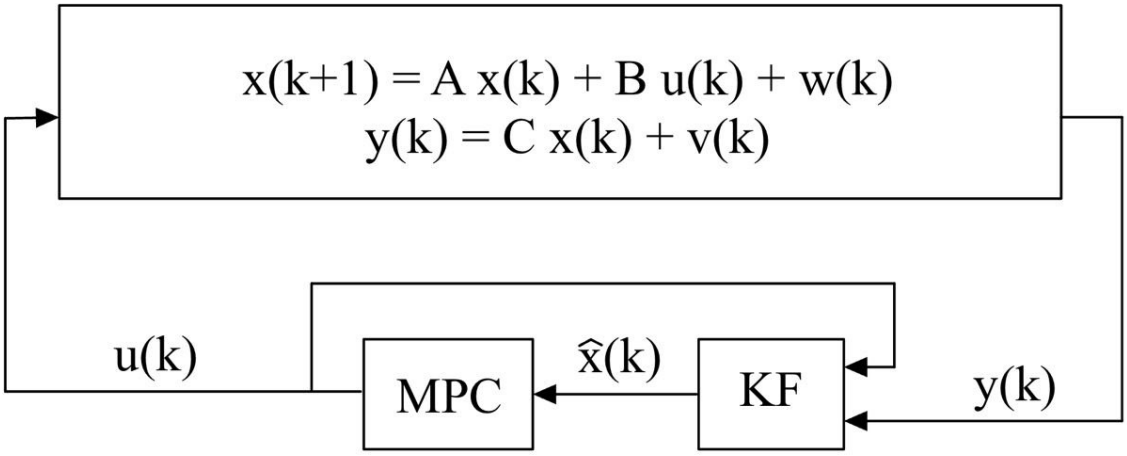

Figure 3.12: Implementation of the Kalman Filter in the model predictive control structure

Chapter 4

Modelling of the structure and simulations

4.1 Equations of motion and transfer functions

This chapter describes all the procedures followed for building the model and the strategies used to obtain the various results with different control algorithms.

The equation of motion of a base-excited lumped mass single-degree-of-freedom structure can be written as:

$$M\ddot{z}_1 + C\dot{z}_1 + Kz_1 = -M\ddot{z}_g \tag{4.1.1}$$

Where M is the mass of the structure, K is the linear elastic stiffness of the undamped structure C is the damping coefficient of the structure without additive dampers, z_1 is the horizontal displacement of the first floor of the structure, $\ddot{z}_g$ is the earthquake input acceleration to the system, which multiplied by the mass represents a force input.

This equation is the starting point for the model, it does not consider the presence of the fluid viscous damper and allows to have a comparison between a structure with an additive damper and one without it. The viscous dashpot model, presented in chapter 2, has been used to represent the behaviour of the fluid viscous damper mainly because of its simplicity in the implementation and also because it does not need the interpolation of various parameters through shaking-table tests, which would have been prohibitive during the building phase of the model.

The equilibrium relation modelling also the presence of the fluid viscous damper is represented by the following equation:

$$\begin{gathered} m\ddot{z}_1 + c\dot{z}_1 + kz_1 + \eta f(t) = -m\ddot{z}_g \\ with\ f(t) = C(t)|\dot{x}(t)|^{\alpha}\mathrm{sgn}(\dot{x}) \end{gathered} \tag{4.1.2}$$

This equation (with $\eta = 1$) models the presence of a single fluid viscous damper working horizontally to the ground, to model a higher number of dampers it is sufficient to increase the value of η to the number of dampers present in the structure since in that condition the maximum force exerted by the dampers will be higher.

The values considered for the structure m, c and k are scalars and their values are the following:

$$\begin{aligned} m &= 10000\ [kg] \\ k &= 2000000\ [N/m] \\ c &= 2815\ [Ns/m] \end{aligned} \tag{4.1.3}$$

The equations describing the behaviour of the system can be represented in state space form using the following four matrices:

$$A = \begin{bmatrix} 0 & 1 \\ -\frac{k}{m} & -\frac{c}{m} \end{bmatrix}$$

$$B = \begin{bmatrix} 0 & 0 \\ -1 & \frac{1}{m} \end{bmatrix}$$

$$C = \begin{bmatrix} 1 & 0 \\ 0 & 1 \\ -\frac{k}{m} & -\frac{c}{m} \end{bmatrix} \tag{4.1.4}$$

$$D = \begin{bmatrix} 0 & 0 \\ 0 & 0 \\ -1 & \frac{1}{m} \end{bmatrix}$$

These four matrices allow the creation of a state space model with two inputs, the first input is the input force given by the earthquake signal $m\ddot{z}_g$, and the second input is the force given by the semi-active fluid viscous damper. The force given by the damper is considered as a second input because it is more convenient to compute it each time instant, this is because it is a strongly non-linear function, therefore it results impossible to incorporate it inside the state space form in a different way. The images below schematize the structure respectively without the additive semi-active fluid viscous damper and with the semi-active fluid viscous damper.

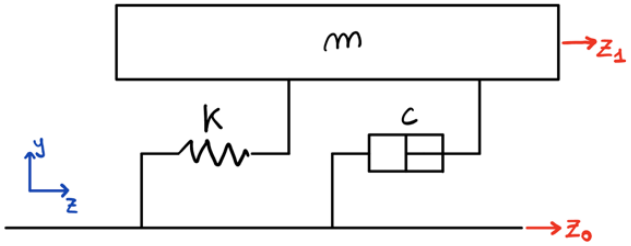

Figure 4.1: Schematic model of the structure without the semi-active damper

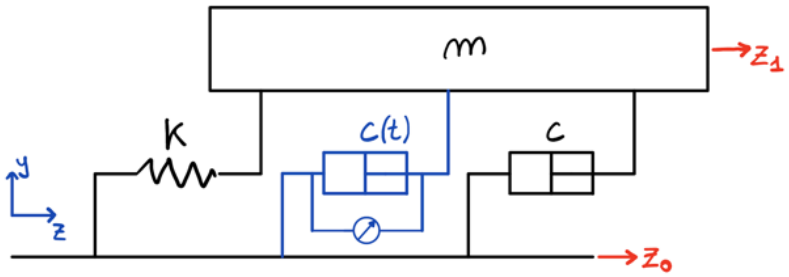

Figure 4.2: Schematic model of the structure with the semi-active damper

Given that the system has two inputs, it has six transfer functions, the first three are relative to the values of displacement, velocity, and acceleration given by the first input, which is the earthquake signal, the last three transfer functions instead relate displacement, velocity, and acceleration with the second input, which is the input force given by the damper. The transfer functions of the structure without the damper, which are also the ones in the multi-input structure relating the earthquake input to the states of the system, are the first three ones reported below in equation 4.1.5. The natural period of the structure is equal to $T = 0.4443s$, and the resonance frequency is equal to $14.1421\ Hz$.

The transfer functions are present in equation (4.1.5) here below:

$$
\begin{aligned}
H_{uz_1} &= \frac{-1}{s^2 + 0.2815s + 200} \\
H_{u\dot{z}_1} &= \frac{-s}{s^2 + 0.2815s + 200} \\
H_{u\ddot{z}_1} &= \frac{-s^2}{s^2 + 0.2815s + 200} \\
H_{fz_1} &= \frac{0.0001}{s^2 + 0.2815s + 200} \\
H_{f\dot{z}_1} &= \frac{0.0001s}{s^2 + 0.2815s + 200} \\
H_{f\ddot{z}_1} &= \frac{0.0001s^2}{s^2 + 0.2815s + 200}
\end{aligned}
\tag{4.1.5}
$$

The bode diagrams of each transfer function are present in figure 4.3. The 6 bode diagrams are in the same order of the transfer functions present above starting from the top left position and advancing in reading order.

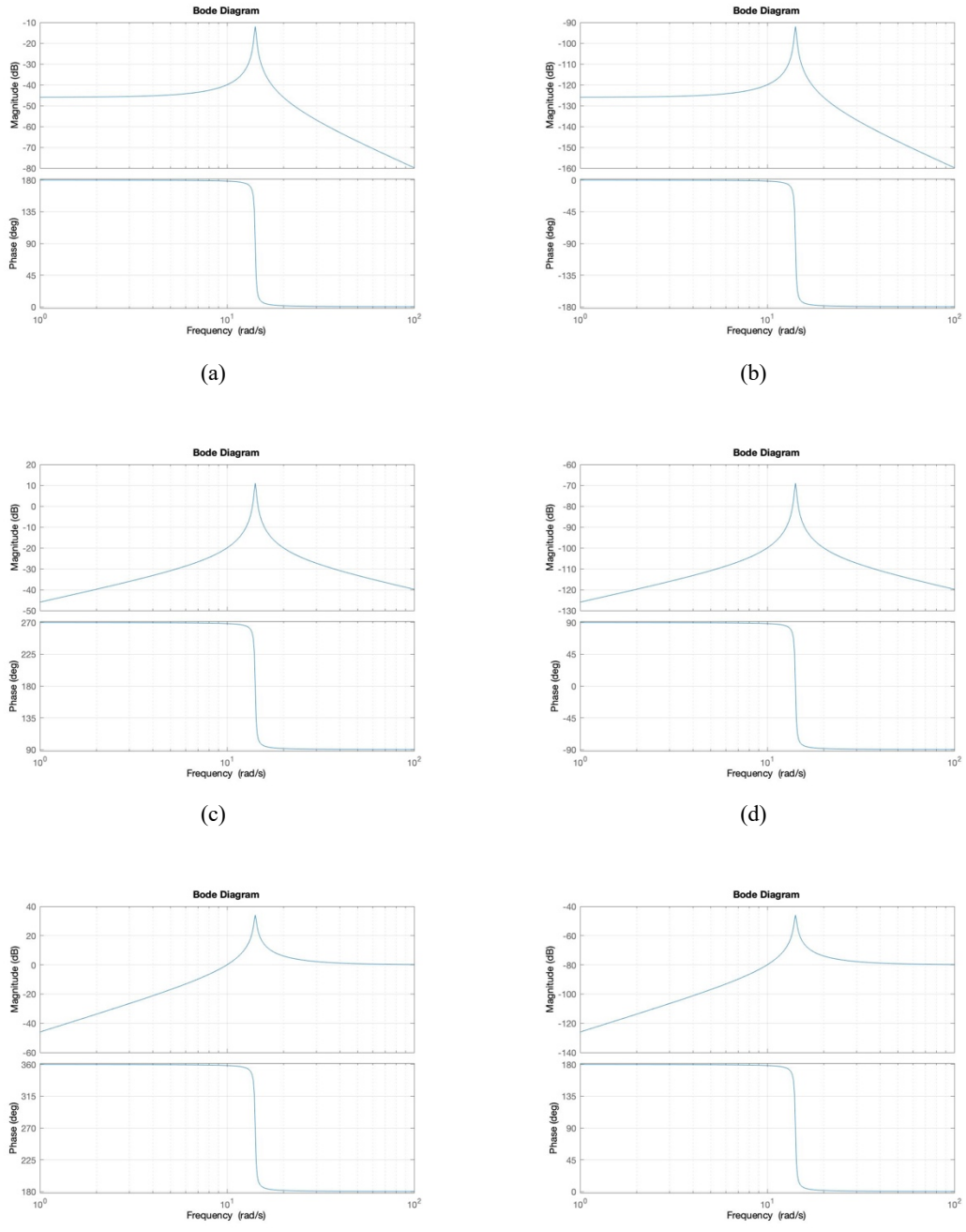

Figure 4.3: Transfer functions of the system, (a) From the earthquake input to the displacement, (b) from the earthquake input to the velocity, (c) from the earthquake input to the acceleration, (d) from the damper force input to the displacement, (e) from the damper force input to the velocity, (f) from the damper force input to the acceleration

4.2 Uncontrolled structure model

The first model realized is also the simplest one, this model does not possess the additive semi-active fluid viscous dampers and gives a reference for the structure behaviour. The earthquake signal, which is a vector containing time and acceleration components, enters the state space model from which displacement, velocity and acceleration are computed each instant through the equations of motion of the system. The state space model in this case represents a system with a single input. The model outputs the three states, which are displacement, velocity, and acceleration of the suspended mass.

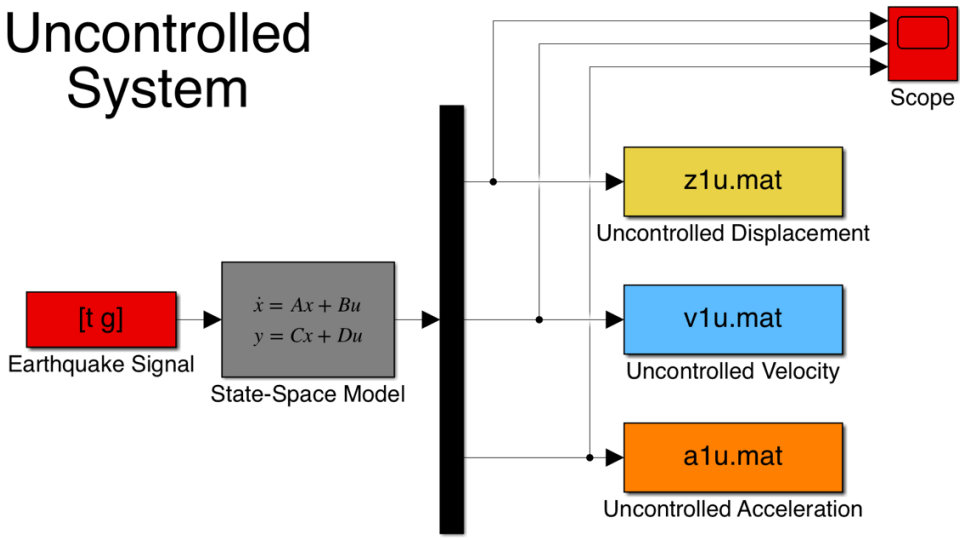

Figure 4.4: Simulink model of a 1 degree of freedom structure showing an uncontrolled system with displacement, velocity, and acceleration as outputs

4.3 Model with uncontrolled fluid viscous damper

The successive level of complexity in the model is achieved by including the presence of the damper in passive form (no control), the force output from the damper as reported in equation (4.1.2) is a function of the velocity of the structure as well as its sign, therefore its signal is measured from the output and through a simple function the output force from the damper is computed. The exponent α is considered equal to 0.1, which is a common value in real-world devices.

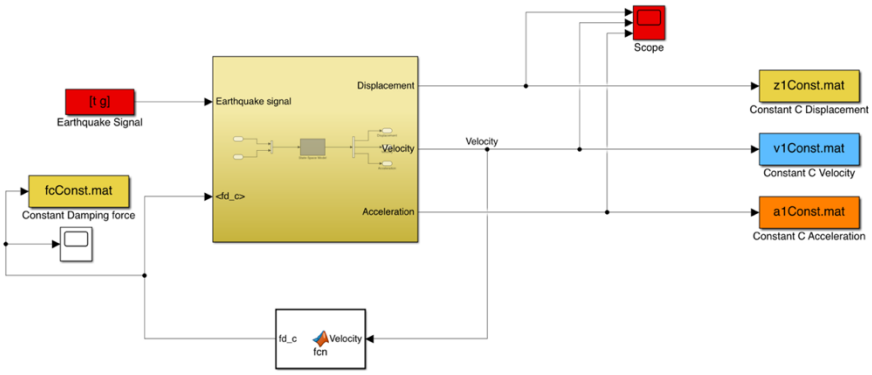

Figure 4.5: Simulink model of a 1 degree of freedom structure with implementation of the input from the fluid viscous damper

The function block present in the feedback loop of the system, shown in figure 4.5, measures the velocity value output from the equations in the state space model and computes the force given by the passive fluid viscous damper in equation (4.1.2) with a constant passive damping coefficient.

This same model has been used with a different input to obtain the graphs relative to the hysteretic behaviour of the structure when subjected to a certain input, specifically sinusoidal inputs and signals covering the whole typical band of frequencies of earthquakes, which in general is considered in the range $1 \div 10\ Hz$. Another kind of input used in these tests is a sinusoidal input with a frequency equal to the resonant frequency of the structure, to simulate a critical input and obtain the relative graphs.

Stimulating the system with a sinusoidal input at the resonant frequency, with unitary amplitude, the following graphs were obtained:

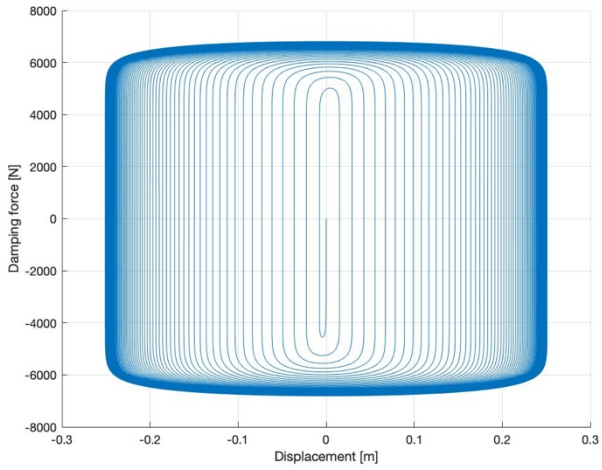

Figure 4.6: Plot of the displacement as a function of the damping force

The first graph, plotting displacement on the x-axis and damping force on the y-axis, results being particularly interesting because of the resemblance with figures 2.7 and 2.8, this clearly shows that the model is a good representation of the actual physical phenomenon.

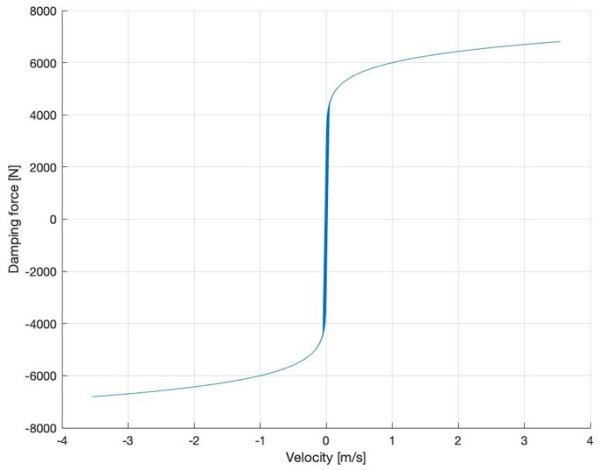

Figure 4.7: Hysteretic plot of the velocity as a function of the damping force in the model

The second graph shows the velocity of the mass on the x axis, while on the y axis the force of the device is shown. Zooming the central portion of the plot is possible to observe the hysteretic behaviour of the component. It is interesting to notice that the subtended area in the velocity vs damping force graph is representative of the energy dissipated by the component, and, more specifically, the area is directly proportional to the value of the α coefficient. The lower the value of α, the more energy is dissipated by the semi-active fluid viscous damper during the motion of the device.

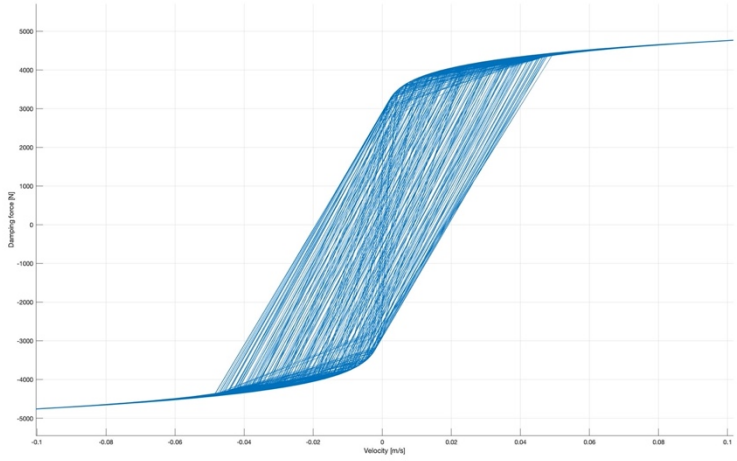

Figure 4.8: Zoom of figure 4.7 plot showing hysteretic behaviour of the device in the model

In figure 4.8 the hysteretic behaviour of the semi-active fluid viscous damper is visible, its presence is representative of a model that simulates properly the physical phenomena during the motion of the structure. The image below shows the plot of the acceleration on the x axis versus the damping force on the y axis, the acceleration values are very high because the sinusoidal input to the structure is at the resonant frequency, therefore the structure is subject to a resonant behaviour and is suffering extreme accelerations. The time course of the diagram is similar to the one plotting displacement versus damping force.

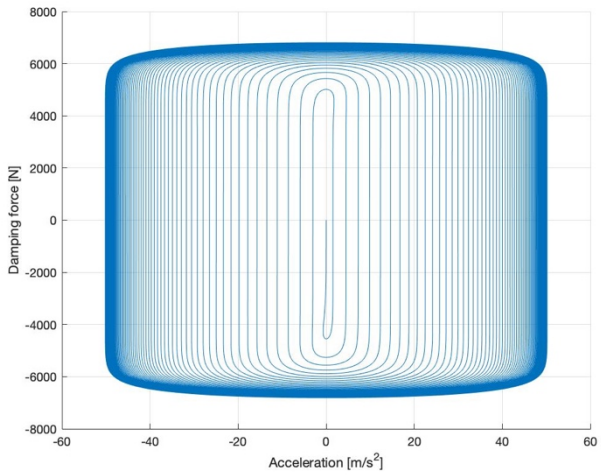

Figure 4.9: Plot of the acceleration versus damping force exerted by the semi-active fluid viscous damper in the model

4.4 Ideal control of the structure

Having obtained the graphs relative to the fundamental characteristics of the structure and the semi-active fluid viscous damper, the first models with an ideal control algorithm were built. Ideal control is referred to the property of the controller to feed back a generic control force into the state space model, and this is not possible because the semi-active device allows only the variation of the damping coefficient inside a certain range. Nevertheless, these kinds of models represent a starting point for the actual control strategy used in the successive steps. The control algorithms used, as anticipated in the previous chapter, are the Proportional-Integrative-Derivative control algorithm, and the Model Predictive Control algorithm.

The first model is the PID ideal control with saturation. In this model, the velocity signal is measured from the output of the state space system, and the error between a reference signal and the actual velocity of the structure is input inside the PID controller. This kind of approach aims at stabilizing the structure as quickly as possible, and this is because the reference to zero

of the velocity signal mathematically speaking refers to a system in a static equilibrium condition. The PID controller in this model also features upper and lower saturation constraints to make the value of the input force comparable with the one of the uncontrolled damper case. It has been tuned with the built-in PID tuner app inside the Simulink environment, through the linearization of the plant represented by the state space model of the structure. The tuning procedure of the controller was carried out by choosing values that represented a compromise between robust behaviour and quick response time.

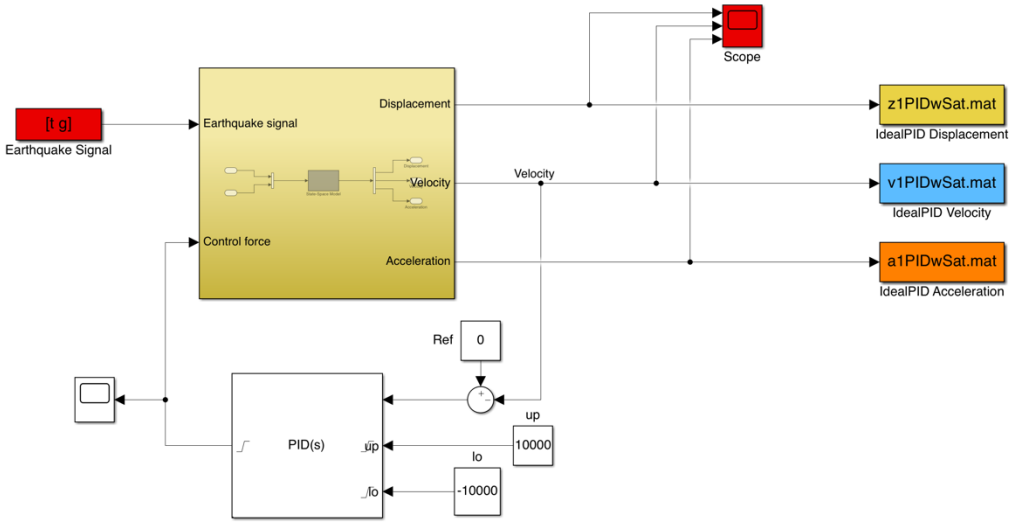

Figure 4.10: Simulink model of a 1 degree of freedom structure implementing ideal PID controller with upper and lower saturation constraints

The second ideal model built has a very similar structure to the first one, but it applies a different control algorithm. This model once again considers a controller able to feed back into the system a control force with upper and lower saturation constraints, it exploits a model predictive control algorithm with a built-in Kalman filtering action. The upper and lower saturation constraints are built-in in the Model Predictive Control block and the entity of the constraints is the same as the ones of the PID controller shown previously. The MPC block observes the velocity output from the state-space model and has a reference to zero, this kind of setting implies that also in this case the objective of the controller is stabilizing the structure as quickly as possible. In this specific MPC controller, the sampling time was set equal to one millisecond and the prediction and control horizons were set to 50 units of sampling time. The Model Predictive Control block linearizes the equations in state space form after the specification of the plant inside the simulation and creates a model to predict the future

behaviour of the system knowing the history of the input/output relation of the transfer function of the plant.

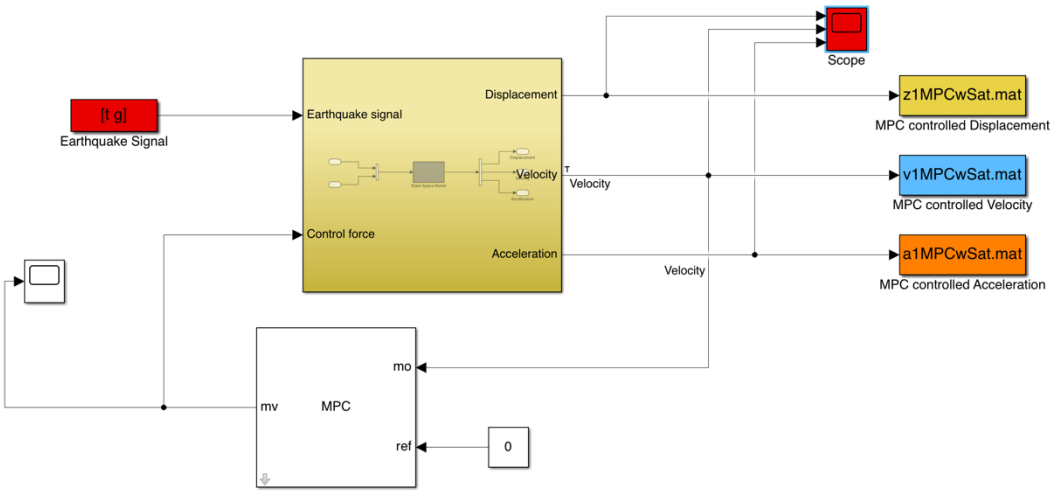

Figure 4.11: Simulink model of a 1 degree of freedom structure implementing ideal MPC controller with upper and lower saturation constraints

4.5 Ideal control versus uncontrolled damper

The models illustrated were used to simulate the behaviour of a structure with the input of the 1940 El Centro earthquake, which was recorded by a strong-motion seismograph on the 19th of May in the southern portion of California. Through the evaluation of the graphs, it is possible to make some considerations on the behaviour of the system. In blue there is the signal with the fluid viscous damper in passive conditions, in green the signal with the ideal PID control, and in red the signal with the ideal MPC control. The displacement signal of the suspended mass present below has a much better behaviour in the Ideal PID and the MPC case, it is also interesting to notice that the behaviour given by the passive (uncontrolled) damper keeps the displacement in the same order of magnitude of the ideal cases.

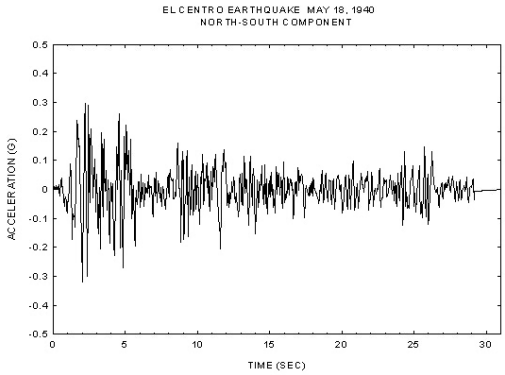

Figure 4.12: Seismograph of the El Centro 1940 earthquake

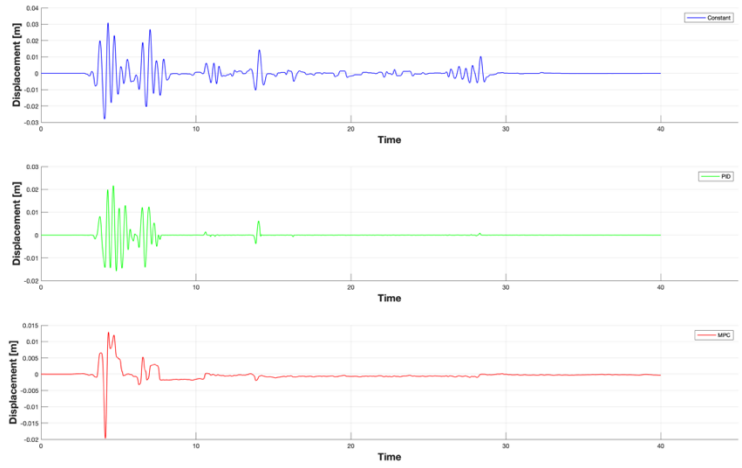

Figure 4.13: Displacement signal of the suspended mass following the earthquake input in constant damper case (blue), ideal PID control with saturation constraints (green) ideal MPC control with saturation constraints (red)

Concerning the velocity signal of the suspended mass, the graph shows a clear improvement using the ideal PID and MPC control algorithms. Comparing the velocity signal with the one relative to the damper in passive working conditions it is possible to notice that the velocity in the constant damper case is not drastically higher than the other two signals.

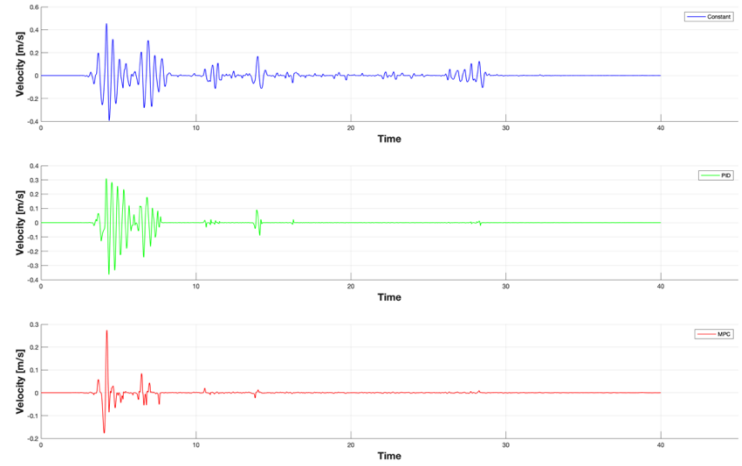

Figure 4.14: Velocity signal of the suspended mass following the earthquake input in constant damper case (blue), ideal PID control with saturation constraints (green) ideal MPC control with saturation constraints (red)

The acceleration signal of the suspended mass in the model represents the most critical aspect in the simulation, the values in the ideal control case and in the passive damper case show the real improvement in the structure behaviour given by the control force. The PID and MPC

control algorithm guarantee a lower acceleration of the structure together with a more stable behaviour throughout the whole simulation.

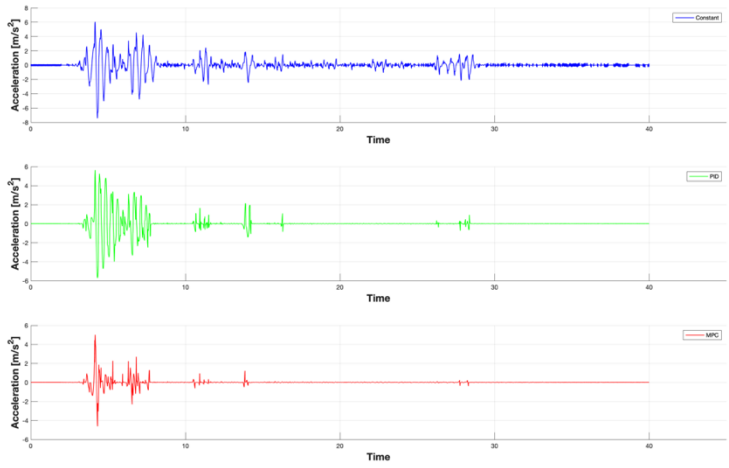

Figure 4.15: Acceleration signal of the suspended mass following the earthquake input in constant damper case (blue), ideal PID control with saturation constraints (green) ideal MPC control with saturation constraints (red)

These graphs show that an ideal control force is capable of effectively reducing the values of acceleration of the suspended mass of the structure, this triggers a chain effect for which also the velocity and the displacement of the mass result lower than in the non-ideal case. The values shown in the graphs above can also be evaluated numerically in the tables showing mean and variance of the three cases under study in this specific case.

Table 4.1: Values for open loop tuning of PID controllers

	Constant damping	PID	MPC
Displacement mean μ	-11.1898×10^{-5}	4.8063×10^{-5}	-26.5464×10^{-5}
Displacement variance σ^2	19.587×10^{-6}	7.3844×10^{-6}	3.4533×10^{-6}
Velocity mean μ	-6.7299×10^{-7}	-0.6415×10^{-7}	-78.227×10^{-7}
Velocity variance σ^2	0.0033109	0.0017866	0.00032571
Acceleration mean μ	-0.0019×10^{-5}	-1.6822×10^{-5}	0.31244×10^{-5}
Acceleration variance σ^2	0.72917	0.56766	0.10084

Some values of the table are not reported in a standard scientific notation, this was chosen to report all the values in the same row with the same order of magnitude to have a more immediate comparison between the digits. From the table, it is possible to notice how the mean and variance absolute values of the Constant damping case are higher than the Ideal PID and

the MPC scenarios, specifically in the acceleration case in which the variance of the Constant damping case results much higher than the others. The bar graphs below show the peak values of each signal with the different control strategies.

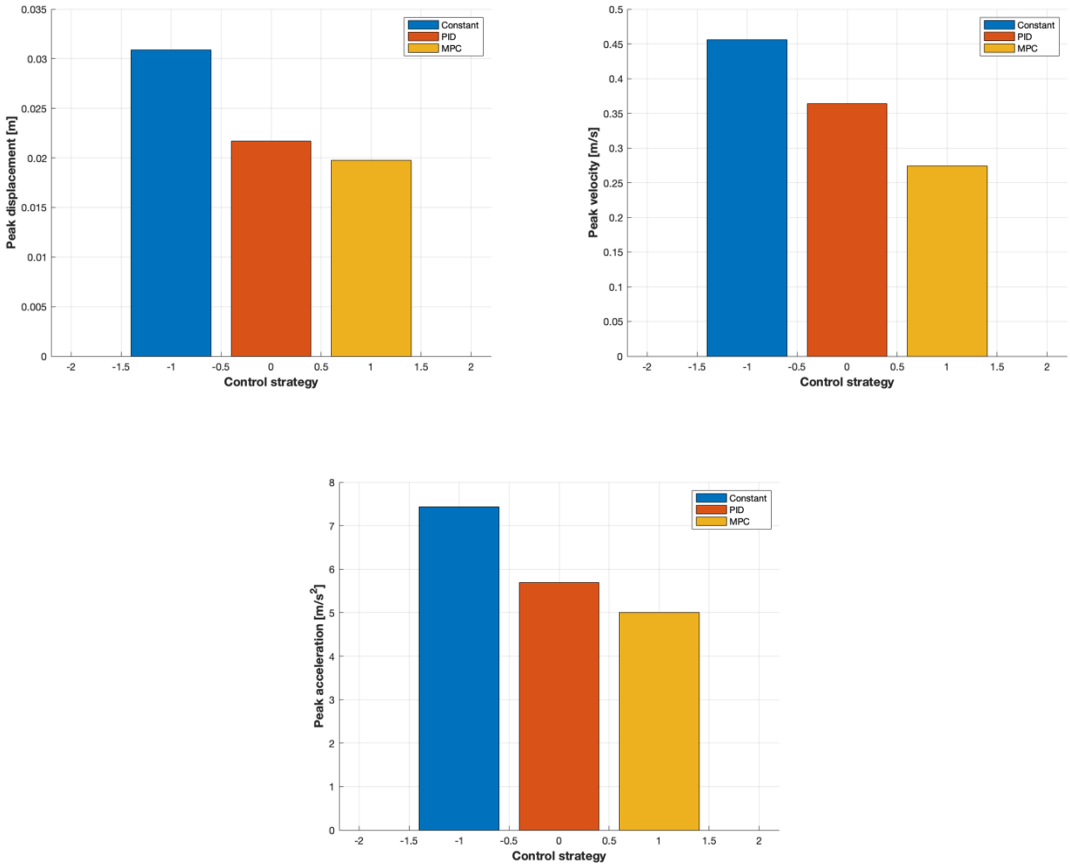

Figure 4.16: Peak values of displacement (top left), velocity (top right), and acceleration (bottom) in constant case (blue) PID case (orange) and MPC case (yellow)

This kind of visualization of the data gives many insights into the differences among the various approaches, in particular, it is clear how the Model Predictive Control algorithm can analyse and forecast the behaviour of the system to have a lower value of velocity and acceleration peak signals. The PID controller instead keeps all the signals below a certain threshold but is not capable to reduce the acceleration and velocity as much as the MPC does, this is certainly related to the capability of the Model Predictive Control algorithm to choose a better ideal control force.

Another unit of comparison between the different control algorithms is the RMSe of the various signals, which was compared again in the form of bar graphs and is reported below.

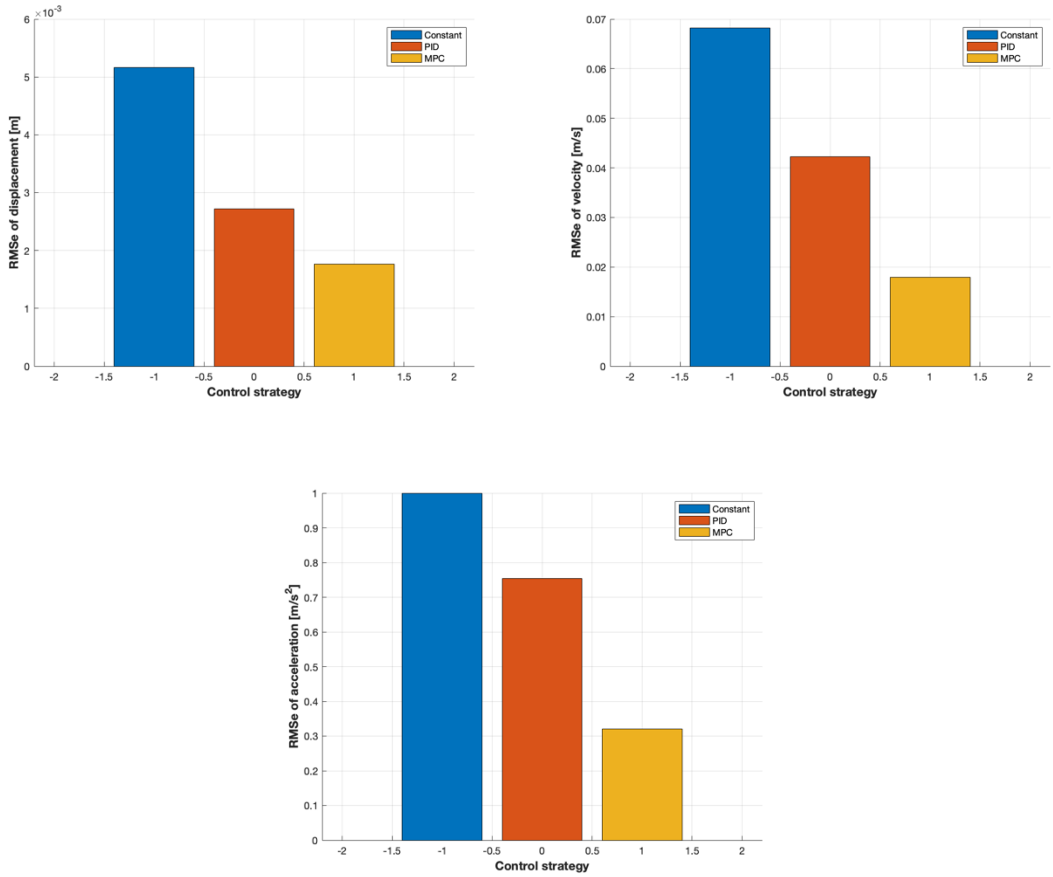

Figure 4.17: RMSe values of displacement (top left), velocity (top right), and acceleration (bottom) in constant case (blue) PID case (orange) and MPC case (yellow)

It is once again clear how both control algorithms give an evident improvement in all three signals of the structure, notably the Model Predictive Control can give better performances from all points of view.

These graphs set a reference for the successive simulations, in which the damper works according to the real mathematical model, therefore simulating the real behaviour of the structure much more effectively.

4.6 Spectral analysis of the signals

A spectral analysis of displacement, velocity and acceleration signals was performed on the constant model to further inspect the behaviour of the system working with the passive damper. The analysis also resulted useful for the choice of the sampling time (chapter 4.7) and were performed using the Signal Analyzer tool in the MATLAB environment.

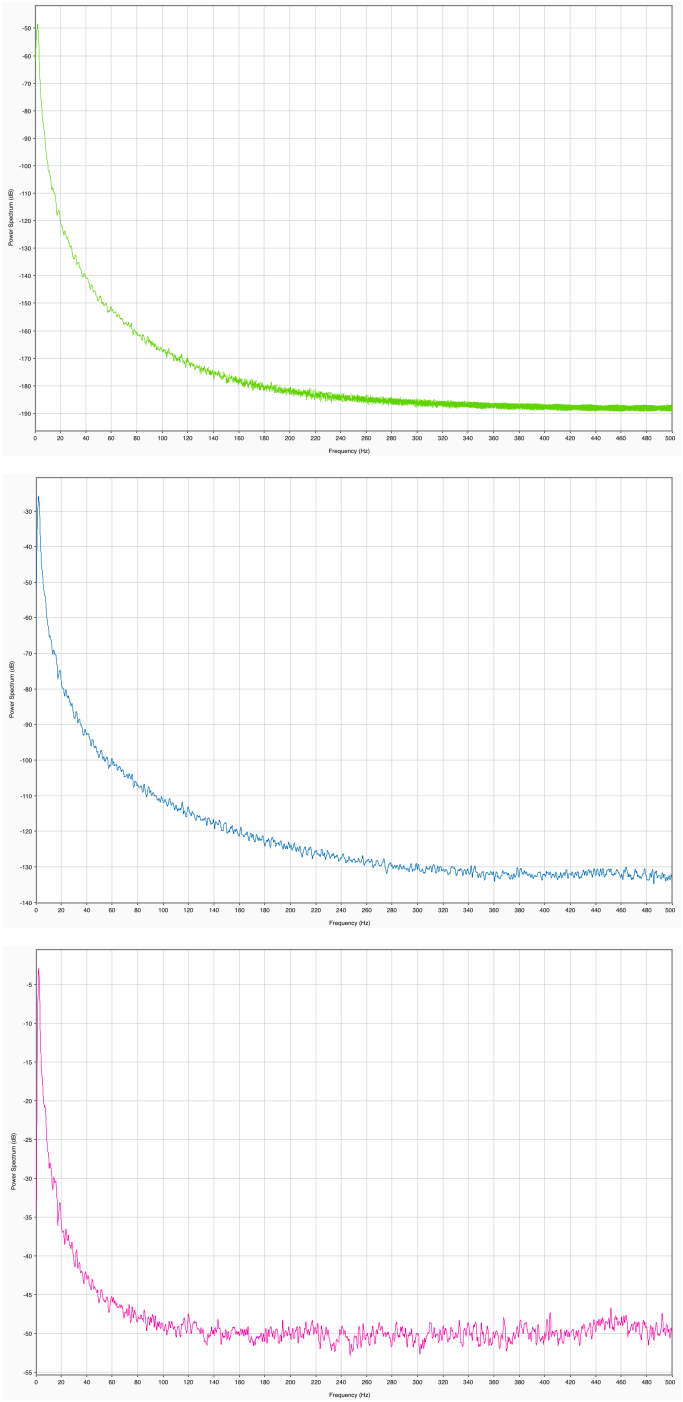

Figure 4.18: Spectral analysis of displacement signal (top), velocity signal (middle) and acceleration signal (bottom).

It is interesting to notice how the power spectrum of the various signals have different orders of magnitude but always show the peak values around 3 Hz. This happens because the typical frequencies related to a seismic input are in the range 1-10 Hz and also due to specific properties of the structure under study, such as the resonant frequency (or the natural period).

4.7 Towards a more realistic model

The successive steps in the study concern the adaptation of the control strategy to the viscous dashpot model, which is strongly nonlinear and also dependent on the velocity of the structure. These considerations imply that the control algorithm must approximate the ideal ones exploited in the previous pages. Different models were built to explore the effect of this control strategy on the behaviour of the structure, also with different sampling times to evaluate how the computational weight of the control algorithm affects the results in terms of the performance of the structure. The choice of the minimum sampling time was performed through a spectral analysis of the velocity signal since it is the one that enters the controller to compute the control input.

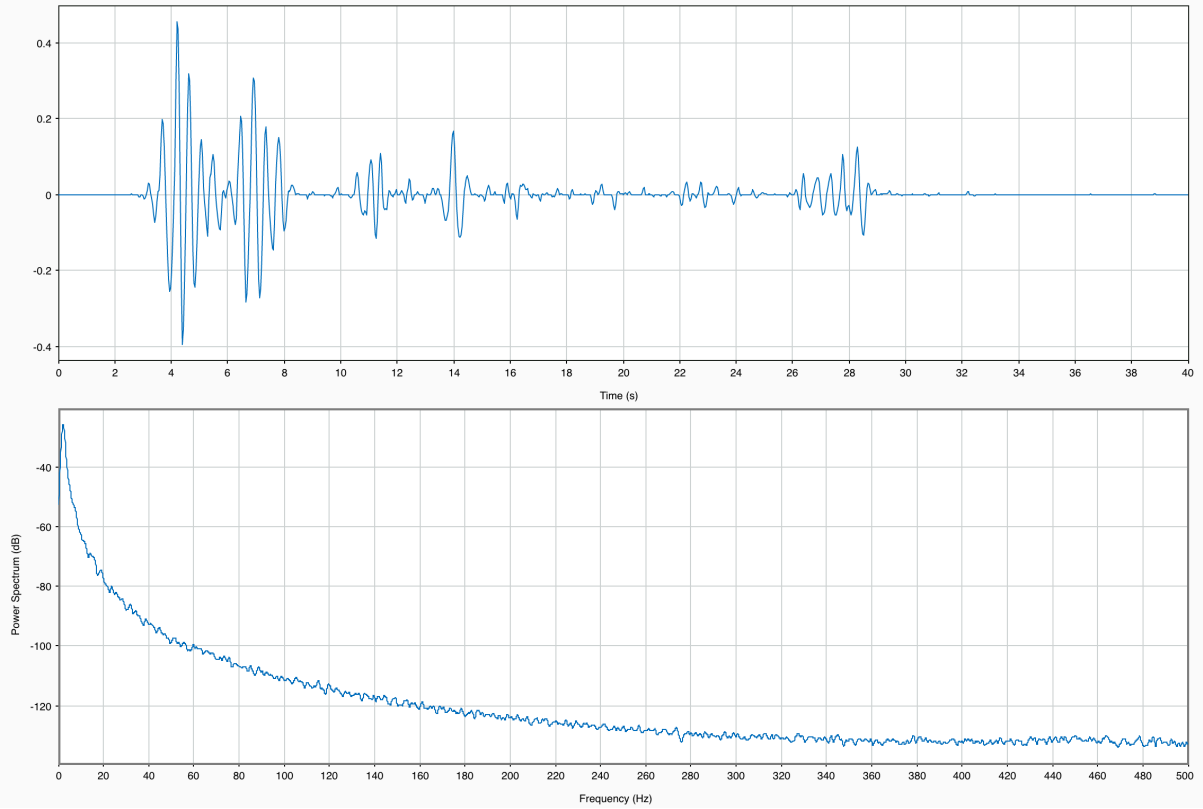

Figure 4.19: Velocity signal of the model in figure 4.4 (above) and spectral analysis of the signal (below).

In figure 4.19 the spectral analysis of the signal shows frequency components up to 500 Hz, with a Power Spectrum of -100 dB at 50 Hz. The components over 50 Hz were neglected due to their low power, from Shannon's theorem the minimum sampling frequency was chosen to be 100 Hz, which was used in the simulations together with a sampling frequency of 1000 Hz to check if the different sampling times perform differently in terms of control algorithm.

To build a model that is based on an optimal control algorithm and also considers the real behaviour of the device a specific strategy was adopted. The ideal controller was used as a reference for the value of the control force to the system, a function computed the value of the damping coefficient of the device needed to obtain the control force input by the controller using the following relation:

$$C(t) = \frac{f(t)}{|\dot{x}(t)|^{\alpha}\mathrm{sgn}(\dot{x})} \tag{4.6.1}$$

Which is obtained from equation (2). If the value of the variable damping coefficient $C(t)$ was inside the attainable range of the device, then it would take that specific value, otherwise, the damping coefficient would saturate at the maximum or minimum limit of the range.

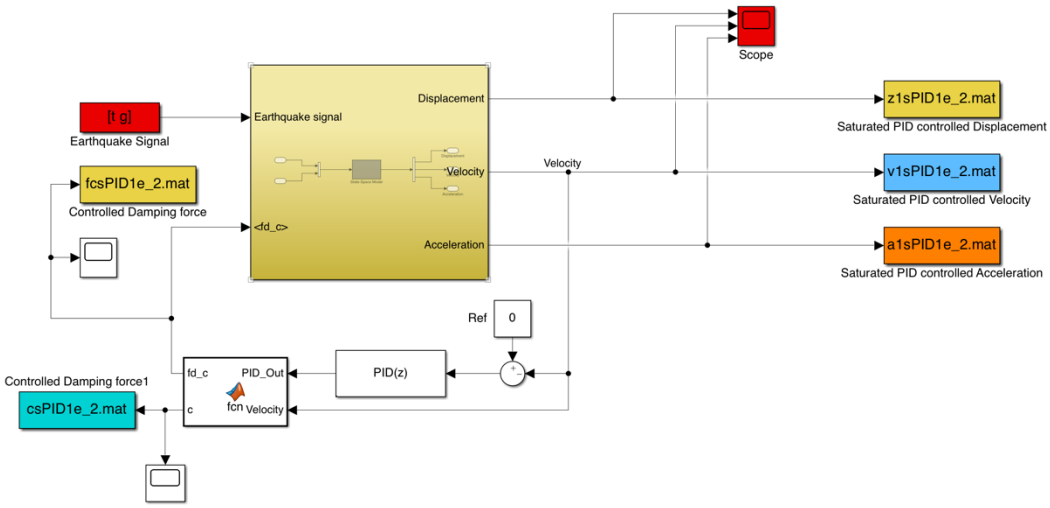

Figure 4.20: Simulink model of a 1 degree of freedom structure implementing PID controller and semi-active fluid viscous damper with a sampling time of one-hundredth of a second

Figure 4.20 shows the model built with the PID controller, choosing a sampling time equal to one-hundredth of a second (100 Hz). A MATLAB function with two inputs, specifically the ideal control force from the PID controller and the velocity from the state space equation of the system computes the value of the damping coefficient and the attainable control force instantaneously to create a feedback loop that models the viscous dashpot model of the semi-active fluid viscous damper. This same model was realized also with a sampling time equal to one millisecond to compare the effectiveness of the results. A variation of this model was built considering the case in which the damper works in a two-stage condition (BangBang strategy). In this case, the damping coefficient can only saturate at the higher or the lower value

depending on if the ideal value of the damping coefficient is above or below a certain threshold. This model was built because typically the semi-active fluid viscous dampers in real-world applications operate in two-stage conditions as mentioned in chapter 2.

A third model with the same structure was built using the MPC control algorithm, again two different sampling times equal to one-hundredth and one-thousandth of a second were applied to simulate different computational weights and to compare the results (respectively 100 Hz and 1000 Hz)

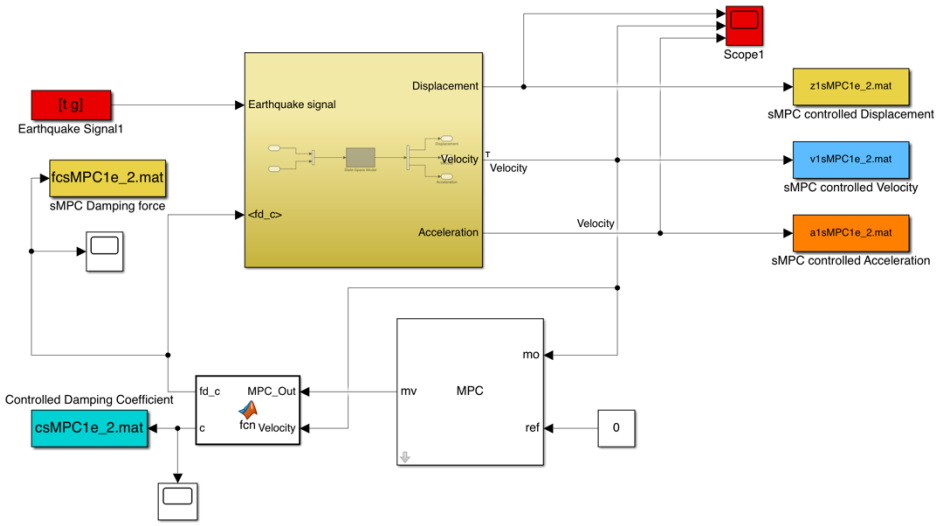

Figure 4.21: Simulink model representing the vibration control of a 1 degree of freedom structure implementing MPC controller and semi-active fluid viscous damper with a sampling time of one-hundredth of a second

Once again, the input from the controller enters a function block that computes the ideal damping coefficient needed to obtain the control force desired from the controller. The function block then outputs the damping coefficient of the device together with the real control force obtained through the viscous dashpot model and inputs it into the system. These models represent an almost physically accurate behaviour of the semi-active fluid viscous damper because the time delay in the variation of the damping coefficient and the noise in the measurement of the velocity signal are still neglected in this modelling phase.

4.8 Results of the viscous dashpot modelling phase

The graphs obtained running the various simulations with different control strategies and sampling times were analysed mainly by exploiting the bar graphs concerning the peak values and the RMSe values of the signals because they give many insights into the ability of the control algorithms to improve the behaviour of the structure through the control of the device.

The three graphs below show the peak values of the displacement, velocity, and acceleration of the suspended mass in the structure. In blue is the signal of the constant damper case, followed by the two MPC simulations with decreasing sampling time, followed again by the four PID simulations, firstly the two with the damping coefficient variable inside the range, and then the two with the two-stage damper (BangBang strategy). Both are in decreasing sampling time.

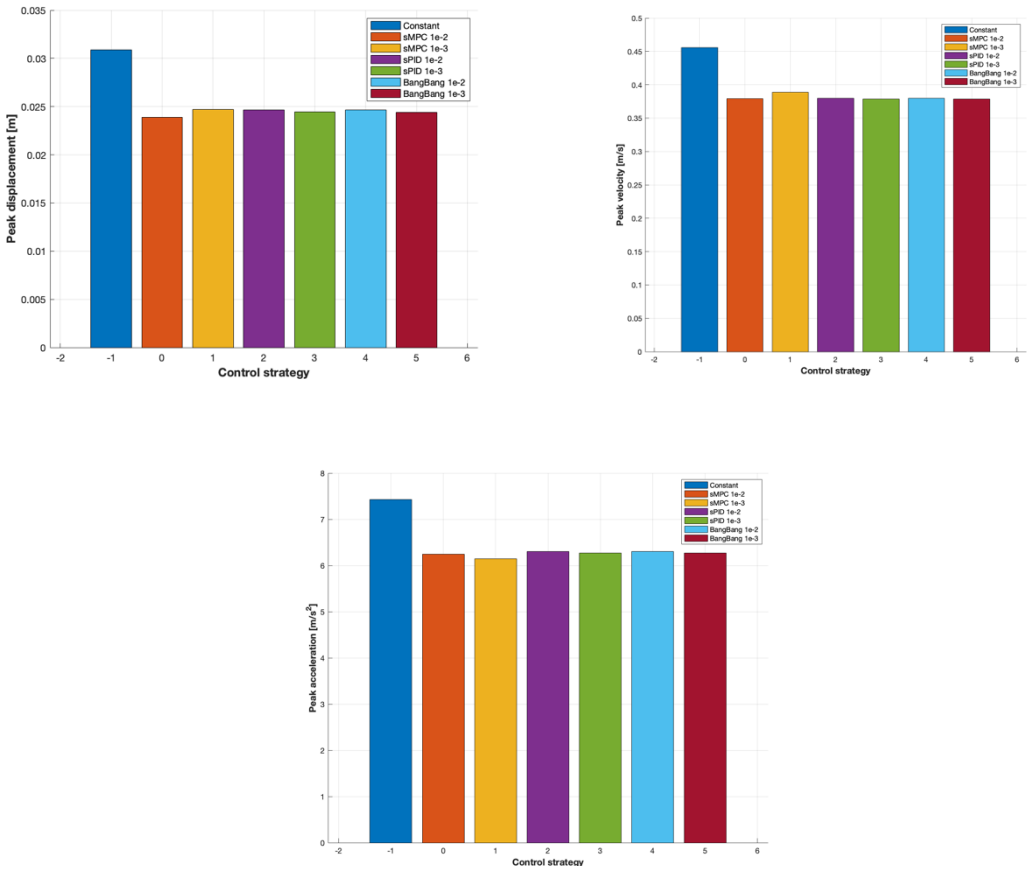

Figure 4.22: Peak values of displacement (top left), velocity (top right), and acceleration (bottom) in constant case (blue), MPC with sampling time 1e-2 (orange), MPC with sampling time 1e-3 (yellow), saturated PID with sampling time 1e-2 (purple), saturated PID with sampling time 1e-3 (green), BangBang with sampling time 1e-2 (light blue), and BangBang with sampling time 1e-3 (dark red).

The first aspect that is evident from the graphs is that any control strategy causes an improvement compared to the behaviour with the constant damper. It is also noticeable that the sampling time of the simulation is not a critical aspect of the peak values of the signals, and that the different control algorithms do not generate any notable improvement in the peaks. Moreover, it is interesting to underline that the results of the PID simulation with the damper able to vary inside the range and the damper in the two-stage form are very similar, this means

that the BangBang strategy works as well as the standard PID one (at reducing the peak values) despite being easier to implement practically in the structure.

The values of RMSe of the signals are interesting to analyse as well:

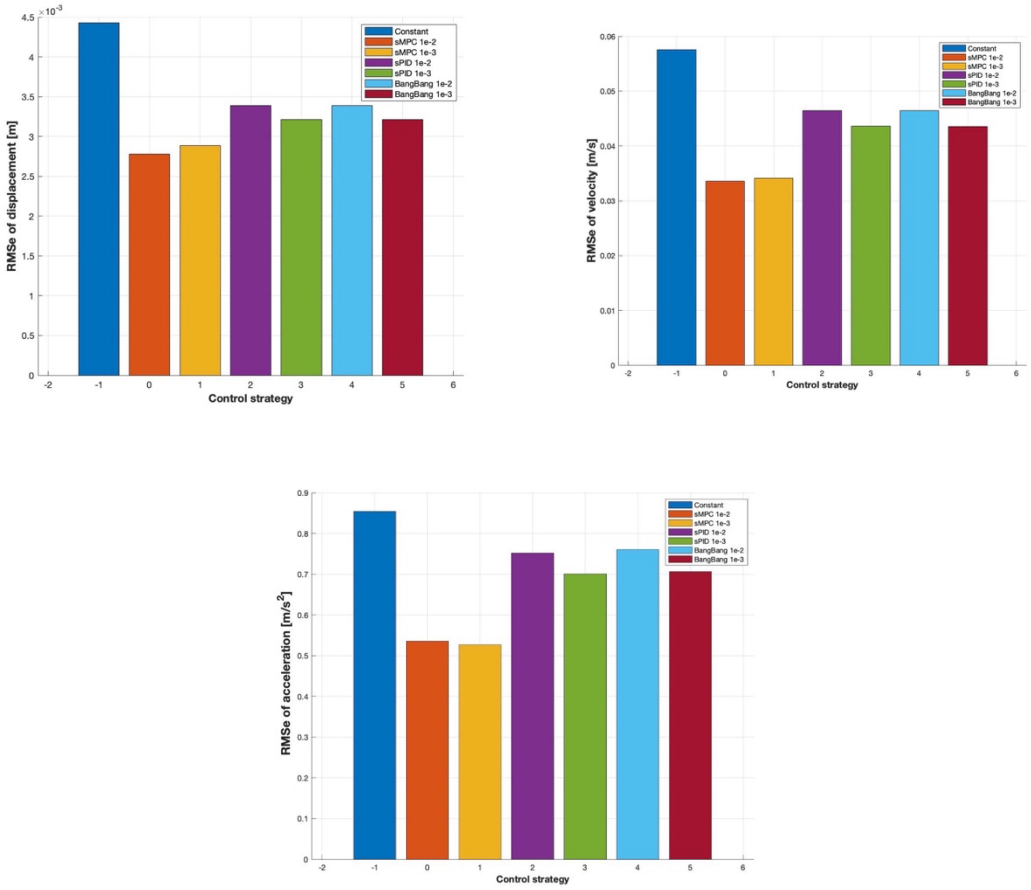

Figure 4.23: RMSe values of displacement (top left), velocity (top right), and acceleration (bottom) in constant case (blue), MPC with sampling time 1e-2 (orange), MPC with sampling time 1e-3 (yellow), saturated PID with sampling time 1e-2 (purple), saturated PID with sampling time 1e-3 (green), BangBang with sampling time 1e-2 (light blue), and BangBang with sampling time 1e-3 (dark red).

The RMSe values of displacement, velocity and acceleration show how, despite not being able of decreasing the peak values of displacement, velocity and acceleration, the Model Predictive Control algorithm still performs better than a standard PID control algorithm, with a decrease of approximately 15% in all signals. Furthermore, it is evident how, also in this case, the BangBang algorithm works as well as the standard PID one even if it is cheaper to install and more convenient from a computational point of view.

4.9 Implementing the delay of the real component

The semi-active fluid viscous damper implements a solenoid valve in the outside loop as illustrated in chapter 2. This valve is a device that requires a certain amount of time to change its position, the delay is typically comprised between 20 and 35 ms. The simulations whose results were shown in the previous pages underline how the ideal semi-active behaviour is effective with both control algorithms (PID and MPC) and were able to improve the performance of the structure by decreasing the peak values and RMSe of displacement, velocity, and acceleration, nevertheless the delay of the physical device was not considered in the model. At this point, the implementation of the delay is a key step to exploring the effectiveness of the real device. The models considered a constant delay of 30 ms, which represents a conservative condition.

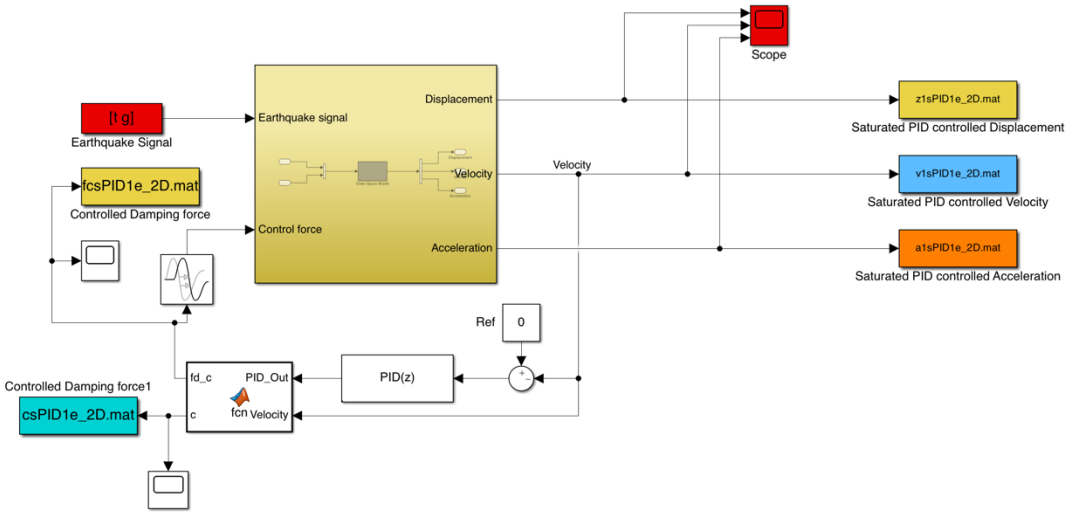

Figure 4.24: Simulink model representing the vibration control of a 1 degree of freedom structure implementing the delay of the real semi-active fluid viscous damper

This same delay implementation was used also for the other simulations, to have a constant reference that allows a linear comparison of the results. Once again, the benchmark for this simulation was done by evaluating peak values and RMSe of displacement, velocity, and acceleration signals.

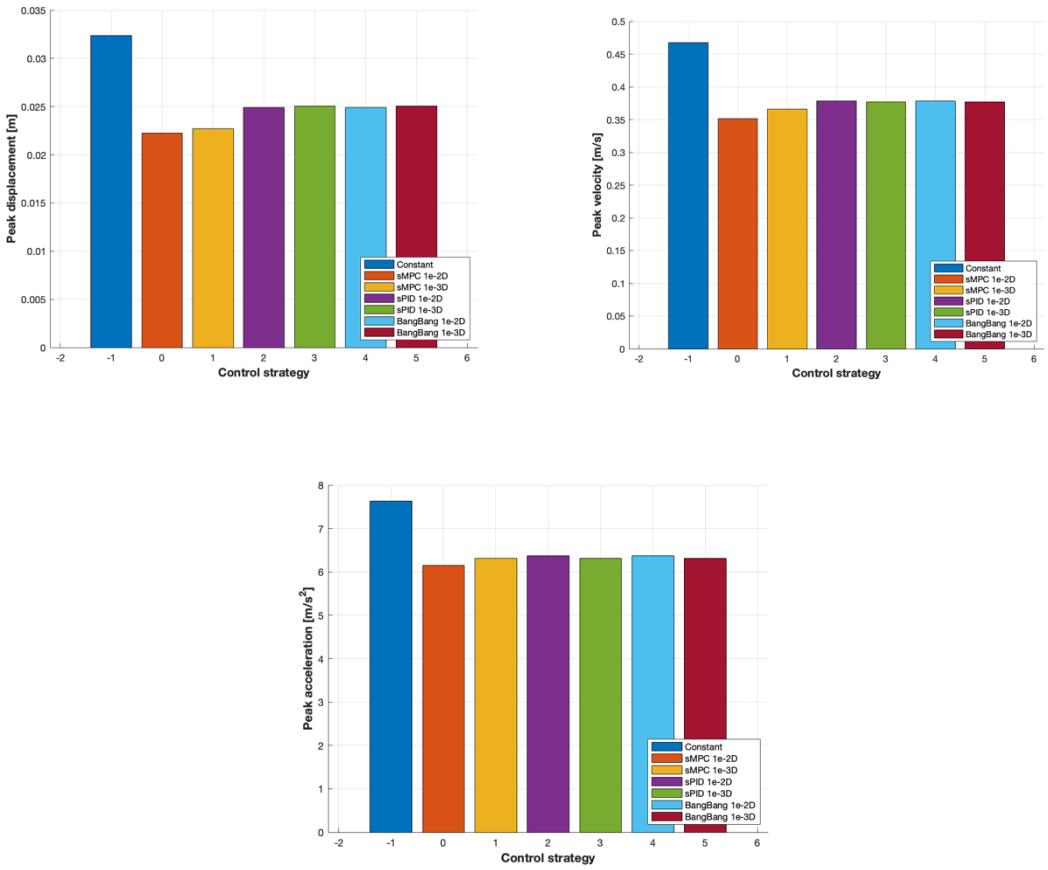

Figure 4.25: Peak values of displacement (top left), velocity (top right), and acceleration (bottom) considering the delay of the solenoid valve of the semi-active fluid viscous damper in constant case (blue), MPC with sampling time 1e-2 (orange), MPC with sampling time 1e-3 (yellow), saturated PID with sampling time 1e-2 (purple), saturated PID with sampling time 1e-3 (green), BangBang with sampling time 1e-2 (light blue), and BangBang with sampling time 1e-3 (dark red).

The first three graphs, present in figure 4.25, show that the peak values are reduced with all the control strategies even if the model now considers the delay of the solenoid valve in the outside loop. This performance improvement results very interesting considering that the delay is a critical aspect from the point of view of the efficiency of the control algorithms. The delay in the input force to the structure represents the main problem in a practical application because it is a factor that directly worsens the quality of the control of the device. It is also interesting to highlight that the entity of the reduction of the peak values is very similar to the one of the simulations without delay (figure 4.20), this implies that the control algorithm is well tuned and does not require a strongly impulsive behaviour from the semi-active device.

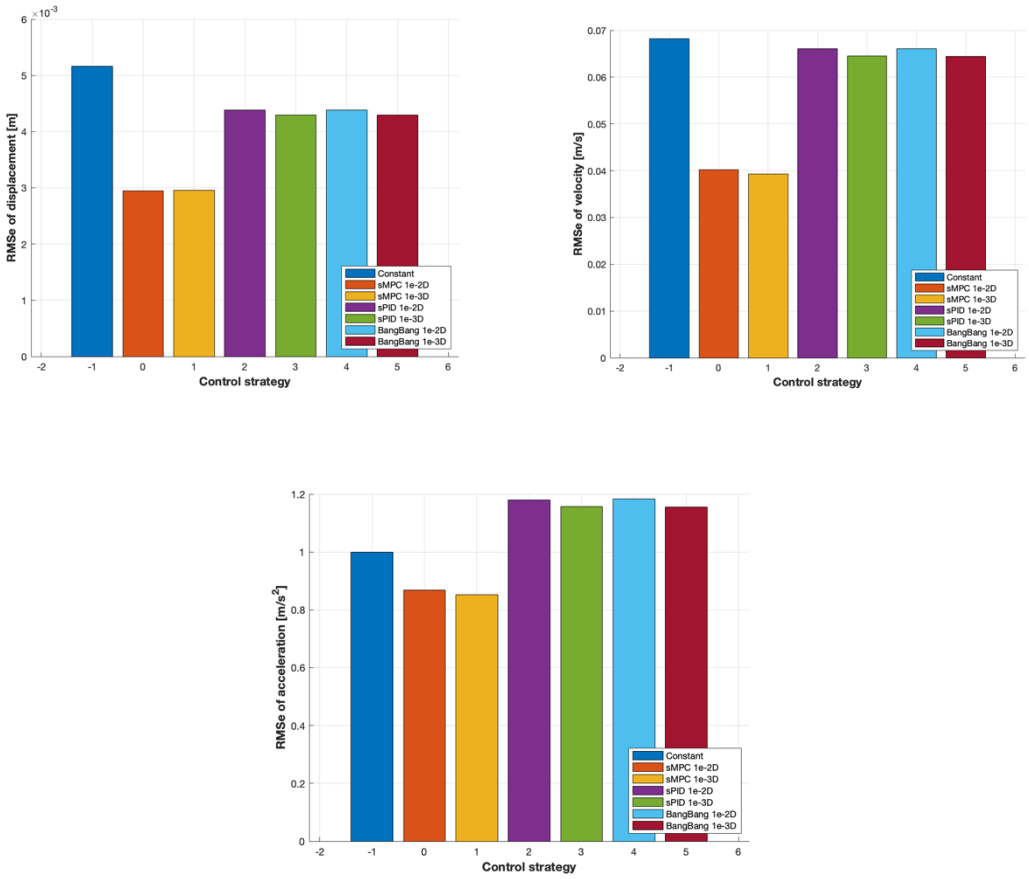

Figure 4.26: RMSe values of displacement (top left), velocity (top right), and acceleration (bottom) considering the delay of the solenoid valve of the semi-active fluid viscous damper in constant case (blue), MPC with sampling time 1e-2 (orange), MPC with sampling time 1e-3 (yellow), saturated PID with sampling time 1e-2 (purple), saturated PID with sampling time 1e-3 (green), BangBang with sampling time 1e-2 (light blue), and BangBang with sampling time 1e-3 (dark red).

In figure 4.26 the graphs show the RMSe values of the model. The results are very interesting and show a trend for which there is a significant difference between the MPC control algorithm and the PID one, plus the introduction of the delay causes a strong variation of the RMSe compared to the previous simulation, present in figure 4.21. In the displacement case, the MPC controller performs significantly better than the PID case, which shows RMSe values very similar to the ones of the constant damper scenario. The RMSe of the velocity signal possesses a similar trend, with the only difference being that the RMSe of the PID simulations is now slightly higher than the constant damper case. The final graph, which is the RMSe of the acceleration shows a different pattern, in which the MPC has a performance level very similar to the constant damper case, while the values of the PID control strategies have values approximately 20% higher than the ones of the constant damper case. The MPC control algorithm performance level is strictly related to its capacity of modifying the response depending on the previous I/O data obtained, a feature that the PID controller does not possess.

The hypothesis for this kind of overall behaviour of the RMSe index and the difference concerning the previous one (without delay) is that the presence of the delay causes a certain degradation of the control loop, therefore making the algorithm less effective at reducing the destabilization of the structure. It is necessary to underline that the simulation was performed with a constant $30\ ms$ delay, which is a condition very close to the worst-case scenario. This data, therefore, can be considered positively in the context of a possible implementation of the semi-active device. In Control theory, the presence of delay in a system is a well-known problem, which can be classified either in loss problems or delay problems [94]. The loss problems happen when the total delay of the system (computing time delay, delayed response of the components, etc) reach a value greater than or equal to the sampling time. The delay problem, instead, happens when the total delay of the system has a value smaller than the sampling time. The context of the last simulation with the delay of the real component falls into the category of loss problems because the entity of the delay is higher than the sampling time chosen for the simulations. In general, the effect of a loss problem to a system result difficult to be analysed for different reasons, such as the fact that the delay must be modelled as a random variable and the different structures of control systems.

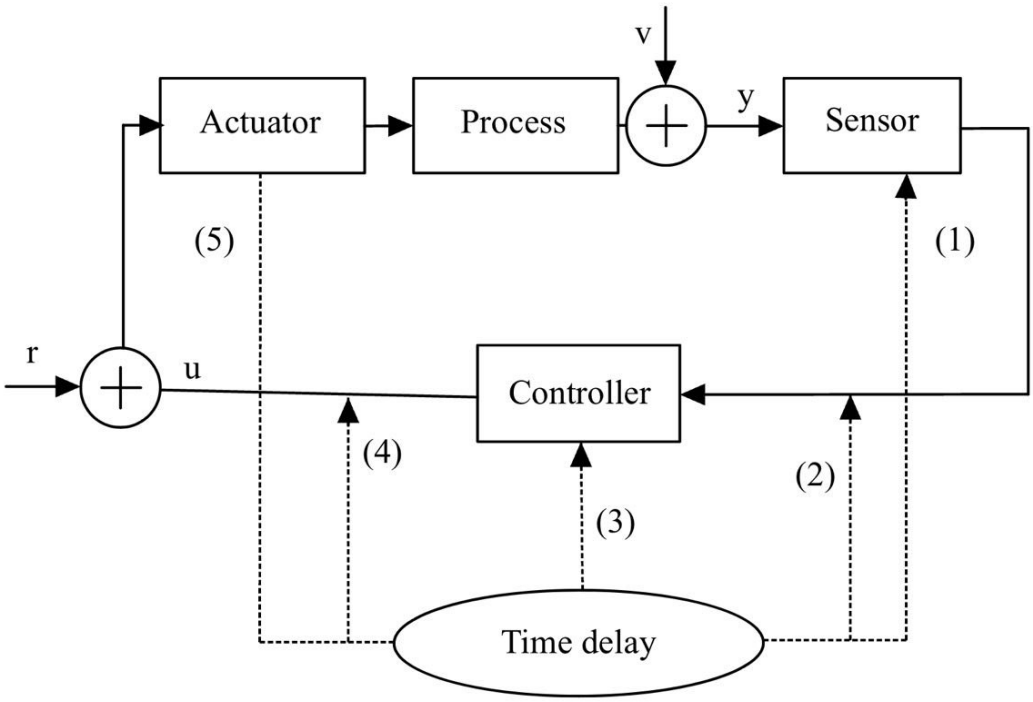

Figure 4.27: Structure of a generic control system and possible sources of delay

Chapter 5

Conclusions

Firstly, this thesis work is posed in a specific application of the very extended topics of vibration optimization and control theory, it does not aim to treat exhaustively the broad number of mathematical and experimental concepts needed for these engineering applications but to introduce fairly well the various tools needed to approach the problem, research for any improvement in the behaviour of the structures and illustrate the advantages of combining different fields such as mechatronics and structural engineering. This thesis work would not have been realized without the influence and insights offered by the many references present in the bibliography, which occasionally explore more in-depth some specific points, and at times move in different research directions, nevertheless, they were fundamental because of the thorough analysis of many subjects, representing the pillars of this work. Likewise, hopefully, this thesis will someday contribute to research and enrich the vast world of scientific knowledge.

After posing the fundamental tools of the control algorithms needed in the third chapter, the fourth chapter explores how it is possible to model in Simulink environment a simple structure relying on the physical equations of motion, initially without a feedback loop and successively including it in the model. A linear model was built because it is more well-fit for the implementation of the various strategies, and it has a reduced level of complexity and computational weight. The comparison between the results of the simulations and the theoretical results presented in chapter 2 allowed to verify the correctness of the model and therefore continue the analysis, introducing the various control algorithms and progressively decreasing the level of approximation at each new simulation. The behaviour of the control algorithms highlighted in general a better performance by the Model Predictive Control than the Proportional Integrative Derivative control structure, the choice of two different sampling frequencies (100 Hz and 1 KHz) showed that the behaviour of the structure improves in both cases and allowed to inspect the possibility of implementing the control algorithm in a real application since the microcontrollers available off the shelf nowadays certainly have enough computing power. In real-world implementations often a trade-off between performance and

complexity of the system is necessary, and for this reason, frequently the PID controller with a BangBang strategy is chosen over other solutions. Although the diagrams in figure 4.25 and 4.26 showed a partial improvement for the BangBang strategy, in which only the peak values decreased with respect to the case in which the damper was in a passive working condition, it is necessary to underline that the MPC control algorithm poses at each sampling instant an optimization problem, which must be solved with a numerical algorithm, has to be feasible, and may have stability issues if the robustness to noises is not considered in the design; the PID, on the other hand, has a much simpler structure, in which the algorithm operates thanks to the different parameters (gains) that are set and fixated in the design procedure without any specific real-time requirement and the noises are typically filtered with low pass filters. Finally, the BangBang strategy considers only two levels of damping coefficient in the device, corresponding to a fully open valve (minimum damping) and a fully closed valve (maximum damping) which is less problematic than having a variable damping coefficient inside the available range.

Appendix A

1. Control theory results useful for the application

This appendix contains some basic results of control theory reported here for completeness and sometimes applied in a specific civil engineering context. The appendix is preparatory for chapter 3 of the thesis.

To analyze the consequences of a control strategy to a simple structure model, let us consider a structure with n-degrees of freedom that can be modelled as a mass-spring-damper system. The equilibrium of forces of the system is written as:

$$\boldsymbol{M}\ddot{\boldsymbol{x}}(t) + \boldsymbol{C}\dot{\boldsymbol{x}}(t) + \boldsymbol{K}\boldsymbol{x}(t) = \boldsymbol{D}\boldsymbol{u}(t) + \boldsymbol{E}\boldsymbol{f}(t) \tag{A.1.1}$$

In which $\boldsymbol{M}$, $\boldsymbol{C}$ and $\boldsymbol{K}$ represent, respectively, the mass, damping and stiffness matrices $(n \times n)$, $\boldsymbol{x}(t)$ represents the n-dimensional displacement vector, the $n \times m$ matrix $\boldsymbol{D}$ represents the position of the actuators, $\boldsymbol{u}(t)$ is the m-dimensional vector of the actuator forces, $\boldsymbol{E}$ is the $n \times r$ matrix representing the location of the excitement and $\boldsymbol{f}(t)$ is the r-dimensional vector of the external excitation.

Let us consider a control strategy in which the control vector $\boldsymbol{u}(t)$ is linearly proportional to $\boldsymbol{x}(t)$, $\dot{\boldsymbol{x}}(t)$ and $\boldsymbol{f}(t)$. The control force fed back to the system is given by

$$\boldsymbol{u}(t) = \overline{\boldsymbol{C}}\dot{\boldsymbol{x}}(t) + \overline{\boldsymbol{K}}\boldsymbol{x}(t) + \overline{\boldsymbol{E}}\boldsymbol{f}(t) \tag{A.1.2}$$

In which $\overline{\boldsymbol{C}}$, $\overline{\boldsymbol{K}}$ and $\overline{\boldsymbol{E}}$ are the respective gains that can be a function of time as well.

By substituting equation (A.1.2) in equation (A.1.1) the following relation is obtained

$$\boldsymbol{M}\ddot{\boldsymbol{x}}(t) + (\boldsymbol{C} - \boldsymbol{D}\overline{\boldsymbol{C}})\dot{\boldsymbol{x}}(t) + (\boldsymbol{K} - \boldsymbol{D}\overline{\boldsymbol{K}})\boldsymbol{x}(t) = (\boldsymbol{E} + \boldsymbol{D}\overline{\boldsymbol{E}})\boldsymbol{f}(t) \tag{A.1.3}$$

It is possible to notice, comparing equation (A.1.3) with equation (A.1.1), that feedback control acts on the system modifying the stiffness and the damping matrices, which represent the structural parameters, in a way that aims at optimizing the structural response, and the entity of this modification entirely depends on the control strategy chosen. Feedforward control, conversely, acts aiming at a reduction of the excitation received by the system.

By contrast, the effect of passive control on a system is less complete, as a matter of fact, in this configuration there are no feedback signals, nor the necessity of measuring any stimulation because there is no possibility of acting on the system through actuators, in fact, passive control is also referred to as "structure redesign".

To clarify the difference between the two strategies, let us consider once again the mass-spring-damper system, but this time in a static condition

$$\boldsymbol{M}\ddot{\boldsymbol{x}}(t) + (\boldsymbol{C} + \Delta\boldsymbol{C})\dot{\boldsymbol{x}}(t) + (\boldsymbol{K} + \Delta\boldsymbol{K})\boldsymbol{x}(t) = 0 \tag{A.1.4}$$

Passive control chooses a new stiffness (or damping depending on the specific type of device) *before* the system is put into motion meaning that $\Delta\boldsymbol{C}$ and $\Delta\boldsymbol{K}$ cannot be modified in real-time. By comparing these two strategies, it is clear that the first one has a much more radical effect on the system and is able to enhance in a better way the dynamic performances.

To analyze thoroughly the control theory, it is necessary to introduce the state equation form, which is fundamental for computer simulations, single-input-single-output (SISO) and multi-input-multi-output (MIMO) systems, as well as time-varying and stochastic systems.

A relevant amount of configurations can be modelled by a set of first-order differential equations which can be described as

$$\dot{z}(t) = g(z(t), u(t), t) \tag{A.1.5}$$

In which $z(t)$ is the *state* vector of the system, $u(t)$ is the *input* vector that is representative of external forces and also disturbances. $u(t)$ can either be controlled or fixated by external factors. For linear time-invariant systems (LTI) the equation reduces to

$$\dot{z} = Az + Bu \tag{A.1.6}$$

Therefore, equation (A.1.6) represents the state-space form of a LTI system, which is the focus of this dissertation, considering that structural systems can be represented fairly well by this kind of model.

Let us consider a two-story structure, typically the state vector is chosen to be the horizontal displacement of the building, considering that the main components of the input (wind, earthquakes) are directed perpendicularly to the ground direction. The equations of motion of the system are

$$\begin{gathered} m_1\ddot{x}_1(t) + c_1\dot{x}_1(t) - c_2[\dot{x}_2(t) - \dot{x}_1(t)] + \\ +k_1x_1(t) - k_2[x_2(t) - x_1(t)] = u_1(t) \end{gathered} \tag{A.1.7}$$

$$m_2\ddot{x}_2(t) + c_2[\dot{x}_2(t) - \dot{x}_1(t)] + k_2[x_2(t) - x_1(t)] = u_2(t)$$

In which m_i, c_i and k_i represent respectively mass, damping coefficient and stiffness associated with the i-th story of the structure and $u_i(t)$ the external force related to the i-th floor.

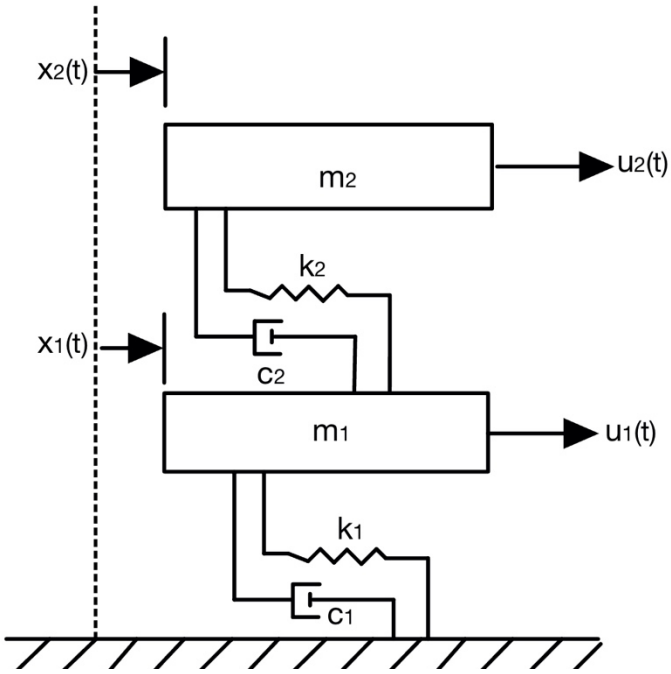

Figure A.1: Scheme of a two-story structure

The process to convert the equilibrium of the system (A.1.7) into state space form starts by selecting the state vector of the system

$$z = [x_1 \quad x_2 \quad y_1 \quad y_2]^T \tag{A.1.8}$$

Where the superscript T refers to the transpose of the vector. Equation (A.1.7) can now be rewritten as:

$$\begin{gathered} \dot{x}_1 = y_1 \\ \dot{x}_2 = y_2 \\ m_1\dot{y}_1 = -c_1 y_1 + c_2(y_2 - y_1) - k_1 x_1 + k_2(x_2 - x_1) + u_1 \\ m_2\dot{y}_2 = -c_2(y_2 - y_1) - k_2(x_2 - x_1) + u_2 \end{gathered} \tag{A.1.9}$$

With this notation, it is now possible to reconstruct the equations in the form given in (A.1.6) in which A, B and u are defined as:

$$A = \begin{bmatrix} 0_2 & I_2 \\ K & C \end{bmatrix} \qquad B = \begin{bmatrix} 0_2 \\ M^{-1} \end{bmatrix} \qquad u = \begin{bmatrix} u_1 \\ u_2 \end{bmatrix} \tag{A.1.10}$$

Where I_2 is the $2\ x\ 2$ identity matrix, 0_2 is the $2\ x\ 2$ null matrix and M^{-1} is the inverse of the mass matrix.

$$K = \begin{bmatrix} -\frac{k_1 + k_2}{m_1} & \frac{k_2}{m_1} \\ \frac{k_2}{m_2} & -\frac{k_2}{m_2} \end{bmatrix} \tag{A.1.11}$$

$$C = \begin{bmatrix} -\frac{c_1 + c_2}{m_1} & \frac{c_2}{m_1} \\ \frac{c_2}{m_2} & -\frac{c_2}{m_2} \end{bmatrix} \tag{A.1.12}$$

$$M = diag[m_1 \quad m_2] \tag{A.1.13}$$

The state vector can be representative of any physical quantity that is of interest for the application, therefore not necessarily a displacement or a velocity.

2. Solution of the state equation

Considering the LTI case and the simplified case given by

$$\dot{z} = Az \tag{A.2.1}$$

Having as the initial value of the state vector

$$z(t_0) = z_0 \tag{A.2.2}$$

It is possible to prove that the solution to equation (A.2.1) always exists and can be written as

$$z(t) = \Phi(t, t_0) z_0, \qquad t \geq t_0 \tag{A.2.3}$$

Where $\Phi(t, t_0)$ is referred to as *transition matrix* in literature and is the solution of the differential equation in matrix form

$$\Phi(t, t_0) = A\Phi(t, t_0), \qquad \Phi(t, t_0) = I \tag{A.2.4}$$

In which $\Phi(t, t_0)$ has the specific formulation

$$\Phi(t, t_0) = \Phi(t - t_0) = e^{(t - t_0)A} = 1 + (t - t_0)A + \frac{1}{2!}[(t - t_0)A]^2 + \cdots \tag{A.2.5}$$

Which converges for any A. The elements of $\Phi(t, t_0)$ can straightforwardly be written down when A, called *system matrix*, can be diagonalized. Let us consider A to be a $n \times n$ matrix with eigenvalues λ_j, with $j = 1, \cdots, n$ and eigenvectors η_j, with $j = 1, \cdots, n$, this implies

$$\eta_j^T \eta_j = 1, \qquad j = 1, \cdots, n \tag{A.2.6}$$

Introducing the $n \times n$ matrix T and the $n \times n$ matrix Λ

$$T = [\eta_1, \eta_2, \dots, \eta_j] \tag{A.2.7}$$

$$\Lambda = diag[\lambda_1, \lambda_2, \dots, \lambda_j] \tag{A.2.8}$$

It is possible to write A as a function of T and Λ:

$$A = T\Lambda T^{-1} \tag{A.2.9}$$

And this is a fundamental result because it allows writing the transition matrix as

$$\Phi(t - t_0) = e^{(t-t_0)A} = Te^{(t-t_0)\Lambda} T^{-1} \tag{A.2.10}$$

With

$$e^{(t-t_0)\Lambda} = diag[e^{(t-t_0)\lambda_1}, e^{(t-t_0)\lambda_2}, \dots, e^{(t-t_0)\lambda_n}] \tag{A.2.11}$$

The diagonalization is feasible when the quantity of linearly independent eigenvectors for each eigenvalue is equal to its multiplicity, otherwise, other mathematical instruments are needed such as the Jordan form, not investigated in this dissertation.
Considering now the most general case introduced in (A.1.6)

$$\dot{z} = Az + Bu \tag{A.2.12}$$

The solution of the state equation is obtained through the Lagrange equation

$$z(t) = e^{At} z_0 + \int_{0_-}^{t} e^{A(t-\tau)} Bu(\tau) d\tau = z_{zi}(t) + z_{zs}(t) \tag{A.2.13}$$

And, as noticeable, the solution of an LTI system can be split into two independent contributions: $z_{zi}(t)$, zero-input response and $z_{zs}(t)$, zero-state response. The first one corresponds to the response of the state of the system considering only the initial conditions and no external inputs, while the second one is the complementary term giving information about the behaviour of the system with null initial conditions and only the influence of the input.
The output response can be derived from the following equation

$$y(t) = Cz(t) + Du(t) \tag{A.2.14}$$

Where C is the $q \times n$ *output matrix* and D is the $q \times p$ *input-output matrix.* By substituting equation (A.2.12) in equation (A.2.13) it is possible to obtain

$$y(t) = Ce^{At}z_0 + C\int_{0_-}^{t} e^{A(t-\tau)}Bu(\tau)d\tau + Du(t) = y_{zi}(t) + y_{zs}(t) \tag{A.2.15}$$

And, also, in this case, the response can be split into two contributions: $y_{zi}(t)$, the zero-input output response and $y_{zs}(t)$, the zero-state output response. In the control theory context, to decrease the computational weight of the procedure and avoid solving differential equations, the Laplace transform is exploited

$$F(s) = \mathcal{L}\{f(t)\} = \int_{0}^{\infty} f(t)\, e^{-st}dt \tag{A.2.16}$$

With $f(t)$ being a unilateral time function $f(t)$: $\mathbb{R}^+ \to \mathbb{R}$, the unilateral Laplace transform of $f(t)$ is a complex function $F(s)$: $\mathbb{C} \to \mathbb{C}$, and $s = \sigma + j\omega$. The inverse Laplace transform is defined as

$$f(t) = \mathcal{L}^{-1}\{F(s)\} = \frac{1}{2\pi j}\int_{\sigma-j\omega}^{\sigma+j\omega} F(s)\, e^{st}ds, \quad t \in \mathbb{R}^+ \tag{A.2.17}$$

The Laplace transform possesses some important properties, illustrated below:

- **Linearity** – Being $f_1(t)$ and $f_2(t)$ unilateral time functions, with $F_1(s) = \mathcal{L}\{f_1(t)\}$, $F_2(s) = \mathcal{L}\{f_2(t)\}$ and $c_1, c_2 \in \mathbb{R}$, then:

$$\mathcal{L}\{c_1f_1(t) + c_2f_2(t)\} = c_1F_1(s) + c_2F_2(s)$$

- **Time integration** – Assuming $f(t)$ equal to an integrable unilateral time function with $F(s) = \mathcal{L}\{f(t)\}$, then:

$$\mathcal{L}\left\{\int_{0}^{t} f(t)dt\right\} = \frac{F(s)}{s}$$

- **Time derivation** - Assuming $f(t)$ equal to a n-times derivable unilateral time function with $F(s) = \mathcal{L}\{f(t)\}$, then:

$$\mathcal{L}\{\dot{f}(t)\} = sF(s) - f(0_-)$$
$$\mathcal{L}\{\ddot{f}(t)\} = s^2F(s) - sf(0_-) - \dot{f}(0_-)$$
$$\vdots$$
$$\mathcal{L}\{f^{(n)}(t)\} = s^nF(s) - s^{n-1}f(0_-) - s^{n-2}\dot{f}(0_-) - \cdots - f^{(n-1)}(0_-)$$

- **Time convolution** - Being $f_1(t)$ and $f_2(t)$ unilateral time functions, with $F_1(s) = \mathcal{L}\{f_1(t)\}$, $F_2(s) = \mathcal{L}\{f_2(t)\}$ the convolution product admits Laplace transform and is:

$$f_1(t) * f_2(t) = \int_{0_-}^{t} f_1(t-\tau) \cdot f_2(\tau)d\tau = \int_{0_-}^{t} f_1(\tau) \cdot f_2(t-\tau)d\tau$$
$$\mathcal{L}\{f_1(t) * f_2(t)\} = F_1(s) \cdot F_2(s)$$

- **Time delay** – Let $f(t)$ a unilateral time function with $F(s) = \mathcal{L}\{f(t)\}$, then:

$$\mathcal{L}\{f(t-\tau)\} = F(s)e^{-\tau s}$$

- **Final value theorem** - Being $f(t)$ a unilateral time function with $F(s) = \mathcal{L}\{f(t)\}$ and supposing that all the roots of the denominator polynomial of $sF(s)$ have strictly negative real part, then:

$$\lim_{t\to\infty} f(t) = \lim_{s\to 0} sF(s)$$

- **Initial value theorem** - Being $f(t)$ a unilateral time function with $F(s) = \mathcal{L}\{f(t)\}$, then:

$$\lim_{t\to 0} f(t) = \lim_{s\to\infty} sF(s)$$

Through the Laplace transform, the set of equations given by (A.1.6) and (A.2.13) becomes

$$Z(s) = (sI - A)^{-1}z_0 + (sI - A)^{-1}BU(s)$$
$$Y(s) = C(sI - A)^{-1}z_0 + [C(sI - A)^{-1}B + D]U(s) \quad \text{(A.2.18)}$$

Where $Z(s)$ and $Y(s)$ are respectively the Laplace transform of the state vector and the output vector. In presence of zero initial conditions ($z_0 = 0$) the solution of a LTI dynamical system

can be expressed in terms of the *transfer function* of the system, defined as the ratio between the Laplace transforms of the system output and input

$$H(s) = \frac{Y(s)}{U(s)} \tag{A.2.19}$$

3. Frequency response

Considering a LTI system in the frequency domain, it is possible to analyze the response through an input of the form:

$$u(t) = ae^{j\omega t}, \qquad u(0) = 0, \qquad t \geq 0 \tag{A.3.1}$$

Substituting in (A.1.6), the following steady state solution of the state equation is obtained:

$$z(t) = H(j\omega)ae^{j\omega t} \tag{A.3.2}$$

In which:

$$H(j\omega) = (j\omega I - A)^{-1}B \tag{A.3.3}$$

Is referred to as the *frequency response matrix*. It is very important since its knowledge leads directly to the solution of the state equation for a LTI system. This happens because, thanks to the linearity of the system, the superposition principle can be applied, and also because the input can in general be represented as a sum of sinusoids. It can be noticed that it is equal to the transfer function $H(s)$ in which the Laplace variable s has been substituted with $j\omega$.

4. Stability

In the context of LTI systems analysis, it is possible to distinguish two different kinds of stabilities. The first one is called *internal stability* and refers to the boundedness of the zero-input response of the state equation for any initial state z_0. The second type of stability is called *bounded-input-bounded-output* stability and relates to the boundedness of the zero-state response in presence of any input $u(t)$. Stability is probably the most important feature of a LTI system. System matrix A has n eigenvalues λ_j and eigenvectors $\eta_j, j = 1, \cdots, n$, the state as a function of time can be written as

$$z(t) = \sum_j g_j e^{\lambda_j t}\, \eta_j \tag{A.4.1}$$

Where g_j are real numbers function of the initial state z_0. Therefore, the stability features of a LTI system are given by the eigenvalues λ_j. A LTI system is *internally stable* if and only if all the eigenvalues have a real part smaller or equal to zero and those with a null real part have unitary minimal polynomial multiplicity.

A LTI system is *asymptotically stable* if and only if all the eigenvalues have a real part strictly smaller than zero.

Since real-world physics systems are not perfectly linear, they are typically linearized around a certain equilibrium point, therefore it is more interesting to analyze the stability in terms of a given equilibrium point of the system. Considering the state equation in the form:

$$\dot{z}(t) = Az(t), \qquad z(t_0) = z_0 \tag{A.4.2}$$

An *equilibrium point* z_e of the system is defined such as:

$$Az_e = 0 \tag{A.4.3}$$

Which is unique if the system matrix A is nonsingular. Lyapunov stability theorem states that an equilibrium state z_e is said to be *stable* if, for any t_0 and $\alpha > 0$ there exist a number $\delta(t_0, \alpha) \in \mathbb{R}$ such that:

$$\|z_0 - z_e\| \leq \delta \tag{A.4.4}$$

Which implies

$$\|z(t) - z_e\| < \varepsilon \tag{A.4.5}$$

(True for all $t \geq t_0$. In the case in which δ is not a function of t_0, the equilibrium state is called *uniformly stable*. Lyapunov stability is not a "strong" kind of stability, therefore criteria with stricter requirements are also introduced in this context.

An equilibrium state z_e is referred to as *asymptotically stable* if for any time instant there exists a constant $\delta > 0$, which can also be a function of the initial conditions, such that:

$$\|z_0 - z_e\| \leq \delta \tag{A.4.6}$$

With

$$\|z(t) - z_e\| \to 0, \qquad t \to \infty \tag{A.4.7}$$

And this condition implies that the state converges to the equilibrium point as the time converges to infinity when the state is closer than δ to the equilibrium point.

An equilibrium state z_e is referred to as *exponentially stable* if there exists two real constants $\alpha, \beta > 0$, such that

$$\|z(t) - z_e\| \leq \alpha e^{-\beta(t-t_0)}\|z_0\|, \qquad t \geq t_0 \tag{A.4.8}$$

For any z_0. This condition implies that the state of an *exponentially stable* system converges to the equilibrium point in an exponential fashion without regard to the initial conditions. For linear systems, however, the stability of an equilibrium state also implies the stability of any other solution.

5. Controllability and Observability

In control theory, some basic questions about the characteristics of the system to be controlled have to be asked, because they are necessary to properly operate on the system under study. Controllability (also referred to as reachability in literature) refers to the ability of a system to switch from an initial state to any other one due to the effect of the input $u(t)$.

A dynamic system $\dot{z} = Az + Bu$, is said *reachable* if and only if the *reachability matrix*

$$M_R = [B \quad AB \quad \cdots \quad A^{n-1}B] \tag{A.5.1}$$

is full rank (rank equal to n).

Observability analyzes if the dynamical system allows one to determine the state simply by knowing the input and output time course.

A dynamic system $\dot{z} = Az + Bu;\ y(t) = Cz(t) + Du(t)$ is said *observable* if and only if the *observability matrix*

$$M_O = [C \quad CA \quad \cdots \quad CA^{n-1}]^T \tag{A.5.2}$$

is full rank (rank equal to n).

Bibliography

[1] Adeli H., "High-performance computing for large-scale analysis, optimization and control", Journal of Aerospace Engineering, ASCE, 13(1), pp. 1–10.

[2] Adeli H., Cheng N.T., "Concurrent genetic algorithms for optimization of large structures", Journal of Aerospace Engineering, ASCE, 7(3), pp. 276–296.

[3] Adeli H., Hsu H.L., "Optimization of space trusses on a vector multiprocessor", Journal of Aerospace Engineering, ASCE, 7(1), pp. 120–126.

[4] Adeli H., Hung, S.L., "A concurrent adaptive conjugate gradient learning algorithm on MIMD machines", Journal of Supercomputer Applications, MIT Press, 7(2), pp. 155–166.

[5] Adeli H., Kamal O., "Concurrent analysis of large structures – I – algorithms", Computers and Structures, 42(3), pp. 413–424.

[6] Adeli H., Kamal O., "Concurrent analysis of large structures – II – applications", Computers and Structures, 42(3), pp. 425–432.

[7] Adeli H., Kamal O., Parallel Processing in Structural Engineering, Elsevier Applied Science, London.

[8] Adeli H., Kumar S., "Concurrent structural optimization on a massively parallel supercomputer", Journal of Structural Engineering, ASCE, 121(11), pp. 1588–1597.

[9] Adeli H., Kumar S., "Distributed finite element analysis on a network of workstations—algorithms", Journal of Structural Engineering, ASCE, 121(10), pp. 1448–1455 (1995).

[10] Adeli H., Kumar S., "Distributed genetic algorithms for structural optimization", Journal of Aerospace Engineering, 8(3), pp. 156–163.

[11] Adeli H., Saleh A. "Integrated structural/control optimization of large adaptive/smart structures", International Journal of Solids and Structures, 35(28–29), pp. 3815–3830.

[12] Adeli H., Saleh, A., "Optimal control of adaptive/smart bridge structures", Journal of Structural Engineering, ASCE, 123(2), pp. 218–226.

[13] Adeli H., Soegiarso R., High-Performance Computing in Structural Engineering, CRC Press, Boca Raton, Florida.

[14] Agrawal A.K., Yang J.N., Schmitendorf, W.E. and Jabbari, F. "Stability of actively controlled structures with actuator saturation", Journal of Structural Engineering, 123(11), pp. 1497–1505 (1997).

[15] Bauer H. F., "Oscillations of immiscible liquids in a rectangular container: a new damper for excited structures", Journal of Sound and Vibration, 93(1),117-133.

[16] Bemporad A., Morari M, "Control of systems integrating logic, dynamics, and constraints", Automatica, vol. 35, no. 3, pp. 407–427.

[17] Bemporad A., Morari M, Dua V., E.N. Pistikopoulos, "The explicit linear quadratic regulator for constrained systems", Automatica, vol. 38, no. 1, pp. 3–20.

[18] Bemporad A., Morari M., "A multiparametric quadratic programming algorithm with polyhedral computations based on nonnegative least squares", IEEE Trans. Automatic Control, vol. 60, no. 11, pp. 2892–2903.

[19] Bergman D. M., Goel S. C., "Evaluation of cyclic testing of steel-plate devices for added damping and stiffness", Rep. No. UMCE 87-10, University of Michigan, Ann Arbor, Michigan.

[20] Bhardwaj M.K., Datta, T.K., "Semi-active fuzzy control of seismic response of building frame", Journal of Structural Engineering, 132(5), pp. 791–799.

[21] Borrelli F., Bemporad A., Morari M., (2017), "Predictive Control for Linear and Hybrid Systems", Cambridge: Cambridge University Press.

[22] Chang K. C., Chen S. J., Hsu C. J., Chou F.P., Lai M. L, "Inelastic seismic behavior of a three-story steel frame with added viscoelastic dampers", Proc. First World Conference on Structural Control, Vol. 2, TP3-117-TP3-126.

[23] Chang K. C., Soong T. T., Oh S.T., Lai M. L., "Seismic behavior of steel frame with added viscoelastic dampers", Journal of Structural Engineering, 121(10), 1418-1426.

[24] Chase J.G., Breneman S.E., Smith, H.A., "Robust H∞ static output feedback control with actuator saturation", Journal of Engineering Mechanics, 125(2), pp. 225–233.

[25] Constantinou M. C., Symans M. D., "Experimental and analytical investigation of seismic response of structures with supplemental fluid viscous dampers", NCEER Rep. 92-0032, State University of New York at Buffalo, Buffalo, N.Y.

[26] Crowe, J., Johnson, M., PID control. In M. Johnson, & M. Moradi (Eds.), "PID Control: New Identification and Design Methods", London: Springer.

[27] D. Bernardini, A. Bemporad, "Stabilizing model predictive control of stochastic constrained linear systems", IEEE Trans. Automatic Control, vol. 57, no. 6, pp. 1468–1480.

[28] Dong P., Fan J., "Semiactive Wind Response Control of 76-Story Benchmark Building with Smart Piezoelectric Friction Dampers", Advanced Materials Research, 250-253, 2196–2201.

[29] Dyke S.J., Caicedo J.M., Turan G., Bergman L.A., Hague, S., "Phase I benchmark control problem for seismic response of cable-stayed bridges", Journal of Structural Engineering, 129(7), pp. 857–872.

[30] F.D. Torrisi, A. Bemporad, HYSDEL, "A tool for generating computational hybrid models", IEEE Trans. Contr. Systems Technology, vol. 12, no. 2, pp. 235–249.

[31] Fisco N.R., Adeli, H., Smart structures: Part I—Active and semi-active control. Scientia Iranica, 18(3), 275–284, DOI:10.1016/j.scient.2011.05.034.

[32] Foutch D.A., Wood S. L., Brady P. A., "Seismic retrofit of nunductile reinforced concrete frames using viscoelastic dampers", Proc., of ATC 17-1 on Seismic Isolation, Passive Energy and Active Control, Vol. 2, 605-610.

[33] Fujino Y., Pacheco B. M., Chaiseri P., Sun L. M., "Parametric studies on tuned liquid damper (TLD) using circular containers by a free oscillation experiments", Structural Engineering/Earthquake Engineering, 5(2), 381s-391s.

[34] Guclu R., Yazici, H. "Vibration control of a structure with ATMD against earthquake using fuzzy logic controllers", Journal of Sound and Vibration, 313(1–2), pp. 36–49.

[35] Guéraud R., Noël-Leroux J. P., Livolant M., Michalopoulos A. P., "Seismic isolation using sliding-elastomer bearing pads", Journal of Nuclear Engineering and Design, 84, 363-377.

[36] Hiemenz G.J., Choi Y.T., Wereley, N.M. "Seismic control of civil structures utilizing semi-active MR braces", Computer-Aided Civil and Infrastructure Engineering, 18(1), pp. 31–44.

[37] Housner G.W., Bergman L.A., Caughey T.K., Chassiakos A.G., Claus R.O., Masri S.F., Skelton R.E., Soong T.T., Spencer B.F., Yao J.T.P., "Structural control: Past, present, and future", Journal of Engineering Mechanics Volume 123, Issue 9, Pages 897 – 971 September 1997, 10.1061/(ASCE)0733-9399(1997)123:9(897).

[38] Hsu H.L., Adeli H., "A microtasking algorithm for optimization of structures", International Journal of Supercomputer Applications, 5(2), pp. 81–90.

[39] Hung S.L., Adeli H., "A parallel genetic/neural network learning algorithm for MIMD shared memory machines", IEEE Transactions on Neural Networks, 5(60), pp. 900–909.

[40] Hung S.L., Adeli, H., "Parallel backpropagation learning algorithms on cray Y-MP8/864 supercomputer", Neurocomputing, 5(6), pp. 287–302.

[41] Ikeda Y., Sasaki M., Sakamoto M., Kobori T., "Active mass driver system as the first application of active structural control", Earthquake Engineering and Structural Dynamics, 30(11), pp. 1575–1595.

[42] Jabbari, F., Bobrow J.E., "Vibration suppression with resettable device", Journal of Engineering Mechanics, 128(9), pp. 916–924.

[43] Jangid R. S., Datta T. K., "Seismic behaviour of base-isolated buildings: a state-of-the-art review", Proc. Instn Ciu. Engrs Structs & Bldgs. 1995.110, May, 186-203.

[44] Kareem A., "The next generation of tuned liquid dampers", Proc., First World Conference on Structural Control, Vol. 1, WP3-3-WP3-12.

[45] Kasai K., Fu Y., Lai M. L., "Finding of temperature-insensitive viscoelastic frames" Proc., First World Conference on Structural Control, Vol. 1, WP3-3-WP3-12.

[46] Kumar S., Adeli H., "Distributed finite element analysis on a network of workstations—implementation and applications", Journal of Structural Engineering, ASCE, 121(10), pp. 1456–1462.

[47] Kurino H., Tagami J., Shimzu K., Kobori T., "Switching oil damper with built-in controller for structural control", Journal of Structural Engineering, 129(7), pp. 895–904.

[48] Li G. Q., Shen Z. Y., Choo B. S., "A ring-like pendulum for reducing seismic response of tall chimneys", Proc., First World Conference on Structural Control, 1, WP-80-WP4-86.

[49] Li H.J., Hu S.L.J., Jakubiak C. "H2 active vibration control of offshore platform subjected to wave loading", Journal of Sound and Vibration, 263(4), pp. 709–724.

[50] Lin P.Y., Chung L.L., Loh C.H., "Semiactive control of building structures with semiactive tuned mass damper", Computer-Aided Civil and Infrastructure Engineering, 20(1), pp. 35–51.

[51] Liu Y., Gordaninejad F., Evrensel C., Wang X., Hitchcock G., "Comparative study on vibration control of a scaled bridge using fail-safe magneto-rheological fluid dampers", Journal of Structural Engineering, 137(5), pp. 743–751.

[52] Lobo R. F., Bracci J. M., Shen K. L., Reinhorn A. M., Soong T. T., "Inelastic response of R.C. structures with viscoelastic braces", Earthquake Spectra, 9(3), 419-446.

[53] Loh C.H., Chang C.M., "Application of centralized and decentralized control to building structure: analytical study", Journal of Engineering Mechanics, 134(11), pp. 970–982.

[54] Loh C.H., Lynch J.P., Lu K.C., Wang Y., Chang C.M., Lin P.Y., Yeh T.H., "Experimental verification of a wireless sensing and control system for structural control using MR dampers", Earthquake Engineering and Structural Dynamics, 36(10), pp. 1303–1328.

[55] Makris N., Constantinou M. C., Dargush G. F., "Analytical model of viscoelastic liquid dampers", Journal of Structural Engineering, ASCE, 119, 3310-3325.

[56] Makris, N., & Constantinou, M. C., "Spring-viscous damper systems for combined seismic and vibration isolation", Earthquake Engineering & Structural Dynamics, 21(8), 649–664.

[57] Matsuhisa H., Gu R., Nishihara O., Otake Y., Sato K., "Vibration reduction of a gondola lift by dynamic absorbers", Proc., First World Conference on Structural Control, 1, WP4-70-WP4-79.

[58] Moon S.J., Bergman L.A., Voulgaris P.G., "Model predictive control of wind-excited building: benchmark study", Journal of Engineering Mechanics, 129(1), pp. 71–78.

[59] Mostaghel N., Khodaverdian M., "Dynamics of resilient friction base isolator (R-FBI)", Earthquake Engineering and Structural Dynamics, 15, 379-390.

[60] Nishitani A., Nitta Y., Ikeda Y., "Semi-active structural-control based on variable slip-force level dampers", Journal of Structural Engineering, 129(7), pp. 933–940.

[61] Noble B., "Applied Linear Algebra Prentice-Hall", Englewood Cliffs N.J.

[62] Palazzo B., Petti L., "Seismic response control in base isolated systems using tuned mass dampers", Proc., First World Conference on Structural Control, FP5, 29-38.

[63] Pall A. S., Marsh C., "Response of friction damped braced frames", Journal of Struct. Div., ASCE, 108(6), 1313-1323

[64] Pan P., Zamfirescu D., Nakashima M., Nakashima M., Nakayasu N., Kashiwa H., "Base-isolation design practice in Japan: introduction to the post-Kobe approach", Journal of Earthquake Engineering, 9:1, 147-171, DOI: 10.1080/13632460509350537.

[65] Park H.S., Adeli H., "Distributed neural dynamics algorithms for optimization of large steel structures", Journal of Structural Engineering, ASCE, 123(7), pp. 880–888.

[66] Patten W.N., Mo C., Kuehn J., Lee, J., "A primer on design of semiactive vibration absorbers (SAVA)", Journal of Engineering Mechanics, 124(1), pp. 61–68.

[67] Pong W. S., Tsai C. S., Lee G. C. "Seismic study of building frames with added energy-absorbing devices" NCEER Rep. No. 94-0016, State University of New York at Buffalo, Buffalo, N.Y.

[68] Pong W. S., Tsai C. S., Lee G.C. "Seismic study of viscoelastic dampers and TPEA devices for high rise buildings" Proc., First World Conference on Structural Control, Vol. 1, WP3-23-WP3-32

[69] Renzi E., Serino G., "Testing and modeling a semi-actively controlled steel frame structure equipped with MR dampers", Structural Control and Health Monitoring, 11(3), pp. 189–221.

[70] Robinson W. H., "Lead-rubber hysteretic bearings suitable for protecting structures during earthquakes", Earthquake Engineering and Structural Dynamics 10, 593-604.

[71] Rodellar J., Ma.osa V., and Monroy C., "An active tendon control scheme for cable-stayed bridges with model uncertainties and seismic excitation", Structural Control and Health Monitoring, 9(1), pp. 75–94.

[72] Saleh A., Adeli H., "Microtasking, macrotasking, and autotasking for optimization of structures", Journal of Aerospace Engineering, ASCE, 7(2), pp. 156–174 .

[73] Saleh A., Adeli H., "Optimal control of adaptive building structures under blast loading", Mechatronics, 8(8), pp. 821–844.

[74] Saleh A., Adeli H., "Parallel eigenvalue algorithms for large-scale control optimization problems", Journal of Aerospace Engineering, ASCE, 9(3), pp. 70–79.

[75] Saleh A., Adeli H., "Robust parallel algorithms for solution of the Riccati equation", Journal of Aerospace Engineering, ASCE, 10(3), pp. 126–133.

[76] Saleh A., Adeli, H. "Microtasking, macrotasking and autotasking for structural optimization", Journal of Aerospace Engineering, ASCE, 7(2), pp. 156–174.

[77] Saleh A., Adeli, H. "Parallel algorithms for integrated structural and control optimization", Journal of Aerospace Engineering, ASCE, 7(3), pp. 297–314.

[78] Saleh, A. and Adeli, H. "Optimal control of adaptive/smart building structures", Computer-Aided Civil and Infrastructure Engineering, 13(6), pp. 389–403.

[79] Sarma K.C., Adeli H., "Bi-level parallel genetic algorithms for optimization of large steel structures", Computer-Aided Civil and Infrastructure Engineering, 16(5), pp. 295–304.

[80] Setareh M., Ritchey J.K., Murray T.M., Koo J.H., Ahmadian M., "Semi-active tuned mass damper for floor vibration control", Journal of Structural Engineering, 133(2), pp. 242–250.

[81] Shen K. L., Soong T.T., Chang K. C., Lai M. L., "Seismic behaviour of reinforced concrete frame with added viscoelastic dampers", Engrg. Struct.,17(5), 372-380.

[82] Soegiarso R., Adeli H., "Impact of vectorization on large-scale structural optimization", Structural Optimization, 7(1), pp. 117–125.

[83] Soong T. T., Spencer Jr B. F., "Active, semi-active and hybrid control of structures", Bulletin of the New Zealand Society for Earthquake Engineering, 10.5459/bnzsee.33.3.387-402.

[84] Soong T.T., Spencer B.F., "Active structural control: theory and practice", Journal of Engineering Mechanics 118: 1282–1285.

[85] Su L., Ahmadi G., Tadjbakhsh I.G., "A comparative study of base isolation system", Journal of Engng Mech. Am. Soc. Civ. Engrs, 115, 1976-1992

[86] Sun L., Goto Y., "Applications of fuzzy theory to variable dampers for bridge vibration control", Proc., First World Conference on Structural Control, WP1.31-40.

[87] Tsai C. S., Chen H. W., Hong C. P., Su Y. F., "Design of steel triangular plate energy absorbers for seismic-resistant construction", Earthquake spectra, 9(3), 505-528.

[88] Tsiatas G. and Daly K., "Controlling vibrations with combination viscous/friction mechanisms" Proc., First World Conference on Structural Control, Vol. 1, WP4-3-WP4-11.

[89] Tsiatas G., Olson C., "Frictionally damped braced frames" Proc., Seventh Engineering Mech. Specialty Conf., VPI, Blacksburg, Va.

[90] Wakahara T., Ohyama T., Fujii K., "Suppression of wind induced vibration of a tall building using tuned liquid damper", Proc., Symp. On Serviceability of Build.

[91] Welt F., Modi V. J., "Vibration damping through liquid sloshing: part I – a nonlinear analysis" Proc., Diagnostics, Vehicle Dynamics and Specific Topics, ASME, Des. Engrg. Div., Vol. 18-5, 149-156.

[92] Whittaker A. S., Bertero V. V., Thompson C. L., Alonso L. J., "Seismic testing of steel plate energy dissipation devices", Earthquake Spectra, 7(4), 563-604.

[93] Wu J.C., Yang J.N., "Active control of transmission tower under stochastic wind", Journal of Structural Engineering, 124(11), pp. 1302–1312.

[94] Xianzhong Cui, Shin K. G., "Computing time delay and its effects on real-time control systems". IEEE Transactions on Control Systems Technology, 3(2), 218–224.

[95] Xu Y.L., Chen J., Ng, C.L., Qu W.L. "Semi-active seismic response control of buildings with podium structure", Journal of Structural Engineering, 131(6), pp. 890–899.

[96] Xu Y.L., Qu W.L., Chen Z.H., "Control of Wind-Excited Truss Tower Using Semiactive Friction Damper", Journal of Structural Engineering, 127(8), 861–868.

[97] Zadeh L.A., Desoer C.A., "Linear System Theory: The State Space Approach" McGraw-Hill, NY

[98] Zhang R. H., Soong T. T., "Seismic design of viscoelastic dampers for structural application" Journal of Structural Engineering, ASCE 118(5), 1375-1392.

[99] Zhang R. H., Soong T. T., Mahmoodi P., "Seismic response of steel frame structures with added viscoelastic dampers", Earthquake Engineering and Structural Dynamics, 8, 389-396, 1992.